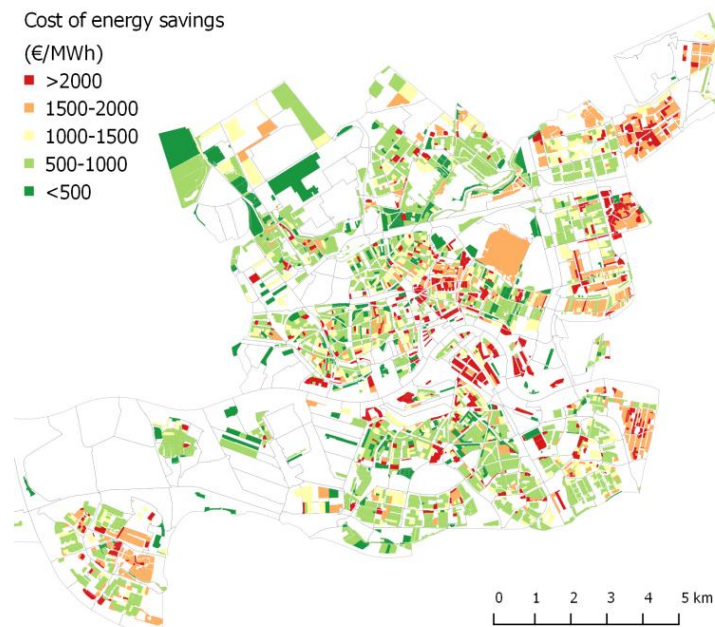


Journal of Energy Challenges and Mechanics

ISSN 2056-9386

<http://www.nscj.co.uk/JECM/>

Volume 3, Issue 4
December 2016



Featured article:

A GIS-based statistical approach to prioritize the retrofit of housing stocks at the urban scale

Alessio Mastrucci^{1}, Olivier Baume², Francesca Stazi³, Ulrich Leopold⁴*

¹International Institute for Applied Systems Analysis, Schlossplatz 1, A-2361 Laxenburg, Austria

²Resource Centre for Environmental Technologies - Public Research Centre Henri Tudor, 6A, avenue des Hauts-Fourneaux, L-4362 Esch-sur-Alzette, Luxembourg

³Dipartimento di Ingegneria Civile, Edile e Architettura - Universita Politecnica delle Marche, Via Brecce Bianche 12, 60131 Ancona, Italy

⁴Luxembourg Institute of Science and Technology, 5 avenue des Hauts-Fourneaux, L-4362 Esch-sur-Alzette.



North Sea Conference & Journal LTD

2 Charlestown Walk, Cove Bay, AB12 3EZ, Aberdeen, Scotland, United Kingdom

<http://www.nscj.co.uk/JECM/> | jecm@nscj.co.uk | +44(0)1224 875635



TABLE OF CONTENTS

pages

Article 1 : Wind power plant resonances <i>Luis Sainz^{1*}, Marc Cheah-Mane^{2*}, Lluís Monjo³, Jun Liang², Oriol Gomis-Bellmunt¹</i> <i>¹Department of Electrical Engineering, ETSEIB-UPC, Av. Diagonal 647, Barcelona 08028, Spain</i> <i>²School of Engineering, Cardiff University, CF24 3AA, Cardiff, U.K</i> <i>³Department of Industrial and Design System Engineering, ESTCE, Univ. Jaume I, Av. de Vicent Sos Baynat, s/n, 12071 Castelló de la Plana, Spain</i>	168- 179
Article 2 : The need for lithium – an upcoming problem for electrochemical energy storages? <i>Daniel Schultz¹, Wilhelm Kuckshinrichs^{1*}</i> <i>¹Institute for Energy and Climate Research – Systems Analysis and Technology Evaluation, Forschungszentrum Jülich, 52425 Jülich, Germany</i>	180- 185
Article 3 : A GIS-based statistical approach to prioritize the retrofit of housing stocks at the urban scale <i>Alessio Mastrucci^{1*}, Olivier Baume², Francesca Stazi³, Ulrich Leopold⁴</i> <i>¹International Institute for Applied Systems Analysis, Schlossplatz 1, A-2361 Laxenburg, Austria</i> <i>²Resource Centre for Environmental Technologies - Public Research Centre Henri Tudor, 6A, avenue des Hauts-Fourneaux, L-4362 Esch-sur-Alzette, Luxembourg</i> <i>³Dipartimento di Ingegneria Civile, Edile e Architettura - Università Politecnica delle Marche, Via Brecce Bianche 12, 60131 Ancona, Italy</i> <i>⁴Luxembourg Institute of Science and Technology, 5 avenue des Hauts-Fourneaux, L-4362 Esch-sur-Alzette.</i>	186- 190
Article 4 : Parametric modeling of producer gas-combustor and heat exchanger integration for micro-gas turbine application <i>Mackay A.E. Okure¹, Wilson B. Musinguzi^{2*}, Terese Løvås³</i> <i>¹School of Engineering, Makerere University, P.O. Box 7062, Kampala, Uganda</i> <i>²Faculty of Engineering, Busitema University, P.O. Box 236, Tororo, Uganda</i> <i>³Department of Energy and Process Engineering, NTNU, Trondheim, Norway</i>	191- 200
Article 5 : Behavior, cutting property and environmental load of machine tool in mist of strong alkaline water <i>Ikuo Tanabe^{1*}</i> <i>¹Department of Mechanical Engineering, Nagaoka University of Technology, 1603-1 Kamitomioka Nagaoka Niigata, 940-2188 Japan</i>	201- 210



[Article 6](#): Korea's policies, R&D investment and competitiveness in the LED industry 211-216

Joon Han¹, Chul-Ho Park^{1}, Ji-Sun Ku¹, Ho-Sik Chon²*

¹Center for Climate Technology Cooperation, Green Technology Center Korea, Seoul, Korea

²Division of Policy Research, Green Technology Center Korea, Seoul, Korea



Wind power plant resonances 风力发电厂的共振

Luis Sainz^{1*}, Marc Cheah-Mane^{2*}, Lluís Monjo³, Jun Liang², Oriol Gomis-Bellmunt¹

¹Department of Electrical Engineering, ETSEIB-UPC, Av. Diagonal 647, Barcelona 08028, Spain

²School of Engineering, Cardiff University, CF24 3AA, Cardiff, U.K

³Department of Industrial and Design System Engineering, ESTCE, Univ. Jaume I, Av. de Vicent Sos Baynat, s/n, 12071 Castelló de la Plana, Spain

sainz@ee.upc.edu

Accepted for publication on 30th July 2016

Abstract - Onshore and offshore wind power plants comprising wind turbines equipped with power converters are increasing in number worldwide. Harmonic emissions in power converters distort currents and voltages, leading to power quality problems. Low order resonances in the collector grid can increase the impact of wind turbine emissions. These resonances may also produce electrical instabilities in poorly damped wind power plants. The paper performs frequency scan with Matlab/Simulink simulations and compares low order frequencies of parallel resonances in onshore and offshore wind power plants. It also investigates the influence of wind power plant variables on resonance. Finally, simplified equivalent circuits of wind power plants are proposed to study low order parallel resonances.

Keywords - Wind power generation, resonance, frequency scan.

I. INTRODUCTION

The presence of wind power plants (WPPs) with wind turbines (WTs) equipped with power electronics is currently increasing in traditional power systems [1]. Several power quality concerns related to harmonic emissions of these WTs are present in WPPs [1] – [6]. These concerns increase with parallel resonances in the WPP collector grid at frequencies close to harmonic emissions. These resonances are due to the interaction between inductors and capacitors of the WPP network, [1], [4] – [9]. Several works study WPP resonance to address harmonic concerns [4] – [9]. The most important WPP harmonic and resonance issues are illustrated in [4], [6], [8]. Recent works also study resonance influence on stability of WT converters [10] – [12]. Low order resonances are the most worrisome because they can be close to low order harmonic emissions of power converters and to the poorly damped frequency range. Resonance studies are mainly based on frequency scan analysis, which establishes the frequency range and peak impedance values of resonances. A few works include analytical expressions to determine low order parallel resonance frequency [8], [13], [14]. The influence of WPP parameters on resonances is also discussed in most of the

above studies. In order to investigate this influence further, it is necessary to examine WPP resonance frequencies in depth from frequency scan or analytical expressions which characterize resonance frequencies as a function of WPP parameters [14].

The present work analyzes WPP parallel resonance from frequency scan with Matlab/Simulink simulations. It compares low order parallel resonance frequencies in onshore and offshore WPPs. The impact of WPP parameters on resonance is also investigated. Approximated equivalent circuits for analyzing WPP parallel resonance are proposed from the above studies.

II. WIND POWER PLANTS

The configuration of a generic WPP layout is shown in Fig. 1. Type 4 WTs are supplied from the strings of the $N_r \times N_c$

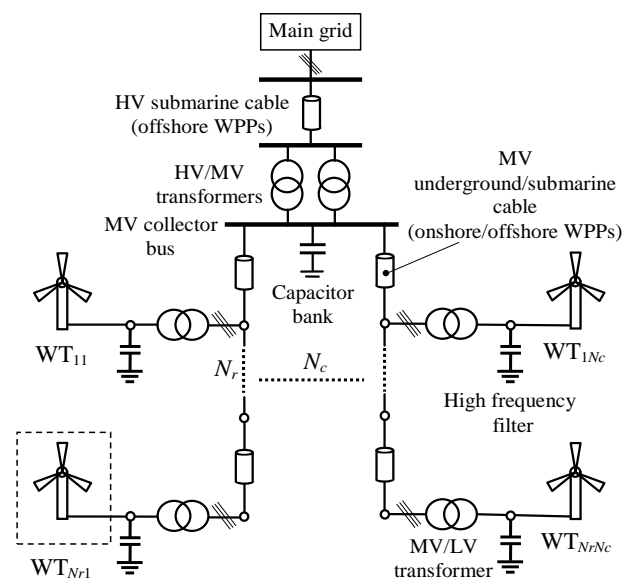


Fig.1. Wind power plant layout

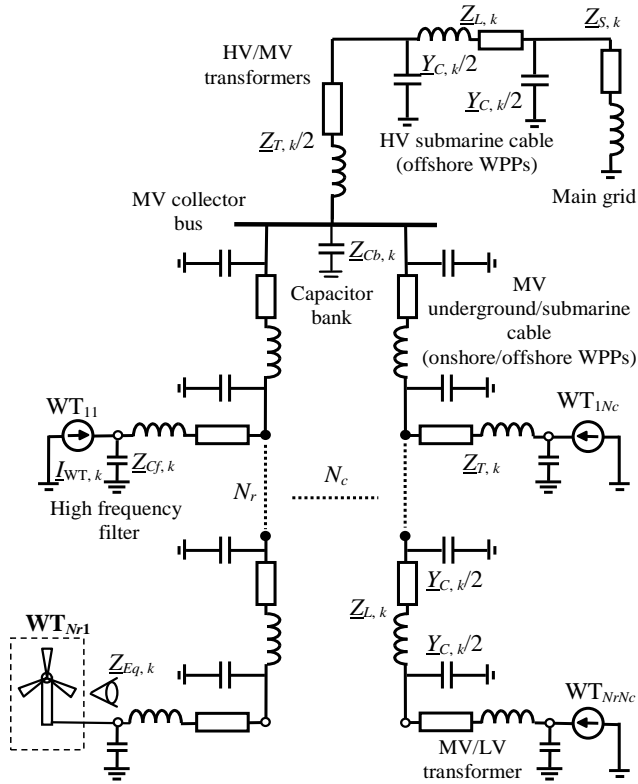


Fig.2. Wind power plant equivalent circuit

collector grid through step-down medium to low voltage (MV/LV) transformers. High frequency filter capacitors are usually installed on the grid-side of WT converters to mitigate frequency switching harmonics [4], [5]. The strings are interconnected with medium voltage (MV) underground cables in onshore WPPs and MV submarine cables in offshore WPPs. These cables are clustered at the MV collector bus [4], [5], [6] – [10], [13]. In onshore WPPs, capacitor banks can also be connected to this bus in order to compensate reactive power. The MV collector bus is connected to the main grid with two step-down high to medium voltage (HV/MV) transformers in parallel. In onshore WPPs, the transformers are directly connected to the main grid while, in offshore WPPs, high voltage (HV) submarine cables are used to link the transformers to the main grid on shore.

Voltage distortion of the WPP collector grid usually remains below standard limits because WT converter harmonic emissions are generally low [2], [3], [15], [16]. However, parallel resonances may increase distortion above these limits and affect WT operation if the resonance frequency is close to WT converter emission harmonics [4], [5]. These resonances may also affect stability of WT converters [10] – [12]. The frequency scan method is commonly used in the literature to characterize the resonance problem at WT terminals and approach harmonic penetration and WT stability studies.

II. WIND POWER PLANT HARMONIC MODEL

In order to perform frequency scan, the WPPs are characterized by the equivalent circuit in Fig. 2, and the equivalent harmonic impedance $Z_{Eq, k}$ at the WTs must be determined to identify resonance frequencies. To do that, the harmonic impedances of the main grid, $Z_{S, k}$, HV/MV and MV/LV transformers, $Z_{T, k}$, HV and MV underground/submarine cables, $Z_{L, k}$, capacitor bank, $Z_{Cb, k}$, and high frequency filters, $Z_{Cf, k}$, are modeled as follows [4], [5], [7]:

$$\begin{aligned}
 Z_{S, k} &= \frac{U_o^2}{S_s} \frac{1}{\sqrt{1 + \tan^2 \varphi_s}} (1 + jk \tan \varphi_s) \\
 Z_{T, k} &= \varepsilon_{cc} \frac{U_{N, s}^2}{S_N} \frac{1}{\sqrt{1 + \tan^2 \varphi_{cc}}} (1 + jk \tan \varphi_{cc}) \\
 Z_{L, k} &= Z_{Lx, k} \frac{\sinh(\gamma_{x, k} D)}{\gamma_{x, k}} \quad Y_{C, k} = Y_{Cx, k} \frac{\tanh(D\gamma_{x, k}/2)}{\gamma_{x, k}/2} \\
 Z_{Cb, k} &= -j \frac{1}{k} \frac{U_{Nb}^2}{Q_{Cb}} \quad Z_{Cf, k} = -j \frac{1}{C_f k \omega_1},
 \end{aligned} \tag{1}$$

where $k = f_k/f_1$ (with f_k and f_1 being the analyzed harmonic frequency and the main grid fundamental frequency, respectively), $\omega_1 = 2\pi \cdot f_1$ and,

- U_o , S_s and $\tan \varphi_s$ are the main grid open-circuit voltage,

TABLE 1. WPP PARAMETERS (WTs OF $P_{WT} = 5$ MW)

Main grid	U_o (f_1)	150 kV (50 Hz)
	S_s	$(10 \dots 100) \cdot N_r N_c P_{WT}$
	$\tan \varphi_s$	20 pu
HV/MV transformers	$U_{N, H}/U_{N, M}$	150/33 kV
	S_N	125 MVA
	ε_{cc} ($\tan \varphi_{cc}$)	0.1 pu (12 pu)
MV/LV transformer	$U_{N, M}/U_{N, L}$	33/0.69 kV
	S_N	5 MVA
	ε_{cc} ($\tan \varphi_{cc}$)	0.05 pu (12 pu)
HV submarine cable (offshore WPPs)	R_x	0.032 Ω /km
	L_x	0.401 mH/km
	C_x	0.21 μ F/km
	D_{HV}	1 to 50 km
MV underground /submarine cable (onshore/offshore WPPs)	R_x	0.041 Ω /km
	L_x	0.38 mH/km
	C_x	0.23 μ F/km
	D_{MV}	0.5 to 1 km
Compensation and filter equipment	Q_{Cb}	0 ... 50 Mvar
	C_f	1000 μ F

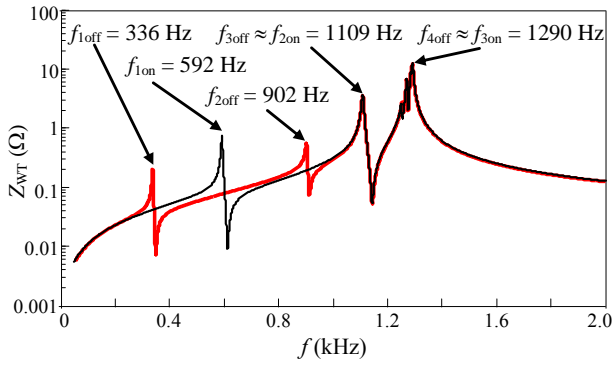


Fig. 3. Frequency scan of 8x5 onshore (black line) and offshore (red line) WPPs (data in Table 1, with $S_S = 2500$ MVA, $D_{HV} = 25$ km, $D_{MV} = 1$ km and $Q_{Cb} = 0$ Mvar)

short-circuit power and X_S/R_S ratio at the point of coupling.

- $U_{N,p}/U_{N,s}$, S_N , ε_{cc} and $\tan\phi_{cc}$ are the HV/MV and MV/LV transformer rated primary/secondary voltages and power, per-unit short-circuit impedance and X_{cc}/R_{cc} ratio.
- $\gamma_{x,k} = (Z_{Lx,k} \cdot Y_{Cx,k})^{1/2}$ is the propagation constant of the cable, $Z_{Lx,k} = R_x + jL_x k \omega_1$ and $Y_{Cx,k} = jC_x k \omega_1$ are the cable distributed parameters and D is the cable length.
- U_{Nb} and Q_{Cb} are the capacitor bank rated voltage and reactive power consumption (i.e., the capacitor bank size).
- C_f is the WT high frequency filter capacitor.

The transformers are modeled as RL equivalent circuits and the WTs are modeled as ideal current sources. These models are accurate enough to analyze the influence of WPP parameters on low order resonances. The WT current source model is commonly chosen to perform frequency scan studies because it offers a useful insight into low order parallel resonance analysis [1], [4], [5] [8], [13]. Table 1 shows usual WPP parameter values.

II. ONSHORE AND OFFSHORE WPP RESONANCES

The frequency response of an 8x5 onshore and an 8x5 offshore WPP (data in Table 1) is determined to compare their low order parallel resonances. Both WPPs consist of 40 type 4 WTs (i.e., full-scale VSC WTs), each with a rated capacity of 5 MW, arranged in five strings of 33 kV underground/submarine cables. These strings collect eight WTs (separated 1 km from each other) at the collector substation. This substation is directly connected to the main grid in the onshore WPP and by a 25 km submarine cable in the offshore WPP. The short circuit power of the main grid is 2500 MVA and capacitor banks are not connected to the collector bus of the onshore WPP (i.e., $Q_{Cb} = 0$ Mvar). The results of the equivalent harmonic impedance $Z_{Eq,k}$ at WT_{N1} (see Fig. 2) are illustrated in Fig. 3. From these results, it can be noted that

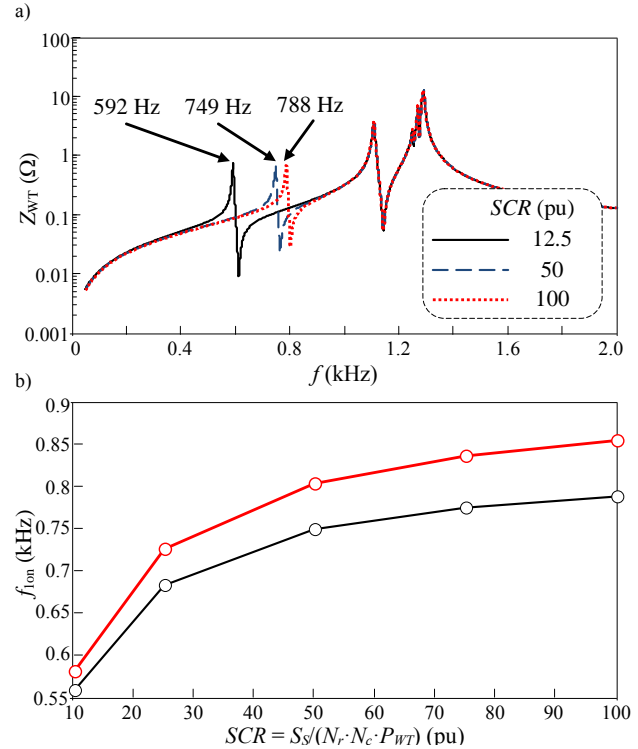


Fig. 4. Influence of the short circuit ratio, SCR , of the main grid on 8x5 onshore WPP resonance (data in Table 1, with $D_{MV} = 1$ km and $Q_{Cb} = 0$ Mvar): a) Frequency scan. b) Frequency of first parallel resonance vs Short circuit ratio (black lines: Equivalent circuit in Fig. 2; red lines: Equivalent circuit in Fig. 19)

- WPP connection to shore by the HV submarine cable is the only difference between the onshore and offshore WPPs. The difference between the first parallel resonances of the onshore WPP (at $f_{1on} = 592$ Hz) and offshore WPP (at $f_{1off} = 336$ Hz) is due to the transversal capacitors of the cable. These capacitors shift the parallel resonance to low order frequencies, which are close to WT harmonic emissions.
- The HV submarine cable of the offshore WPP also produces a parallel resonance at $f_{2off} = 902$ Hz which does not appear in the onshore WPP. The frequency of this parallel resonance depends on the cable length, as is analyzed in Subsection 4.3.
- Parallel resonances above 1 kHz (i.e., $f_{3off} \approx f_{2on}$ and $f_{4off} \approx f_{3on}$) are not affected by the capacitors of the HV submarine cable, thus being similar in both WPPs.

III. ONSHORE WPP RESONANCE STUDY

The frequency response of the 8x5 onshore WPP in Section II (data in Table 1) is analyzed to study the influence of the main grid short circuit ratio, $SCR = S_S / (N_r \cdot N_c \cdot P_{WT})$, WPP layout (i.e., number of WTs and strings N_r , and N_c), MV underground cable length, D_{MV} , and capacitor bank size, Q_{Cb} , on low order parallel resonances. To study the influence of these parameters, Matlab/Simulink simulations are made by varying their values. In these simulations, frequency scan is

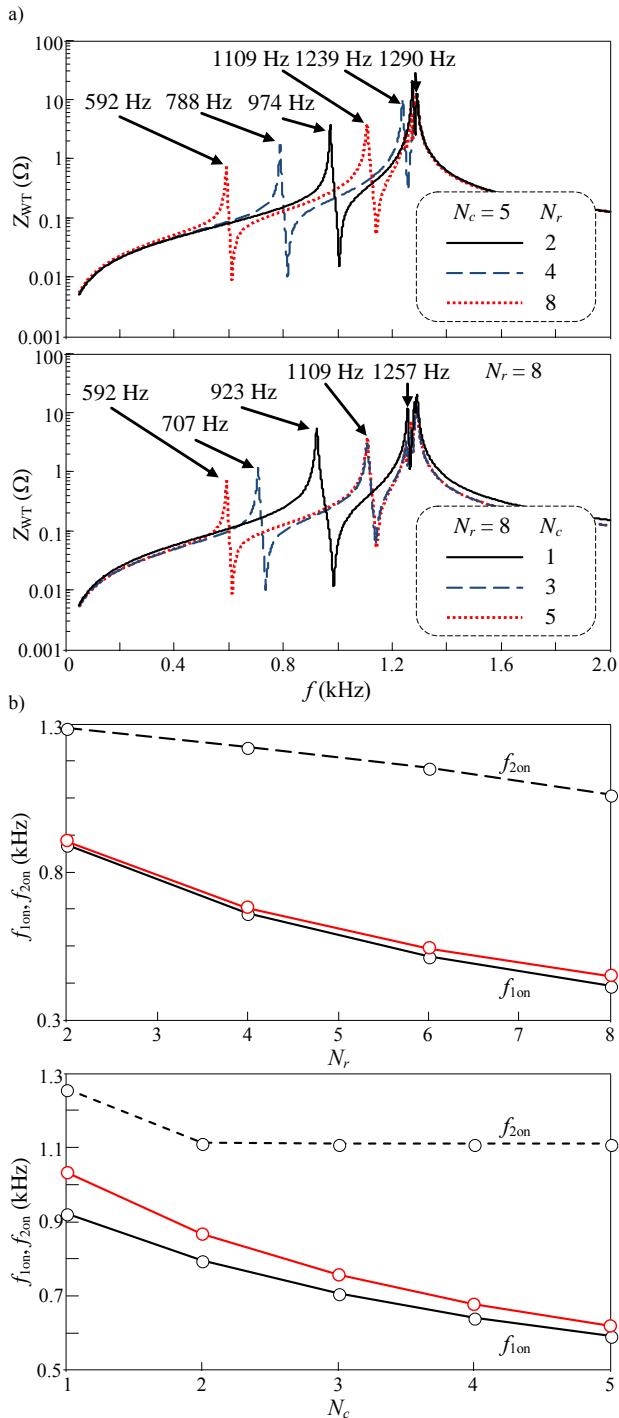


Fig. 5. Influence of WPP layout on onshore $N_r \times N_c$ WPP resonance (data in Table 1, with $SCR = 12.5$ pu, $D_{MV} = 1$ km and $Q_{Cb} = 0$ Mvar): a) Frequency scan. b) Frequency of first and second parallel resonances vs N_r and N_c (black lines: Equivalent circuit in Fig. 2; red lines: Equivalent circuit in Fig. 19)

performed at WT_{Nr1} (see Fig. 2) and the equivalent harmonic impedance $Z_{Eq,k}$ is obtained. Subsequently, the frequency of the parallel resonances is numerically identified from the frequency scan.

3.1. INFLUENCE OF SHORT CIRCUIT RATIO

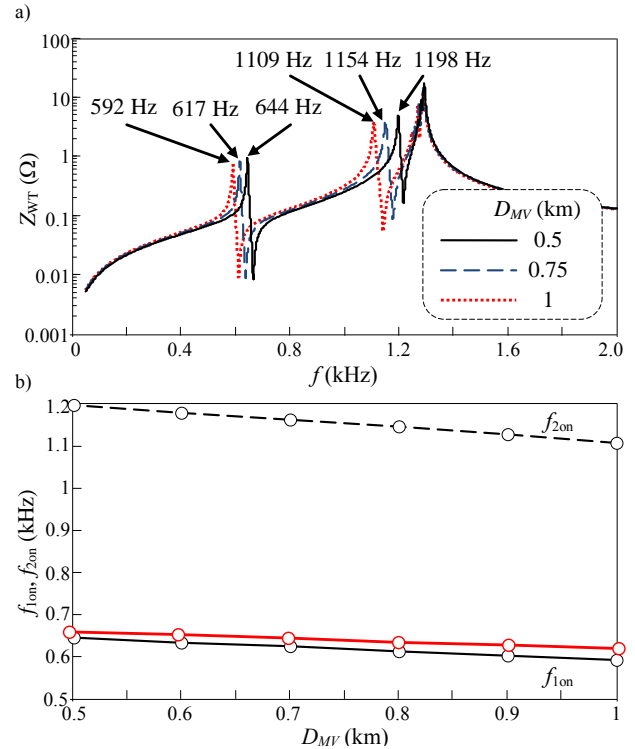


Fig. 6. Influence of MV underground cable length, D_{MV} , on 8x5 onshore WPP resonance (data in Table 1, with $SCR = 12.5$ pu and $Q_{Cb} = 0$ Mvar): a) Frequency scan. b) Frequency of first and second parallel resonances vs MV underground cable length (black lines: Equivalent circuit in Fig. 2; red lines: Equivalent circuit in Fig. 19)

In order to study the influence of the short circuit ratio, SCR , of the main grid on parallel resonance, Matlab/Simulink simulations are made by varying the short circuit ratio value from 10 to 100 (i.e., $S_S = 2000$ MVA to 20000 MVA considering the 8x5 WPP with 5 MW WTs in the study). As an example, the frequency scan of the equivalent harmonic impedance $Z_{Eq,k}$ at WT_{Nr1} for three values of the short circuit ratio ($SCR = 12.5, 50$ and 100) is shown in Fig. 4(a). From these results, it can be noted that

- Small values of the short circuit ratio (i.e., grids that tend to be weak) lead to high values of the main grid inductances (1), which shift the first parallel resonance, f_{1on} , to low frequencies.
- The other parallel resonances are not affected by the main grid inductance, and therefore they are not affected by the short circuit ratio.

The influence of short circuit ratio on the first parallel resonance, f_{1on} , is illustrated with black lines in Fig. 4(b). It can be observed that grids that tend to be weak (i.e. grids with low short circuit ratios) can shift the first parallel resonance to the low frequency range because of the large values of the main grid inductances. Thus, weak grids can produce onshore WPP resonances close to WT harmonic emissions.

3.2. INFLUENCE OF WIND POWER PLANT LAYOUT

In order to study the influence of the number of WTs, N_r , and strings, N_c , on parallel resonance, Matlab/Simulink

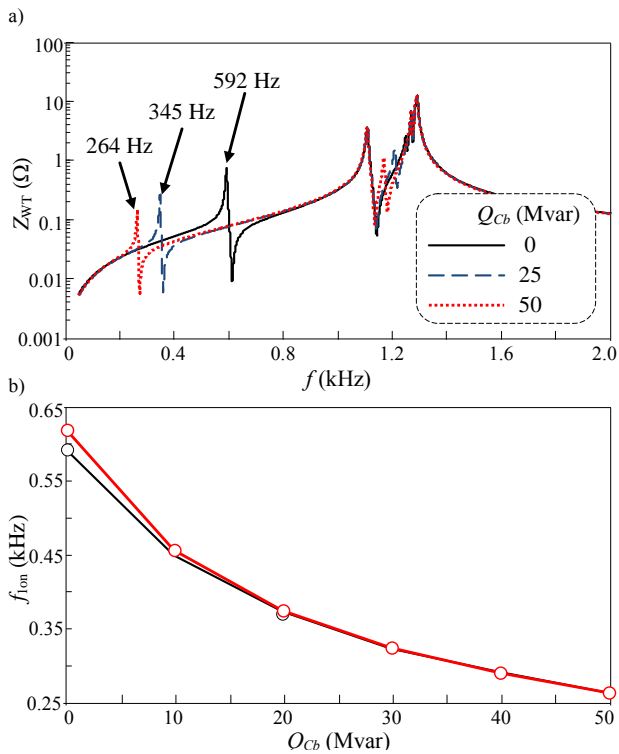


Fig. 7. Influence of capacitor bank size, Q_{Cb} , on 8x5 onshore WPP resonance (data in Table 1, with $SCR = 12.5$ pu and $D_{MV} = 1$ km): a) Frequency scan. b) Frequency of first parallel resonance vs Capacitor bank size (black lines: Equivalent circuit in Fig. 2; red lines: Equivalent circuit in Fig. 19)

simulations are made by varying the N_r value from 2 to 8 and the N_c value from 1 to 5. As an example, the frequency scan of the equivalent harmonic impedance $Z_{Eq,k}$ at WT_{Nr1} for three values of N_r ($N_r = 2, 4$ and 8) and for three values of N_c ($N_c = 1, 3$ and 5) is shown in Fig. 5(a). From these results, it can be noted that

- High number of the WTs and strings shift the first and second parallel resonances, f_{1on} and f_{2on} , to low frequencies.

The influence of WPP layout on the first and second parallel resonances f_{1on} and f_{2on} is illustrated with black lines in Fig. 5(b). It can be observed that parallel resonances are closer to low order harmonics in large onshore WPPs than in small onshore WPPs because parallel resonance frequencies move to lower order harmonics with increasing the number of WTs and strings. An exhaustive study of this influence is presented in [14].

3.3. INFLUENCE OF MV UNDERGROUND CABLE LENGTH

In order to study the influence of MV underground cable length, D_{MV} , on parallel resonance, Matlab/Simulink simulations are made by varying the cable length value from 0.5 km to 1 km. As an example, the frequency scan of the equivalent harmonic impedance $Z_{Eq,k}$ at WT_{Nr1} for three values of the cable length ($D_{MV} = 0.5, 0.75$ and 1 km) is shown in Fig. 6(a). From these results, it can be noted that

- High values of the MV cable length shift the first and second parallel resonances, f_{1on} and f_{2on} , to low

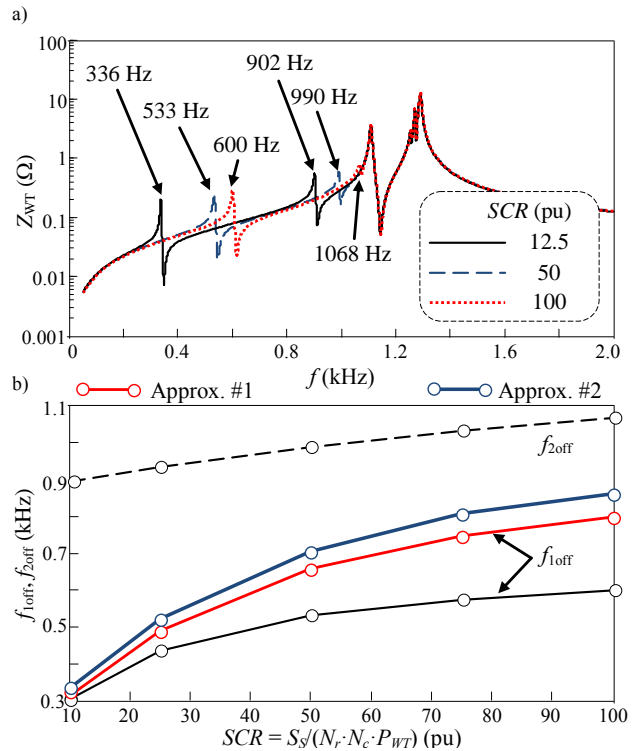


Fig. 8. Influence of short circuit ratio, SCR , of the main grid on 8x5 offshore WPP resonance (data in Table 1, with $D_{HV} = 25$ km and $D_{MV} = 1$ km): a) Frequency scan. b) Frequency of first and second parallel resonances vs Short circuit ratio (black lines: Equivalent circuit in Fig. 2; red and blue lines: Equivalent circuit in Fig. 19)

frequencies because of the higher value of transversal capacitors of the cable. However, these resonance frequencies exhibit a low sensitivity to MV cable length.

- The other parallel resonance is not affected by cable length.

The influence of MV cable length on the first and second parallel resonances f_{1on} and f_{2on} is illustrated with black lines in Fig. 6(b). It can be observed that, although the frequency of the parallel resonances is only slightly affected by cable length, it decreases with long MV underground cables. Thus, WPPs with WTs far away from each other can produce onshore WPP resonances close to WT harmonic emissions.

3.4. INFLUENCE OF CAPACITOR BANK SIZE

In order to study the influence of capacitor bank size, Q_{Cb} , on parallel resonance, Matlab/Simulink simulations are made by varying the reactive power consumption value of the capacitor bank from 0 Mvar to 50 Mvar. As an example, the frequency scan of the equivalent harmonic impedance $Z_{Eq,k}$ at WT_{Nr1} for three values of the capacitor bank size ($Q_{Cb} = 0, 25$ and 50 Mvar) is shown in Fig. 7(a). From these results, it can be noted that

- High values of capacitor bank size shift the first parallel resonance, f_{1on} , to low frequencies because of the increase in capacitors connected to the collector bus.
- The other parallel resonances are slightly affected by capacitor bank size.

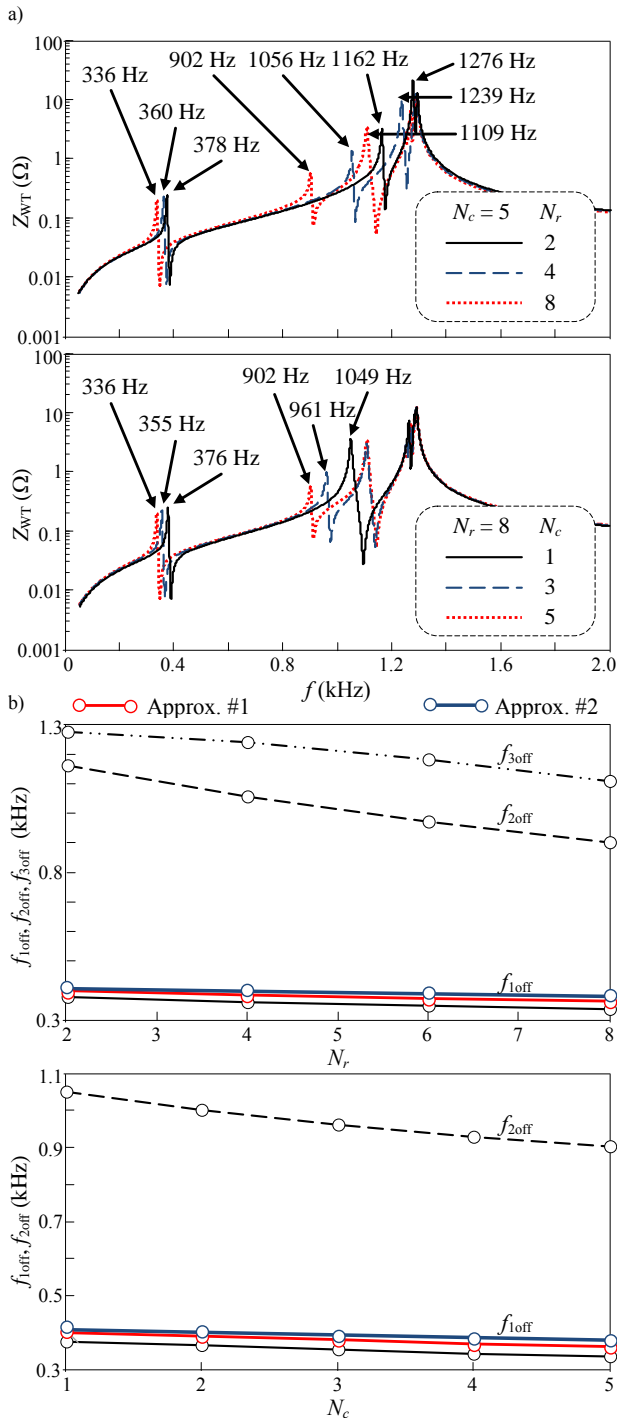


Fig. 9. Influence of WPP layout on $N_r \times N_c$ offshore WPP resonance (data in Table 1, $SCR = 12.5$ pu, $D_{HV} = 25$ km and $D_{MV} = 1$ km): a) Frequency scan. b) Frequencies of first, second and third parallel resonances vs N_r and N_c (black lines: Equivalent circuit in Fig. 2; red and blue lines: Equivalent circuit in Fig. 19)

The influence of capacitor bank size on the first parallel resonance, f_{1off} , is illustrated with black lines in Fig. 7(b). It can be observed that larger capacitor bank sizes lead to lower frequency values of the first parallel resonance. Thus, reactive power compensation at the collector bus can produce onshore WPP resonances close to WT harmonic emissions. An

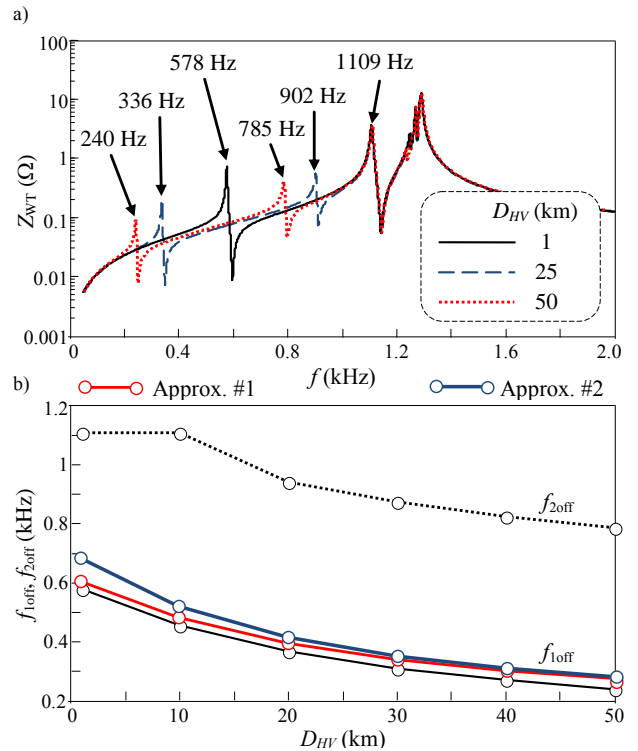


Fig. 10. Influence of HV submarine cable length D_{HV} on 8x5 offshore WPP resonance (data in Table 1, with $SCR = 12.5$ pu and $D_{MV} = 1$ km): a) Frequency scan. b) Frequency of first and second parallel resonances vs MV submarine cable length (black lines: Equivalent circuit in Fig. 2; red and blue lines: Equivalent circuit in Fig. 19)

exhaustive study of capacitor size influence is presented in [14].

IV. OFFSHORE WPP RESONANCE STUDY

The frequency response of the 8x5 offshore WPP in Section II (data in Table 1) is analyzed to study the influence of the main grid short circuit ratio, $SCR = S_S / (N_r \cdot N_c \cdot P_{WT})$, WPP layout (i.e., number of WTs and strings, N_r and N_c), HV submarine cable length, D_{HV} , and MV submarine cable length, D_{MV} , on low order parallel resonances. To do this, Matlab/Simulink simulations are made by varying their values. A frequency scan at WT_{N_r-1} (see Fig. 2) is performed in these simulations and the equivalent harmonic impedance $Z_{Eq,k}$ is obtained. Subsequently, the frequency of the parallel resonance is numerically identified from the frequency scan.

4.1. INFLUENCE OF SHORT CIRCUIT RATIO

In order to study the influence of short circuit ratio, SCR , of the main grid on parallel resonance, Matlab/Simulink simulations are made by varying the short circuit ratio value from 10 to 100 (i.e., $S_S = 2000$ MVA to 20000 MVA considering the 8x5 WPP with 5 MW WTs in the study). As an example, the frequency scan of the equivalent harmonic impedance $Z_{Eq,k}$ at WT_{N_r-1} for three values of the short circuit ratio ($SCR = 12.5, 50$ and 100 pu) is shown in Fig. 8(a). From these results, it can be noted that

- Similarly to onshore WPPs, small values of the short circuit ratio (i.e., grids that tend to be weak) lead to high values of the main grid inductances (1), which shift the first and second parallel resonances to low frequencies, f_{1off} and f_{2off} .
- The other parallel resonances are not affected by the main grid impedance, and therefore they are not affected by the short circuit ratio.

The influence of short circuit power on the first and second parallel resonances f_{1off} and f_{2off} is illustrated with black lines in Fig. 8(b). It can be observed that grids that tend to be weak (i.e., grids with small short circuit ratios) can shift the first and second parallel resonances to a low frequency range because of the large values of the main grid inductances. Thus, weak grids can produce offshore WPP resonances close to WT harmonic emissions.

4.2. INFLUENCE OF WIND POWER PLANT LAYOUT

In order to study the influence of the number of WTs, N_r , and strings, N_c , on parallel resonance, Matlab/Simulink simulations are made by varying the N_r value from 2 to 8 and the N_c value from 1 to 5. As an example, the frequency scan of the equivalent harmonic impedance $Z_{Eq,k}$ at WT_{Nr1} for three values of N_r ($N_r = 2, 4$ and 8) and for three values of N_c ($N_c = 1, 3$ and 5) is shown in Fig. 9(a). From these results, it can be noted that

- High number of the WTs and strings shift the first and second parallel resonances, f_{1off} and f_{2off} , to low frequencies.

The influence of WPP layout on the first and second parallel resonances, f_{1off} and f_{2off} , is illustrated with black lines in Fig. 9(b). It can be observed that parallel resonances are closer to low order harmonics in large offshore WPPs than in small offshore WPPs because parallel resonance frequencies move to lower order harmonics with increasing the number of WTs and strings.

4.3. INFLUENCE OF HV SUBMARINE CABLE LENGTH

In order to study the influence of HV submarine cable length, D_{HV} , on parallel resonance, Matlab/Simulink simulations are made by varying the cable length value from 1 km to 50 km. As an example, the frequency scan of the equivalent harmonic impedance $Z_{Eq,k}$ at WT_{Nr1} for three values of the cable length ($D_{HV} = 1, 25$ and 50 km) is shown in Fig. 10(a). From these results, it can be noted that

- High values of HV cable length shift the first and second parallel resonances, f_{1off} and f_{2off} , to low frequencies because of the higher value of transversal capacitors of the cable.
- The second parallel resonance, f_{2off} , matches with the third parallel resonance, f_{3off} , for small values of HV cable length and is no longer affected by this parameter.
- The other parallel resonances are not affected by the cable length.

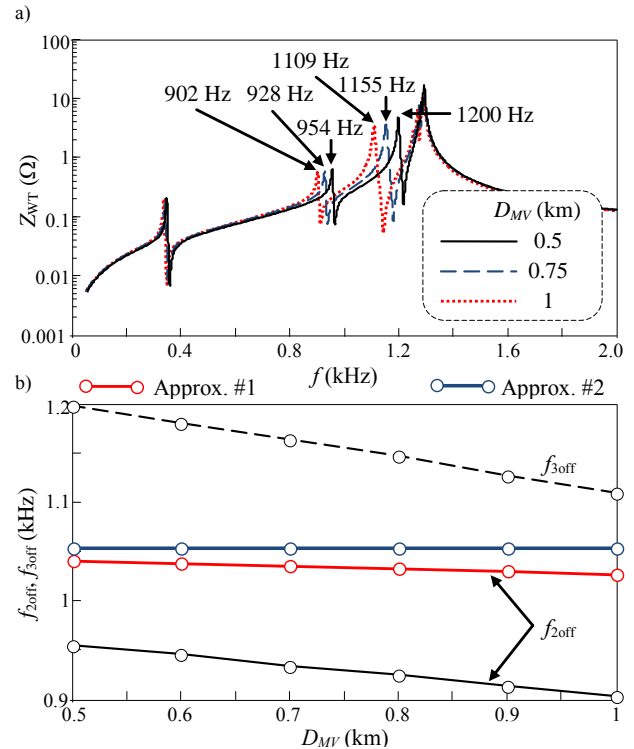


Fig. 11. Influence of MV submarine cable length, D_{MV} , on 8x5 offshore WPP resonance (data in Table 1, with $SCR = 12.5$ pu, and $D_{HV} = 25$ km): a) Frequency scan. b) Frequency of second and third parallel resonance vs MV submarine cable length (black lines: Equivalent circuit in Fig. 2; red and blue lines: Equivalent circuit in Fig. 19)

The influence of HV cable length on the first and second parallel resonances, f_{1off} and f_{2off} , is illustrated with black lines in Fig. 10(b). It can be observed that greater cable lengths lead to lower frequencies of the parallel resonances. Thus, offshore WPPs far from shore can produce resonances close to WT harmonic emissions.

4.4. INFLUENCE OF MV SUBMARINE CABLE LENGTH

In order to study the influence of MV underground cable length, D_{MV} , on parallel resonance, Matlab/Simulink simulations are made by varying the cable length value from 0.5 km to 1 km. As an example, the frequency scan of the equivalent harmonic impedance $Z_{Eq,k}$ at WT_{Nr1} for three values of the cable length ($D_{MV} = 0.5, 0.75$ and 1 km) is shown in Fig. 11(a). From these results, it can be noted that

- High values of MV cable length shift the second and third parallel resonances, f_{2off} and f_{3off} , to low frequencies because of the higher value of transversal capacitors of the cable.
- The low sensitivity of the parallel resonances to MV cable length is similar to that observed in onshore WPPs.
- The other parallel resonances (in particular, the first parallel resonance, f_{1off}) are not affected by the cable length.

The influence of MV cable length on the second and third parallel resonances, f_{2off} and f_{3off} , is illustrated with black lines in Fig. 11(b). It can be observed that, although the frequency

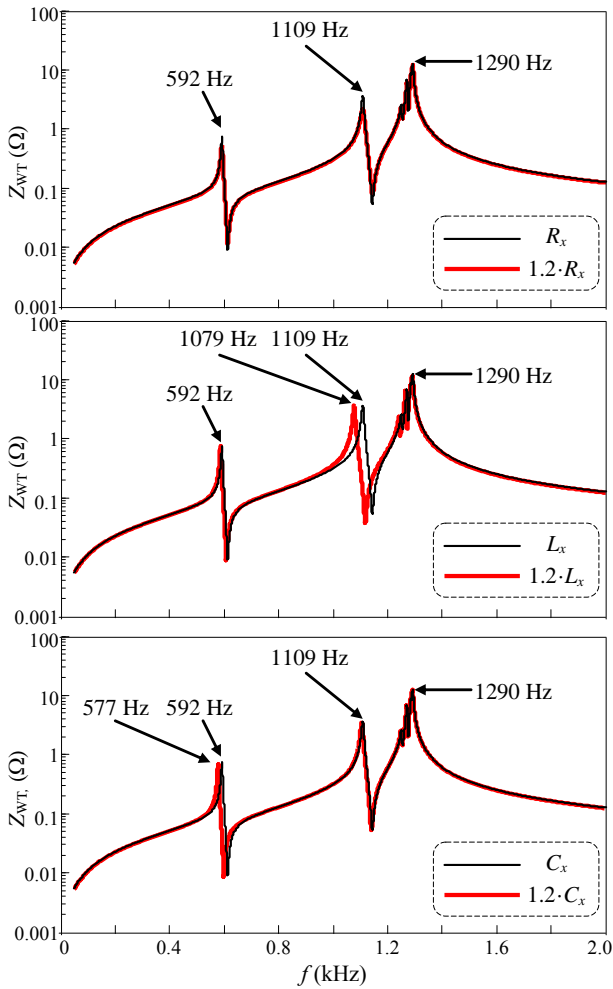


Fig. 12. Influence of MV underground cable electrical parameters on 8x5 onshore WPP resonance (data in Table 1, with $SCR = 12.5$ pu, $D_{MV} = 1$ km and $Q_{Cb} = 0$ Mvar)

of the parallel resonances is only slightly affected by cable length, it decreases with long MV submarine cables. Thus, WPPs with WTs far away from each other can produce resonances close to WT harmonic emissions.

V. INFLUENCE OF WPP ELECTRICAL PARAMETERS

In order to study the influence of WPP electrical parameters on parallel resonance, the frequency scan of the equivalent harmonic impedance $Z_{Eq,k}$ at WT_{Nr1} with the parameter values in Table 1 and with the parameter values increased by 20% is compared for onshore and offshore WPPs.

5.1. ONSHORE WIND POWER PLANTS

The influence of the following electrical parameters is analyzed:

- Electrical parameters of the MV underground cable (Fig. 12). It must be noted that
 - The cable resistance does not affect resonance frequencies. It only damps the frequency response of the WPP.

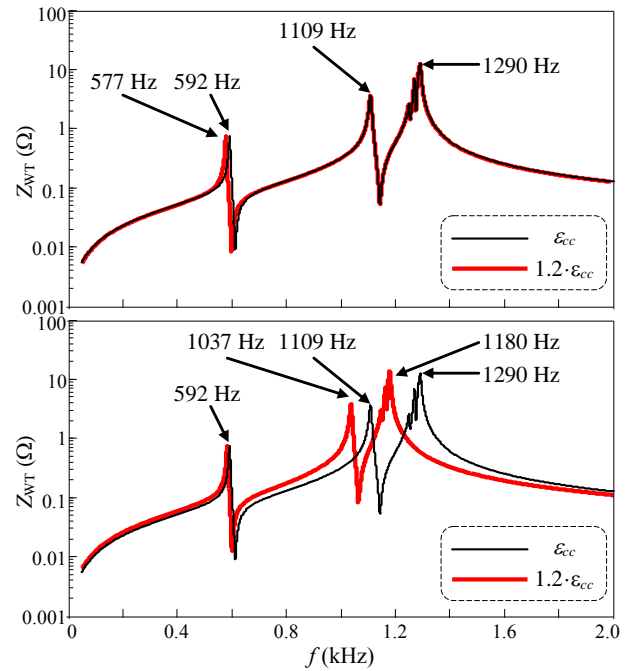


Fig. 13. Influence of HV/MV (top) and MV/LV (bottom) transformer electrical parameters on 8x5 onshore WPP resonance (data in Table 1, with $SCR = 12.5$ pu, $D_{MV} = 1$ km and $Q_{Cb} = 0$ Mvar)

- The cable inductance slightly affects the second parallel resonance, f_{2on} , because this inductance is negligible compared to the equivalent inductance of transformers. Higher inductances result in lower parallel resonance frequencies.
- The cable capacitor slightly affects the first parallel resonance, f_{1on} . Higher capacitor values result in lower parallel resonance frequencies.

These results agree with the influence of MV underground cable length on parallel resonance (see Fig. 6).

- Transformer electrical parameters (Fig. 13). It must be noted that
 - The short-circuit impedance of the HV/MV transformer slightly affects the first parallel resonance, f_{1on} .

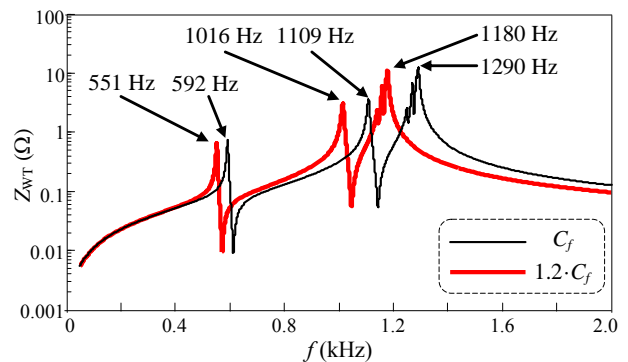


Fig. 14. Influence of WT capacitor filter on 8x5 onshore WPP resonance (data in Table 1, with $SCR = 12.5$ pu, $D_{MV} = 1$ km and $Q_{Cb} = 0$ Mvar)

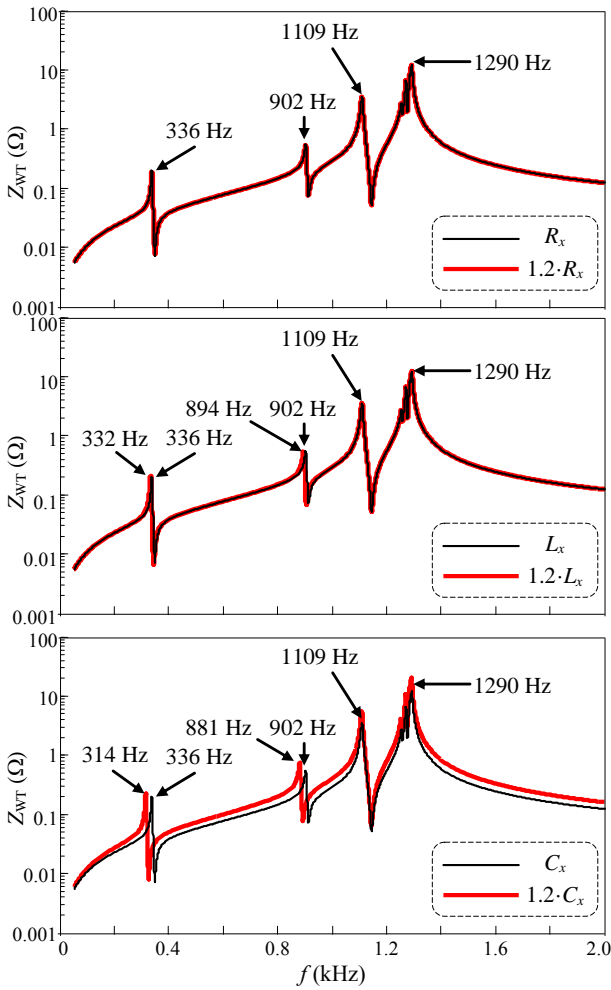


Fig. 15. Influence of HV submarine cable electrical parameters on 8x5 offshore WPP resonance (data in Table 1, with $SCR = 12.5$ pu, $D_{HV} = 25$ km and $D_{MV} = 1$ km)

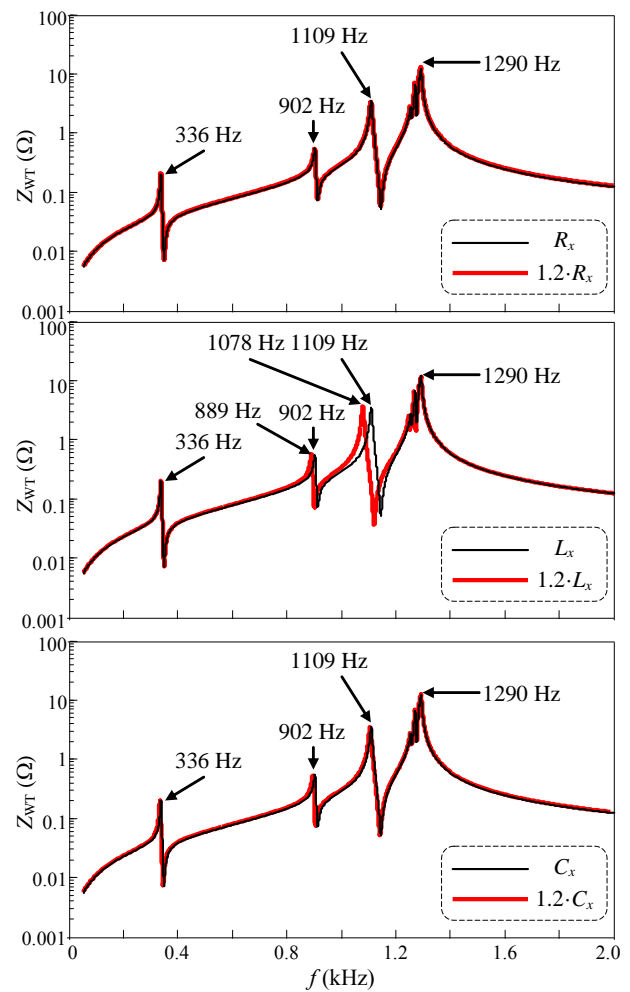


Fig. 16. Influence of MV submarine cable electrical parameters on 8x5 offshore WPP resonance (data in Table 1, with $SCR = 12.5$ pu, $D_{HV} = 25$ km and $D_{MV} = 1$ km)

- The short-circuit impedance of the MV/LV transformer significantly affects the second parallel resonance, f_{2on} .

- WT filter capacitor (Fig. 14). The presence of this capacitor must be considered in onshore WPP resonance studies because it significantly affects all the parallel resonances.

5.2. OFFSHORE WIND POWER PLANTS

The influence of the following electrical parameters is analyzed:

- Electrical parameters of the HV submarine cable (Fig. 15). It must be noted that
 - The cable resistance and inductance do not affect resonance frequencies. The resistance only damps the frequency response of the WPP. They could be neglected compared to the equivalent impedance of transformers for low frequency parallel resonance studies.

- The cable capacitor affects the first and second parallel resonance f_{1off} and f_{2off} . Higher capacitor values lead to lower parallel resonance frequencies.

These results agree with the influence of HV submarine cable length on parallel resonance (see Fig. 10).

- Electrical parameters of the MV submarine cable (Fig. 16).
 - The cable resistance does not affect resonance frequencies. It only damps the frequency response of the WPP.
 - The cable inductance slightly affects the second parallel resonance, f_{2off} , and it significantly affects the third parallel resonance, f_{3off} . Higher inductances lead to lower parallel resonance frequencies.
 - The cable capacitor does not affect parallel resonance.

These results agree with the influence of MV submarine cable length on parallel resonance (see Fig. 11). Thus, electrical parameters of MV submarine cables of offshore WPPs could be neglected because their equivalent impedance

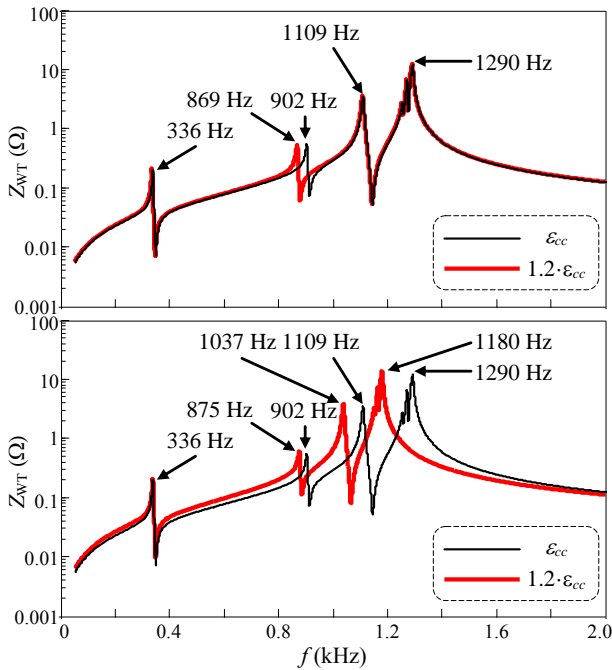


Fig. 17. Influence of HV/MV (top) and MV/LV (bottom) transformer electrical parameters on 8x5 offshore WPP resonance (data in Table 1, with SCR = 12.5 pu, $D_{HV} = 25$ km and $D_{MV} = 1$ km)

is small and only affects the high frequency parallel resonances.

- Transformer electrical parameters (Fig. 17). It must be noted that
 - The short-circuit impedance of the HV/MV transformer slightly affects the second parallel resonance, f_{2off} .
 - The short-circuit impedance of the MV/LV transformer significantly affects the second and third parallel resonance, f_{2off} and f_{3off} .
- WT filter capacitor (Fig. 18). The presence of this capacitor must be considered in offshore WPP resonance studies because it significantly affects all parallel resonances (in particular, the second and third parallel resonances, f_{2off} and f_{3off}).

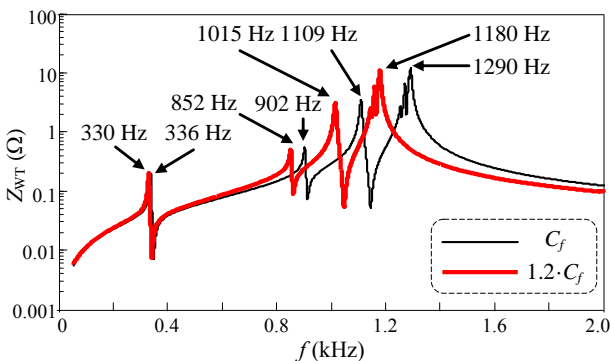


Fig. 18. Influence of WT capacitor filter on 8x5 offshore WPP resonance (data in Table 1, with SCR = 12.5 pu, $D_{HV} = 25$ km and $D_{MV} = 1$ km)

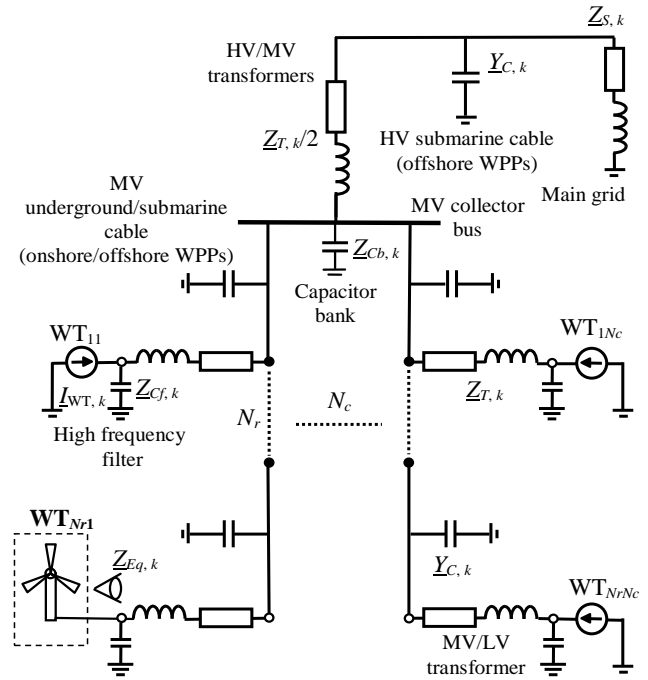


Fig. 19. Wind power plant approximated equivalent circuit

VI. WIND POWER PLANT APPROXIMATED EQUIVALENT CIRCUIT

From the above studies, it can be concluded that the transversal impedances of the WPP cables could be removed from the WPP equivalent circuit in Fig. 2 to easily determine the low order parallel resonances. Thus, the approximated circuit of Fig. 19 is proposed to characterize the low order frequencies of WPP resonances. Moreover, considering the small influence of MV submarine cable capacitors on offshore WPP parallel resonance (see Subsection 5.2), these capacitors could also be neglected in offshore WPP resonance studies. These circuits (circuit in Fig. 19 with and without MV underground/submarine cable capacitors, called approximations #1 and #2, respectively) can be used to study the parallel resonance problem analytically, and thus obtain expressions of the resonance frequencies. The studies in Sections III and IV are performed considering the above approximations (results plotted with red lines from Fig. 4(b) to Fig. 11(b)). The accuracy of the proposed approximations can be checked in these plots. It can be noted that,

- The approximations are valid for small values of the main grid short circuit ratio, which lead to high values of the main grid inductances (see Fig. 4(b) and Fig. 8(b)).
- The approximations are valid to study only the first parallel resonance in onshore and offshore WPPs, f_{1on} and f_{1off} , whereas they do not offer good accuracy for the other parallel resonances (see Fig. 11(b)).
- Approximation #2 is accurate for offshore WPP parallel resonance studies.

VII. CONCLUSION

This paper studied parallel resonance in onshore and offshore WPPs from frequency scan. Extensive Matlab/Simulink simulations were performed to determine the equivalent impedance at WT terminals. The frequency of the parallel resonance was numerically identified from this impedance. The paper compared low order frequencies of parallel resonances in onshore and offshore WPPs and investigated the impact of WPP parameters on resonance. The following conclusions were drawn:

- WT filter capacitors and cables are the factors most and least affecting WPP parallel resonance, respectively.
- Offshore WPPs have parallel resonances at lower order frequencies than onshore WPPs because of the transversal capacitors of the HV submarine cable which connects the WPPs with shore. Moreover, this cable produces a parallel resonance around 1 kHz which does not appear in onshore WPPs.
- Weaker grids lead to parallel resonances closer to low frequencies. This is because grids with low short circuit ratios can produce onshore and offshore WPP resonances close to WT harmonic emissions due to large main grid inductance values.
- Large WPPs have parallel resonance at lower frequencies than small WPPs because of the influence of the number of WTs and strings on resonance.
- Onshore and offshore WPPs with WTs far away from each other have parallel resonances at low order frequencies because of the transversal capacitors of the MV underground cables.
- Reactive power compensation at the onshore WPP collector bus can produce parallel resonances close to WT harmonic emissions.
- Offshore WPPs far from shore have parallel resonances close to low order harmonics.

Based on these conclusions, the paper also proposed approximated equivalent circuits to study low order parallel resonance in onshore and offshore WPPs.

ACKNOWLEDGMENTS

L. Sainz's work was carried out with the financial support of the "Ministerio de Economía y Competitividad" (grant ENE2013-46205-C5-3-R), which the authors gratefully acknowledge.

M. Cheah-Mane's work received funding from the People Programme (Marie Curie Actions) of the European Union Seventh Framework Programme FP7/2007-2013/ under REA grant agreement no. 317221, project title MEDOW.

REFERENCES

- [1] L. H. Kocewiak, *Harmonics in large offshore wind farms*, Thesis for the PhD Degree in Electrical Engineering, Dep. of Energy Technology, Aalborg University, Denmark.
- [2] S. A. Papathanassiou and M. P. Papadopoulos, "Harmonic analysis in a power system with wind generation," *IEEE Trans. Power Delivery*, **21**, (4), pp. 2006-2016, 2006.
- [3] S. T. Tentzerakis and S. A. Papathanassiou, "An investigation of the harmonic emissions of wind turbines," *IEEE Trans. Energy Conversion*, **22**, (1), pp. 150-158, 2007.
- [4] IEEE PES Wind Plant Collector System Design Working Group, "Harmonics and resonance issues in wind power plants," *Proc. of the IEEE Power and Energy Society General Meeting*, July 2011, pp. 1-8.
- [5] K. Yang, *On Harmonic Emissions, Propagation and Aggregation a Wind power Plants*, Thesis for the PhD Degree, Dep. of Engineering Sciences and Mathematics, Lulea University of Technology, Sweden.
- [6] U. Axelsson, U. Holm, M. Bollen and K. Yang, "Propagation of harmonic emission from the turbines through the collection grid to the public grid," *Proc. 22nd Int. Conf. and Exhibition on Electricity Distribution (CIRED 2013)*, 2013, pp. 1-4.
- [7] R. Zheng, M. Bollen and J. Zhong, "Harmonic resonances due to a grid-connected wind farm," *Proc. 14th Int. Conf. on Harmonics and Quality of Power (ICHQP 2010)*, Sept. 2010, pp. 1-7.
- [8] J. Li, N. Samaan and S. Williams, "Modeling of large wind farm systems for dynamic and harmonics analysis," *Proc. IEEE/PES Transmission and Distribution Conference and Exposition*, April 2008.
- [9] F. Ghassemi and K-L Koo, "Equivalent network for wind farm harmonic assessments," *IEEE Trans. on Power Delivery*, **25**, 3, pp. 1808-1815, 2010.
- [10] S. Zhang, S. Jiang, X. Lu, B. Ge and F. Zheng, "Resonance issues and damping techniques for grid-connected inverters with long transmission cable," *IEEE Trans. on Power Electronics*, **29**, 1, pp. 110-120, 2014.
- [11] L. Harnefors, A. G. Yepes, A. Vidal and J. Doval-Gandoy, "Passivity-based controller design of grid-connected VSCs for prevention of electrical resonance instability," *IEEE Trans. on Industrial Electronics*, **62**, 2, pp. 702-710, 2015.
- [12] X. Chen and J. Sun, "A study of renewable energy systems harmonic resonance based on a DG test-bed," *Proc. 26th IEEE Applied Power Electronics Conference and Exposition (APEC 2011)*, March 2011, pp. 995-1002.
- [13] S. Schostan, K.-D. Dettmann, D. Schultz and J. Plotkin, "Investigation of an atypical sixth harmonic current level of a 5 MW wind turbine configuration," *Proceedings of the Int. Conf. on Computer as a tool (EUROCON)*, September 1998.
- [14] LL. Monjo, L. Sainz, J. Liang and J. Pedra, "Study of resonance in wind parks," *Electric Power Systems Research*, **128**, pp. 30-38, 2015.

- [15] EN Standards, *Voltage characteristics of electricity supplied by public electricity networks*, EN 50160 Ed. 3, 2003.
- [16] *IEEE Standard for interconnecting distributed resources with electric power systems*, IEEE Standard 15471, 2005.



The need for lithium – an upcoming problem for electrochemical energy storages?

锂之需要 – 电化学能量储存即将带来的问题?

Daniel Schultz¹, Wilhelm Kuckshinrichs^{1*}

¹*Institute for Energy and Climate Research – Systems Analysis and Technology Evaluation, Forschungszentrum Jülich, 52425 Jülich, Germany*

w.kuckshinrichs@fz-juelich.de

Accepted for publication on 29th November 2015

Abstract - In the context of the transition of energy systems, storage technologies currently attract high attention. As one of the most promising technologies, lithium-ion battery systems could be used not only for zero-emission mobility but also for several purposes surrounding the integration of renewable energy sources into the grid. But if these applications experience a large-scale penetration, manifold natural resources will be required for construction. This work has the aim to identify future demand paths for the essential resource lithium and to clarify whether temporary or even permanent critical situations on the lithium world market are to expect. For this, a simulation model was built, mapping the future market penetration of relevant applications of lithium batteries. By combining with particular material requirements, partly exclusive real data, and adding other demand, the annual total lithium demand can be modelled. Results show that especially when the electric mobility kicks in, an enormous rise in demand for lithium has to be expected, accompanied by considerably additional demand generated by stationary energy storage purposes.

With the pending demand rise in mind, the supply side was analyzed. Due to ongoing technical progress, broadening the quantity of recoverable resources, a situation of permanent scarcity turns out to be unlikely. This will be even truer if lithium recycling becomes profitable and common.

Adopting the flow perspective, a different situation emerges: Presently, Chilean and Australian extraction dominates, but expansion prospects are limited. The installation of extraction capacities at a huge, nearly untouched Bolivian deposit requires much capital and know-how from outside, but the current nationalistic economic policy has the potential to discourage foreign investments. As a result, a temporary physical scarcity on the lithium market is supposable, causing a deficit in supply and an increase in market prices. Furthermore, a Bolivian market entry raises the market power of South American exporters, possibly leading to some kind of collaboration and again causing a risk for the broad penetration of battery technologies.

Keywords - Energy storage, Battery storages, Resource criticality, Lithium, Electric Vehicles.

I. INTRODUCTION

The structural change of energy systems with the main goal of replacing climate-damaging coal, oil and other non-renewable energy sources by renewable energy capacities like wind energy plants or solar collectors represents a complex economic and technical challenge. In the power sector, increasing fluctuating and noncontrollable generation can result in more unstable power supply with higher risks of blackout situations and therefore induced discussions about the necessity of conventional power plants as 'backup capacities' [1] and about an extension of the grid [2]. In the mobility sector, oil fueled transport dominates, while clean alternative traction technologies using hydrogen or electricity still face several technical or economic challenges [3].

Several electrochemical energy storage applications are already in use to overcome handicaps of clean energy. Worldwide a small number of stationary energy storages are operating, providing network stabilization services as well as taking advantage of temporal price differences by storing energy for arbitrage, which helps to balance differing generation and load patterns. Furthermore, batteries are an important power source option for any electric mobility which is independent from an expensive permanent power supply on track. If worldwide mobility is converted to electric traction, a tremendous increase of demand for batteries can arise.

Due to favorable electrochemical characteristics, already reached marketability for several purposes and ongoing research, it is strongly expected that for the energy transition lithium ion batteries will play a major role [4]. For their con-

struction, numerous natural resources will be required, beginning with the essential alkali metal lithium. As lithium is finite, like any natural resource, the question arises whether the lithium supply will be able to meet the demand generated by power, mobility and other markets. A supply bottleneck can be of permanent or temporary nature, depending on the constitution of the market and reserve base. This paper’s aim is to identify possible shortfall situations by connecting future demand scenarios with feasible resource and market conditions.

In Section II, the diffusion of the potential high scale applications stationary energy storages and electric mobility is modelled. In Section III, the resulting demand for lithium is calculated, which provides the basis for a critical examination of the supply side in Section IV. Section V concludes.

II. APPLICATIONS AND DIFFUSION MODELLING

2.1. STATIONARY ENERGY STORAGES

The benefits from stationary energy storages are manifold: If power supply exceeds load, for example due to massive renewable energy generation, batteries can absorb power and avoid uneconomical forced shutting downs. And if load exceeds generation, batteries can offer their stored power and therefore substitute backup generation capacity. Furthermore, placing storages at critical spots of the electricity network could help to cope with bottleneck situations in the short run and also avoid network extension in the long run.

In 2014, around 500 Megawatt (MW) installed capacity was in operation [5]. The individual size of storage systems differs from <1 MW to >30 MW – this modularity is one advantage over dominating pumped hydro storages with a total of around 140 Gigawatt (GW) installed capacity. The future diffusion of battery storages will be influenced by several factors, including the future extension of renewable energy generation, alternative energy storage technologies including power-to-heat and power-to-gas as well as by the legislative and economic framework on the market.

To obtain possible paths of diffusion, two scenarios have been modelled. Scenario ‘Market Niche’ assumes an increase of installed capacity to 300 GW in 2050, whereas scenario ‘Boost’ assumes an upsurge to 1,000 GW. Based on the diffusion research of Rogers [6], an S-curve model was adopted, mathematically expressed by the hyperbolic tangent concept. Fig. 1 shows the capacity numbers each year.

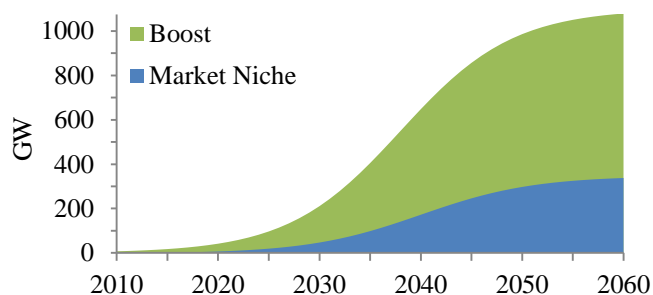


Fig. 1, Installed capacity of stationary energy storages.

By comparing every year with the previous one, the current net construction can easily be calculated. Adding end-of-life replacements, total production is obtained. To include randomness, it is assumed that the life-time of the batteries is normally distributed with a mean of 20 years in scenario ‘Market Niche’ and 14 years in scenario ‘Boost’ and a standard deviation of 2.5 for both scenarios. The resulting total production p.a. can be obtained from Fig. 2 by adding up net construction and replacements for the respective scenario.

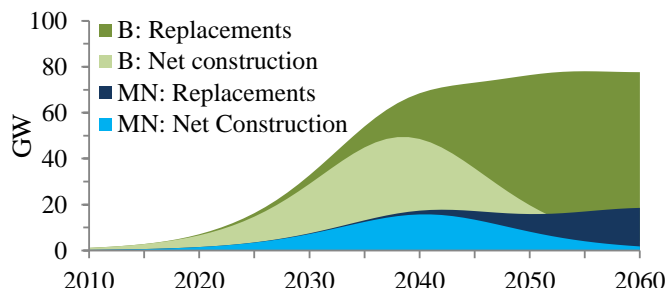


Fig. 2, Net construction and end-of-life replacements of stationary energy storages.

2.2. TRACTION BATTERIES OF ELECTRIC VEHICLES

Despite market potential for other types of vehicles like busses, trucks, trains and ships, the following analysis is focused on electric cars. Today, manifold models are offered, which can be categorized as in Table 1.

TABLE 1, DEFINITIONS OF ELECTRIC CAR TYPES

	Technology	Examples
ICE	Conventional combustion engine	VW Golf, Honda Civic, Ford Focus, etc.
HEV	Combustion and electric engine	Toyota Prius, Honda Insight
PHEV	As HEV, but with plug-in to recharge	Chevrolet Volt, BMW i8
BEV	Electric engine only, recharged by plug-in	Tesla Model S, Nissan Leaf

While cars of the category ‘Internal Combustion Engine’ (ICE) and ‘Hybrid Electric Vehicles’ (HEV) carry comparatively small batteries, provides the option to connect ‘Plug-in Hybrid Electric Vehicles’ (PHEV) and ‘(Full) Battery Electric Vehicles’ (BEV) to the electricity network for battery sizes up to 85 kilowatt hours (kWh, Tesla Model S 85). In the following, the groups of PHEV and BEV are combined and denoted by the term ‘Electric Vehicle’ (EV).

Despite ambitious aims of several governments, worldwide only 665,000 cars out of more than 800 million in total were classified as EV at the end of 2014 [7]. But according to sale statistics, almost half of them were sold only in 2014, more than doubling 2012 sales. Strong distinctions between countries can be obtained: While in Norway more than 11% of all in 2014 sold cars were BEV, China and most other European countries exhibited a share of less than 1% for EV altogether. Only the Netherlands, Sweden and the U.S. (in particular California) reached EV sale quotas of 1% or more. As most

important reasons for these differences, consumer financial incentives, offered by governments, and an available charging infrastructure were found statistically significant [8].

Learning effects and high research effort during the last years led to remarkable technical progress especially in the field of traction batteries, where the energy density (energy per space unit) has been increased and the battery cost (price per energy unit) has been reduced substantially. If this track can be retained and furthermore supported by a proper political framework, chances for a continued increase of market share are pretty good.

Again, for diffusion modeling two scenarios were generated. Starting with 800 million cars today, scenario ‘Moderate’ assumes an increase to 1.5 billion in 2050, based on an improved standard of living in fast-growing regions like China, India, Brazil, Mexico and Indonesia. This is substantially lower than the outlooks from IEA [9] and ExxonMobil [10], assuming 1.9 billion and 1.7 billion cars already in 2040 respectively. For end-of-life replacements a normal distribution with a mean of 15 years and a standard deviation of 2 is assumed. To calculate the number of EV, the chance of every car sold being an EV grows from a little more than 0% today to 40% in 2050. Fig. 3 shows the total stock of cars, divided in electric and non-electric. The annual sales volume of EV grows from 1.25 million in 2020 to 42 million in 2050.

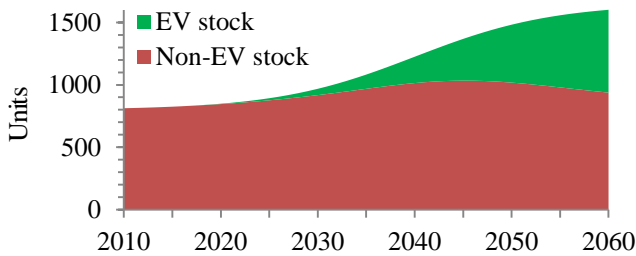


Fig. 3, Total stock of cars in scenario ‘Moderate’.

In scenario ‘Boost’, a total car stock of 2 billion in 2050 is assumed. Furthermore, the mean of the vehicle life-time is lowered to 10 years (standard deviation stays at 2) and in 2050 three of four sold cars are electric (EV share grows to 75%). As can be observed in Fig. 4, this leads to a replacement effect, beginning in the 2030s. The annual EV production experience a boost, starting around 2025 with 10 million and reaching 150 million in 2050 – this is twice the quantity of today’s total car production.

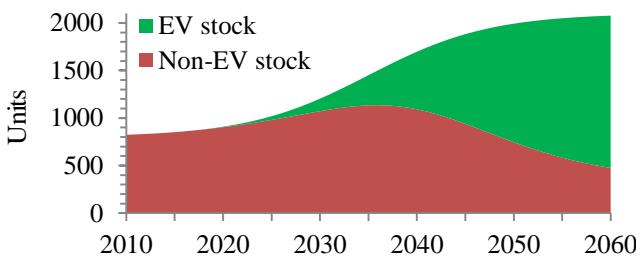


Fig. 4, Total stock of cars in scenario ‘Boost’.

As a change of traction battery within a car’s life-time seems to stay uneconomical, the number of produced traction batteries is equal to sold EV. However, in the average size of traction batteries, the scenarios differ. In scenario ‘Moderate’ it is assumed that PHEV of compact class size dominate, so the battery capacity of every sold EV is projected to be 20 kWh. In scenario ‘Boost’ an average capacity of 30 kWh arises from a higher share of BEV on the one side and large scale penetration of all kinds of cars, including premium models, on the other side. Fig. 5 shows the total demand for battery capacity.

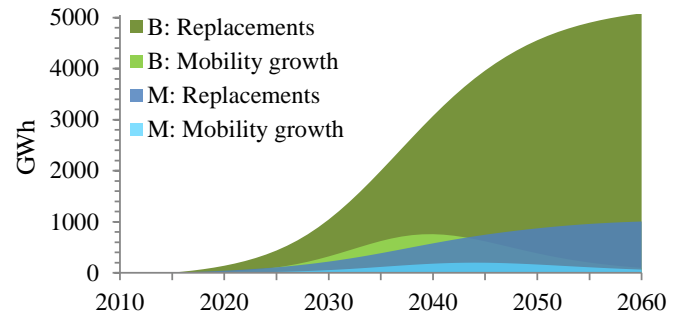


Fig. 5, Annually demanded capacity for EV traction batteries based on scenarios ‘Boost’ and ‘Moderate’.

As can be observed clearly in both scenarios, most electric cars will originate from replacement sells: In times of major mobility growth, around 2030 to 2040, the EV sale quota is still low. When it gets higher, two effects appear: First, usual replacement sales become more and more electric. Second, many cars bought in the major mobility growth period reach their end-of-life and have to be replaced the first time. In sum, especially in the ‘Boost’ scenario, a heavy growth of annually demanded battery capacity, surpassing 4,500 GWh in 2050, results.

III. DEMAND FOR LITHIUM

Today, demand for lithium is mainly generated by industrial applications like ceramics and glass production, its use as lubricants, as well as by manufacturers of batteries for electronic devices like laptops or cellphones. In total, this made up for 33,000 tons in 2014 [11] with a positive trend. In this paper, an increase of 2% p.a. is assumed.

To convert possible future capacity of stationary energy storages and traction batteries into lithium demand figures, it is assumed that only lithium batteries will be produced. This can already be observed as a trend in EV production today, as many PHEV and all important BEV use a lithium ion battery system. For stationary energy storages, data from the 5MW/5MWh WEMAG/Younicos battery farm Schwerin (Germany) is available [12], while for EV a literature review was conducted [13,14]. For the purpose of this paper, it is assumed that 220 kg lithium per MW of stationary energy storage and 150 g per kWh capacity of an EV traction battery is required, which can be converted into 3 kg per EV in scenario ‘Moderate’ and into 4.5 kg per EV in scenario ‘Boost’. To include technical progress in battery production, the re-

quired amount of lithium per battery unit of both applications is lowered by 1% annually.

In a first step, basic lithium demand and both stationary energy storage scenarios were calculated (Fig. 6). While basic demand doubles between 2014 and 2050, the scenarios reach their top level demand around 2040 with 3,000 tons p.a. ('Market Niche') and 12,000 tons p.a. ('Boost'), representing a maximum market share of 6% and 18% respectively.

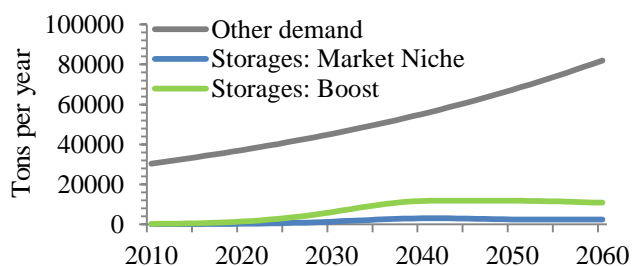


Fig. 6, Basic lithium demand and demand from stationary energy storage construction.

Then, the EV scenarios were calculated (Fig. 7). In scenario 'Moderate', lithium demand begins to increase notably in the 2030s, reaching 70,000 tons p.a. around 2040 and stabilizing at almost 100,000 ton p.a. in the 2050s. Already beginning in the 2030s, the lithium market would be parted into two parts about equally sized: One for EV and one for other applications, including batteries for non-traction use.

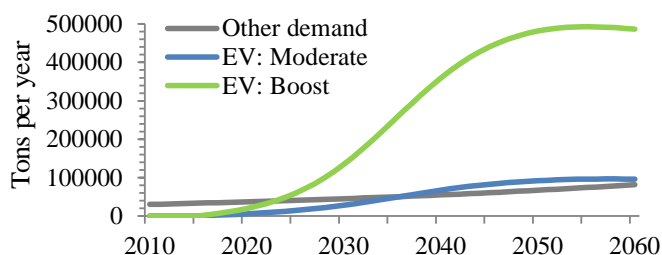


Fig. 7, Basic lithium demand and demand from EV manufacturing.

When considering scenario 'Boost', the numbers increase sharply. Surpassing other demand already in 2023, EV demand reaches a level of 130,000 tons p.a. in 2030 and 480,000 tons p.a. in 2050. The demand side would clearly be dominated by EV traction battery manufacturers, making all other demand minor and expanding the market for lithium sixteen-fold between 2014 and 2050.

IV. POTENTIAL SUPPLY BOTTLENECKS

4.1. THE FEEDSTOCK OF LITHIUM

To analyze whether the supply side is able to cope with potentially soaring demand, the feedstock has to be examined. Today, two Chilean subsurface brine sites and an Australian mine account for the main supply [11], assisted by minor production sites in countries like China, Argentina, Zimbabwe and the US. Some 13.5 million tons are classified as reserves, of which 7.5 million tons are located in Chile, 3.5 million tons in China and 1.5 million tons in Australia. The world resources

are estimated at 40 million tons, including 9 million so far untouched tons in Bolivia.

Comparing these estimates with Section III's lithium demand scenarios with the perspective 2050, no apparent shortage situation emerges. Cumulated basic demand requires 1.75 million tons until 2050, stationary energy storages 62,000 tons ('Market Niche') and 260,000 tons ('Boost') respectively. If EV scenario 'Moderate', which accounts for 1.5 million tons, is added to basic demand and stationary storage scenario 'Boost', a total consumption of 3.5 million tons until 2050 appears – leaving 10 million tons in situ.

If EV scenario 'Boost' is considered instead, accounting for a cumulated demand of 7.7 million tons until 2050, the bulk of reserves will have to be used. Combined with cumulated basic demand and the stationary storage scenario 'Boost', a total demand of 9.7 million tons emerges. Facing reserves of 13.5 million tons, it still leaves almost 30% in situ. However, almost 60% of the reserves are required for EV battery manufacturing, as shown by Fig. 8.

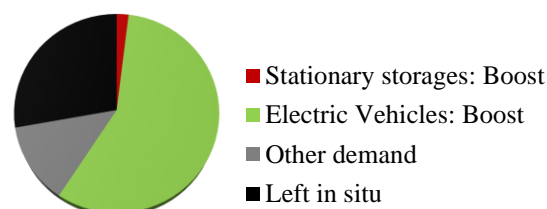


Fig. 8, Usage of reserves until 2050 with both 'Boost' scenarios.

Not only the demand side is uncertain, but also the stock of as reserves classified resources: Known and profitably mineable resources tend to rise with time and interest, as can be frequently observed at the market for oil, because new deposits are found and technical progress makes mining cheaper or even possible. Bearing that in mind, it might be likely that the available reserves of lithium will increase within the next decades, so that the share of reserves left in situ exceeds 30% and the danger of scarcity becomes less present.

Furthermore, particularly if EV traction batteries are widely distributed, a secondary market for recycled lithium could be established. Technically, a recycling rate of approximately 98% is possible already today [15], but due to low quantity and high cost no commercial lithium recycling system exists. But with increasing available quantities, an accepted collection system and a product design that pays attention to subsequent recycling, an effective re-use of wasted battery's lithium could be established. For installation, the well-functioning recycling system for acid car batteries, which covers in Europe nearly 100%, could serve as a guideline. Nevertheless, any recycling operation is time-lagged by nature: The initial amount has always to come from the primary feedstock. For this reason, it is appropriate to analyze the supply side with special focus on the flow perspective.

4.2. RISKS ON THE SUPPLY SIDE

Today, more than one third of lithium is supplied by Australia and Chile, respectively (approximately 13,000 tons p.a. each) [11]. But while Chile exhibits large assets of reserves,

could be the prospects of expanding Australian supply narrowed. Particularly if EV experiences a boom within a short time period, raising lithium demand from 33,000 tons today to 180,000 tons in 2030 and further to 560,000 tons in 2050, other sources will have to be made accessible and developed quickly and simultaneously. But as can be well observed at the extraction of unconventional oil, large amounts of capital and know-how are required for large-scale projects. Adopting this to the extraction of lithium, several possible risks appear: The number of professionals could be insufficient, causing a 'bottleneck of know-how' and resulting in a slow speed of construction and increased costs for completion.

Moreover, large amounts of capital have to be allocated for long-term investments. To invest, actors need favorable surrounding conditions at political and economic levels. In the case of the brine lakes of Bolivia, disposing with approximated 9 million tons the world's largest sources, the political framework could become an issue. Recent acts of nationalization in the telecommunication and even energy sector and depreciative statements of the Bolivian government directed against foreign investors are likely to discourage engagement from outside. A possible result can be observed in allied Venezuela, where projects for the development of heavy oil resources achieve only little or no progress at all, because of missing know-how and capital. If this happens in times with strongly increasing demand for lithium, the risk for a supply shortage at the world market will be raised.

Another possible risk on the supply side is based on its geographic distribution [16]. Today, nearly 60% of the resource base is suspected to be located in South American countries, and due to high Chilean reserves even two-thirds of the reserves are South American. As most battery and car manufacturers are located in Europe, Northern America and Asia, it seems reasonable to expect a high export share for South American lithium. If one takes the oil market as a comparison again, one can observe that big net exporters allied and tried to join forces with the aim of gaining control of the market; they formed the cartel OPEC, which is responsible for several world oil crises with periods of lowered supply and high market prices. If South American net exporting countries unite with the aim of gaining market control and raising their profit, and establish a collaboration as well, another risk of reduced supply on the world market will appear.

In any case, if supply expansion cannot follow an increase in lithium demand, this can affect applications like stationary energy storages and electric mobility for two reasons. First, manufacturers have to cope with a restricted amount of lithium available, potentially leading to problems within the supply chain and resulting in production downtimes in the worst case. Second, the usual market result in situations of supply shortage is a growing price level. At battery manufacturer's level, this is represented by increasing costs for input factors. Especially for products that are being launched onto the market, this could become a considerable handicap, with price sensitive customers bailing out as soon as increasing input costs are forwarded. Today, the price development of lithium is quite stable [11], but this has not to last forever.

V. CONCLUSION

A simulation model was developed and possible paths of market penetration for two possibly large-scale applications of lithium ion batteries were generated. Due to the early market launch stage of both applications, the scenarios differed to a large extent. In all scenarios, a major phase of growing penetration was introduced, followed by a phase of leveling. In the case of stationary energy storages the yearly gross construction rate rises accordingly, with end-of-life replacements replacing net constructions. However, in the case of electric mobility two effects interfere with each other and cause a strong and massive increase of the production of electric cars. First, it is expected that the number of cars worldwide will grow substantially, resulting in EV net constructions. Second, the share of produced cars being electric increases over time. This causes the effect of partly replacing the oil fueled car fleet by electric vehicles, which is due to the high number of cars a large market as well.

Then, the resulting demand for lithium was calculated and confronted with today's lithium demand. It turned out that the lithium need for stationary energy storages could gain a sound market share at the world lithium market. Furthermore, and not surprising, the demand for EV traction batteries has the potential to revolutionize the lithium market, with being even the lithium requirements of scenario 'Moderate' more than all other demand summed up. If EV experiences a boom, the market will change completely and quadruple the first time until 2030 and another time until 2050.

Analyzing data of known lithium sources, this does not seem as a major risk in terms of exhausting world reserves, especially if a market for lithium recycling is introduced. But with possible strongly rising demand in mind, the authors see serious potential for risks on the supply side, which may result in temporary shortage situations and rising price levels at the lithium world market. First, input factor markets for the construction of depletion facilities could face a shortage, for example due to a lack of professionals. Second, an unfavorable investment framework particularly in Bolivia could delay a sufficient buildup of facilities as well. Third, a collaboration of net exports located in South America could try to take advantage of a high market share and ration supply to maximize profits and/or enforce political objectives.

To counteract those potential future risks, the market for lithium on the one side and applications for lithium technologies on the other side should be carefully observed. Furthermore, to keep the recycling option, starting today attention should be paid to product designs making subsequent disassembling and recycling as easy as feasible. To counter shortages in facility construction as well as the time lag between primary and secondary market, preparatory steps for future development of today unused deposits could be carried out already today. In addition, actors could work towards a more cooperative atmosphere to avoid Bolivian solo attempts in developing possibly crucial deposits.

REFERENCES

- [1] H. Weigt. “Germany’s wind energy: The potential for fossil capacity replacement and cost saving”, *Applied Energy*, **86(10)**, pp. 1857-1863, 2009.
- [2] M. Fürsch, S. Hagspiel, C. Jagemann, S. Nagl, D. Lindenberg, and E. Tröster. “The role of grid extensions in a cost-efficient transformation of the European electricity system until 2050”, *Applied Energy*, **104**, pp. 642-652, 2013.
- [3] O. Egbue; S. Long. “Barriers to widespread adoption of electric vehicles: An analysis of consumer attitudes and perceptions”, *Energy Policy*, **48**, pp. 717-729, 2012.
- [4] B. Scrosati; J. Garche. “Lithium batteries: Status, prospects and future”, *Journal of Power Sources*, **195(9)**, pp. 2419-2430, 2010.
- [5] U.S. Department of Energy. “DOE Global Energy Storage Database”, www.energystorageexchange.org, 2015.
- [6] E. Rogers. *Diffusion of Innovations*. Glencoe, Ill., USA: Free Press, 1962.
- [7] International Energy Agency. *Global EV Outlook 2015*. Paris, 2015.
- [8] W. Sierzchula, S. Bakker, K. Maat, and B. van Wee. “The influence of financial incentives and other socio-economic factors on electric vehicle adoption”, *Energy Policy*, **68**, pp. 183-194, 2014.
- [9] International Energy Agency. *World Energy Outlook 2014*. Paris, 2014.
- [10] ExxonMobil. *The Outlook for Energy: A View to 2040*. Irving, Texas, USA, 2015.
- [11] USGS. *Mineral commodity summaries 2015*. Reston, Virginia, USA, 2015.
- [12] J.C. Koj, A. Schreiber, P. Stenzel, P. Zapp, J. Fleer, I. Hahndorf. *Life Cycle Assessment of a large-scale battery system for primary control provision*. Jülich, Germany, 2014.
- [13] S. Konietzko, M. Gernuks. *Ressourcenverfügbarkeit von sekundären Rohstoffen – Potenzialanalyse für Lithium und Kobalt*. LithoRec Final Report, Braunschweig, Germany, 2011.
- [14] H. Vikström, S. Davidsson, M. Höök. “Lithium availability and future production outlooks”, *Applied Energy*, **110**, pp. 252-266, 2013.
- [15] J.H. Miedema, H.C. Moll. “Lithium availability in the EU27 for battery-driven vehicles: The impact of recycling and substitution on the confrontation between supply and demand until 2050”, *Resources Policy*, **38**, pp. 204-211, 2013.
- [16] C. Grosjean, P.H. Miranda, M. Perrin, P. Poggi. “Assessment of world lithium resources and consequences of their geographic distribution on the expected development of the electric vehicle industry”, *Renewable and Sustainable Energy Reviews*, **16**, pp. 1735-1744, 2012.



A GIS-based statistical approach to prioritize the retrofit of housing stocks at the urban scale

基于地理信息系统的统计方法用于城市规模住房存量改造的优先等级处理

Alessio Mastrucci^{1*}, Olivier Baume², Francesca Stazi³, Ulrich Leopold⁴

¹International Institute for Applied Systems Analysis, Schlossplatz 1, A-2361 Laxenburg, Austria

²Resource Centre for Environmental Technologies - Public Research Centre Henri Tudor, 6A, avenue des Hauts-Fourneaux, L-4362 Esch-sur-Alzette, Luxembourg

³Dipartimento di Ingegneria Civile, Edile e Architettura - Universita Politecnica delle Marche, Via Brecce Bianche 12, 60131 Ancona, Italy

⁴Luxembourg Institute of Science and Technology, 5 avenue des Hauts-Fourneaux, L-4362 Esch-sur-Alzette

mastrucc@iiasa.ac.at (Alessio Mastrucci); Ulrich.Leopold@list.lu (Ulrich Leopold)

Abstract - Cities are responsible for about 70% of the overall primary energy consumption in Europe and play a major role in addressing carbon mitigation. In this respect, the housing sector has been identified as a key sector for its high energy savings potential achievable by implementing retrofit measures. However, a detailed characterization of the housing energy consumption profile and spatial distribution is needed to properly assess the energy saving potential at the urban scale and further support sustainable urban planning and energy policies.

This study focused on a statistical approach based on Geographical Information Systems (GIS) developed to identify the energy consumption profile of urban housing stocks, the energy savings potential achievable by implementing retrofit measures and their respective spatial distribution across one entire city. The final energy consumption of individual dwellings is predicted by running a multiple linear regression model based on measured energy consumption available at aggregated level (post-code area level) and GIS data about characteristics of buildings and household. Energy savings potential and cost-effectiveness of standard retrofit measures are subsequently calculated and results are finally displayed as maps for decision support in sustainable urban planning. The methodology was applied to the exemplary housing stock of Rotterdam city, consisting of almost 300,000 units.

Relevant results are provided to prioritize retrofit measures implementation according to energy savings potential and cost-effectiveness. Different types of maps can be produced to show energy consumption and energy saving potential patterns across the city. The methodology is generically applicable to other contexts and provides an effective tool for decision support in carbon mitigation policies of housing stocks at the urban scale.

Keywords – Building stock; Energy savings; Costs; Sustainable urban planning.

I. INTRODUCTION

Cities play a major role in addressing carbon mitigation as they are responsible for about 70% of the overall primary energy consumption in Europe [1]. A significant part of the energy consumption and greenhouse gases emission of cities is attributable to the building sector. As a consequence, the European Directive 2012/27/EU[2] required the Member States a long term strategy for mobilizing investment in this sector. In particular, the housing sector has been identified as one of those with the highest energy savings potential achievable through the implementation of retrofit measure. However, a detailed characterization of the housing energy consumption profile and spatial distribution is needed to properly assess the energy savings potential at the urban scale and further support sustainable urban planning and energy policies. Several types of bottom-up housing stock models have been developed to this end [3]. Statistical models use historical data to attribute final energy consumption to single or groups of buildings using a range of statistical techniques. Even though statistical models are limited in predicting the impact of new technologies, they can efficiently be used to estimate the actual energy consumption profile of the building stock including the effect of the real state of renovation and behavior of occupants. A few statistical models have been already developed for the housing sector, however there is a

lack of studies at the urban scale and taking into account the spatial distribution of energy consumption [4].

The objective of this study was to identify the energy savings and CO2 reduction potential of retrofit measures for urban housing stocks in order to prioritize their implementation across one entire city also using cost-effectiveness criteria. A statistical approach based on Geographical Information Systems (GIS) was developed for this scope. The final energy consumption of individual dwellings was predicted by running a multiple linear regression model based on measured energy consumption available at aggregated level (post-code area level) and GIS data about characteristics of buildings and households. Energy savings potential and cost-effectiveness of standard retrofit measures were subsequently computed using benchmark values and results were finally displayed as maps for decision support in sustainable urban planning.

The methodology was developed as part of the European INTERREG IVB NEW project MUSIC [5] to be implemented into the web-based integrated decision support platform iGUESS [6].

II. CASE STUDY

The housing stock of Rotterdam city, counting 297,312 dwellings in 2012, was taken as a case study. Six typologies of dwellings can be identified, distributed into houses (detached, semi-detached, row-houses) and apartments (maisonette, “galerij” flats, “portiek” flats). Houses account for 24% of the total number of dwellings in Rotterdam with a predominance of row-houses (16%) and a minor share of semi-detached (7%) and detached houses (1%). Apartments represent about 76% of the stock divided into maisonettes (22%), galerij flats (19%) and portiek flats (35%). About 51% of the dwellings were built before 1965, 10% in the period 1965-74, 23% in 1975-1991 and 13% in 1991-2005.

The main energy carrier for space heating, domestic hot water and hob cooking is natural gas, while about 17% of dwellings are connected to the urban heating network. Electricity is mainly used for lighting and appliances and partly for domestic hot water.

Data about dwellings and households were extracted from the GIS address database of the Municipality, including information about floor surface, type of dwelling and period of construction, number of occupants. Measured natural gas consumption are available on a yearly basis at the post-code area level. National building libraries and standards [7,8] were used to apportion the total energy consumption into different end-uses and to estimate the energy saving potential and investment costs for standard retrofit packages.

III. METHODOLOGY

A bottom-up statistical approach based on GIS was developed at the city scale to predict the final energy consumption of the housing stock [4]. Multiple linear regression is used to disaggregate measured natural gas

consumption values available at post-code area level to single dwellings depending on building and household features. The equation at the basis of the model for gas is Eq (1):

$$y = \beta_0 + x_{floor} \beta_{floor} + \sum_i x_{type,i} \beta_{type,i} + \varepsilon \tag{1}$$

where the dependent variable y represents measured yearly average gas consumption per dwelling at post-code level, the independent variable x_{floor} the average floor surface of dwellings, $x_{type,i}$ the percentage of dwellings per type and period of construction (26 combinations) in the post-code, β_0 , β_{floor} , $\beta_{type,i}$ the regression coefficients to be estimated commonly by ordinary least squares technique and ε a random error term. The residuals were carefully analyzed and their spatial distribution displayed at post-code level so to identify areas with higher consumption deviation and detect possible spatial patterns. The software QGIS [9] was used for this scope.

The total natural gas consumption was apportioned into different end uses and the energy savings potential and costs of standard retrofit measures were calculated based on national benchmark values and standards [7,8]. Standard retrofit packages include isolation of external walls, roof and ground floor, windows replacement and boiler replacement according to Dutch regulations (Table 1).

An index to evaluate the cost-effectiveness of retrofit measures $C_{en.sav}$ ($\text{€} / kWh a$) was defined according to Eq (2):

$$C_{en.sav} = I_{retr} / E_{sav} \tag{2}$$

where I_{retr} (€) is the investment cost of the standard retrofit measure package and E_{sav} (kWh) is the yearly energy savings potential. Such index is suitable to prioritize the implementation of retrofit measures for residential buildings across the city.

TABLE 1, STANDARD RETROFIT PACKAGES FOR THE BUILDING ENVELOPE IN THE NETHERLANDS (ADAPTED FROM [7]).

Retrofit package	U-value ($kWh/m^2 K$)	Rc-value ($m^2 K/kWh$)
External wall insulation	0.36	2.53
Roof insulation	0.36	2.53
Ground floor insulation	0.36	2.53
Double Glazing LowE - HR ⁺⁺	1.80	-

Energy consumption and energy savings predicted for single dwellings were aggregated across the city at the block level and their distribution was spatially analyzed using GIS. The block level was selected as the *target level* where to show information useful for decision support in urban planning as this level gives sufficient detail in results and at the same time keeps sensitive data protected (e.g. information for single buildings). Maps were generated at the block level for the total primary energy consumption for space heating and domestic hot water in the current state, the total energy savings potential achievable through standard retrofit measures and the average cost of energy savings.

IV. RESULTS AND DISCUSSION

The multiple linear regression model for the natural gas consumption of the Rotterdam housing stock was found to be significant with coefficients of determination $R^2 = 0.734$ [4]. The model results demonstrated a good accuracy in the prediction. Fig. 1 shows the distribution of predicted against measured average gas consumption for the post-code areas used to fit the model. Deviation of natural gas consumption is in the range of $\pm 20\%$ in 82% of the cases.

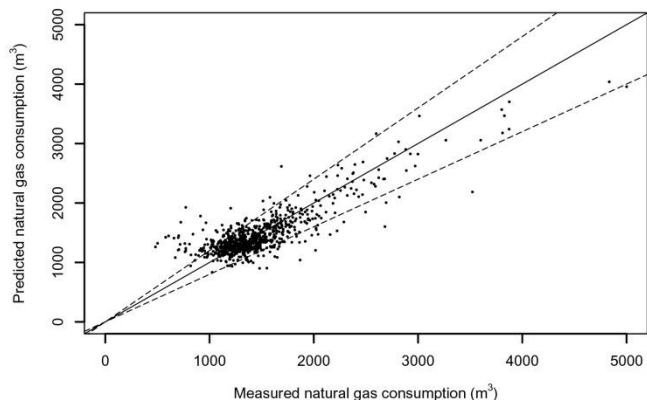


Fig. 1, Average natural gas consumption per dwelling at post-code level: predicted against measured values. The dotted lines contain cases within $\pm 20\%$ error. Adapted from [4].

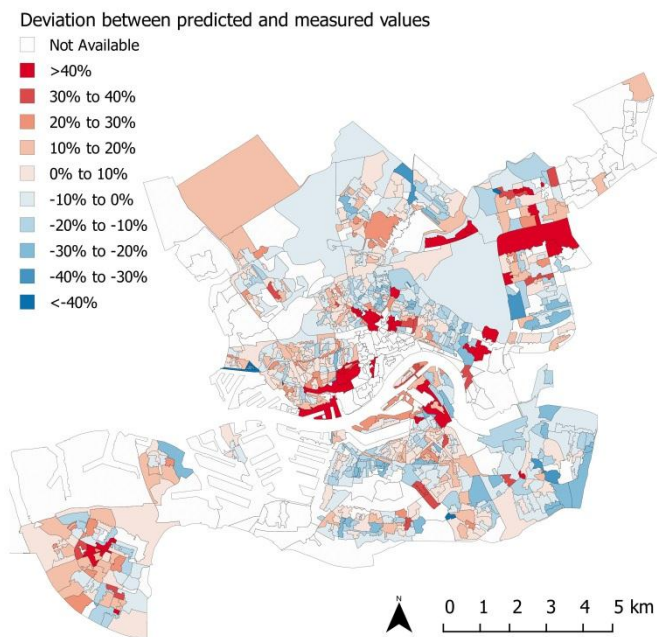


Fig.2, Map of deviation between predicted and measured yearly average natural gas consumption at post-code level in Rotterdam.

The residuals are further displayed on a map at the post-code level to visualize their spatial distribution (Fig.2). Deviations in consumption tend to concentrate in various parts of the city, indicating the possible presence of effects at local scale. Specific configuration of buildings, household composition, income level and other social factors might determine this

effect and must be further analyzed in a future step. The largest deviations were detected for few small areas where only one building with special characteristics is present, such as a big residential complex. Overall, the comparison between fitted and measured values demonstrated that the prediction given by the model is accurate across the city.

The estimated regression coefficients were used to predict the energy consumption of dwellings across the city. Fig. 3 shows the distribution of natural gas consumption predicted by type of dwelling for the whole stock.

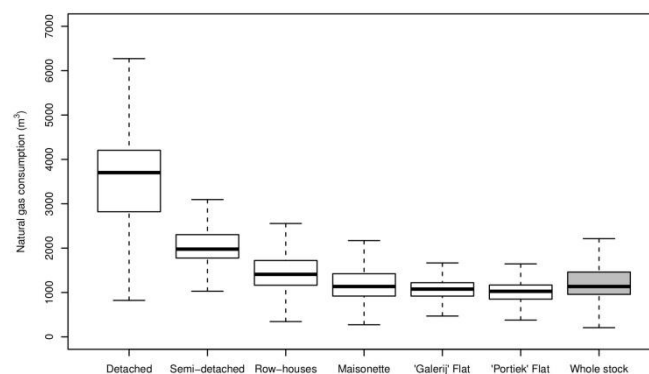


Fig. 3, Distribution of predicted yearly natural gas consumption of dwellings by type for the whole housing stock of Rotterdam.

Gas consumptions are higher for houses than for apartments due to larger floor surface and heated volume. In addition, less compact dwelling types such as detached and semi-detached are more energy consuming because of their relatively large envelope surface area compared to their volume, resulting in higher heat losses.

TABLE 2, ENERGY SAVINGS POTENTIAL FOR SPACE HEATING AND DOMESTIC HOT WATER BY HOUSING TYPE AND PERIOD OF CONSTRUCTION (ADAPTED FROM [4]).

Energy savings potential	Houses	Apartments
Period of construction		
<1946	65 - 68 %	41 - 70%
1946-1964	58 - 68 %	41 - 70%
1965-1974	48 - 61 %	40 - 49%
1975-1991	33 - 40%	24 - 31%
1992-2005	5 - 13%	4 - 13%

The estimated energy savings potential for space heating and domestic hot water associated to the retrofit of residential buildings is reported in Table 2 by dwelling type and period of construction. The potential is higher for older buildings and progressively decreases for more recent ones. The typology has a relative influence on results depending on both different envelope thermal properties and geometry. For instance, insulating buildings with a less compact shape can lead to major energy savings because of the higher influence of the heat losses by transmission on the energy demand.

The values of energy consumption and energy savings potential, calculated at dwelling level, were aggregated at the

block level and displayed as spatial maps for the entire city of Rotterdam (Figs. 4-5).

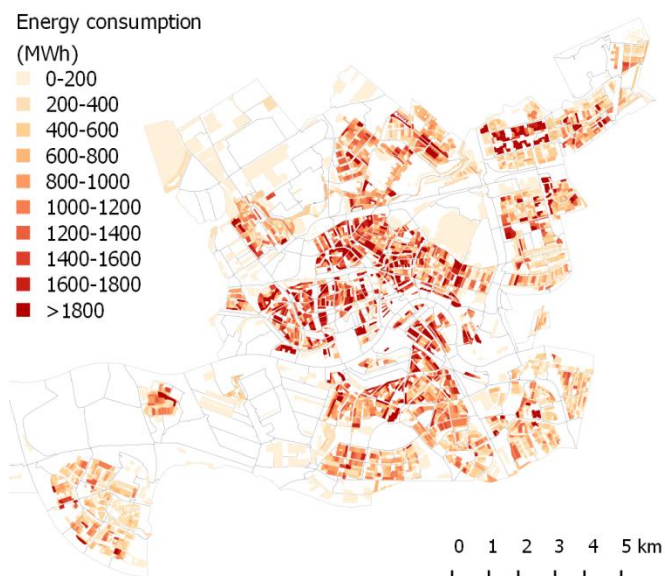


Fig.4, Map of primary energy consumption at block level for space heating and domestic hot water of dwellings across Rotterdam.

Fig. 4 displays maps of primary energy consumption for space heating and domestic hot water of dwellings across the whole city. Higher energy consumption is registered for the city center and adjacent areas characterized by high density and the presence of older flats and row-houses. In contrast, the city suburbs have total lower energy consumption due to a lower density, despite the presence of detached and semi-detached houses more energy consuming.

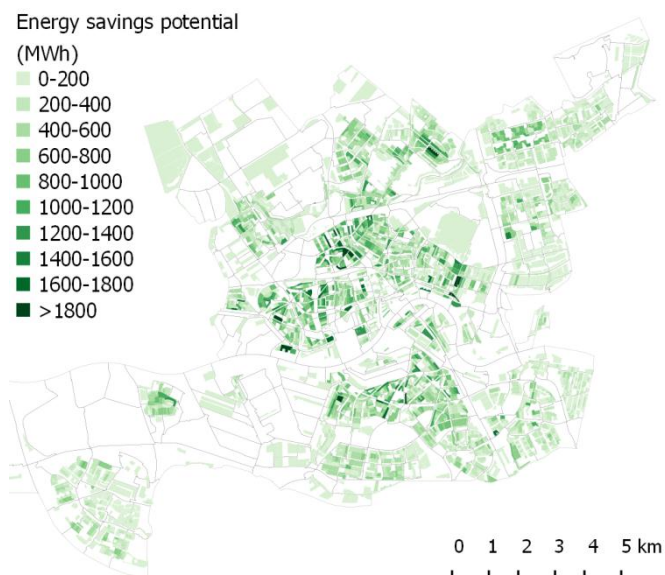


Fig.5, Map of energy savings potential at the block level for space heating and domestic hot water of dwellings across Rotterdam.

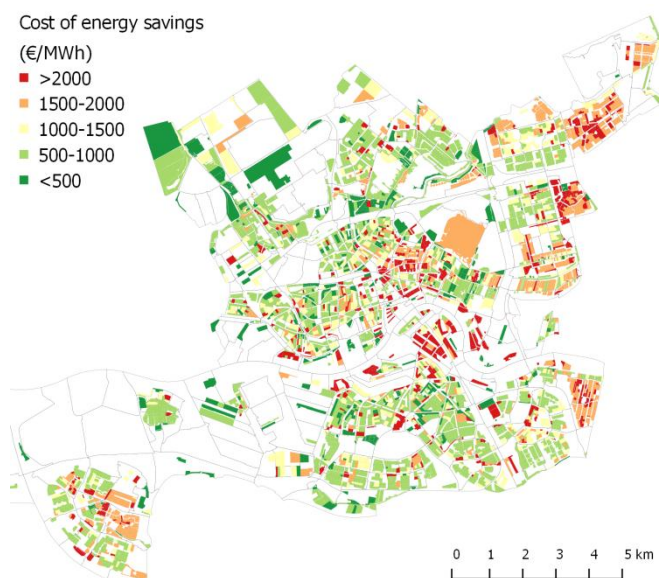


Fig. 6, Map of cost of yearly energy savings at the block level for space heating and domestic hot water of dwellings across Rotterdam.

The map in Fig. 5 shows the energy savings potential for combined space heating and domestic hot water achievable through the implementation of typical retrofit measures for buildings. The map is suitable to identify across the city areas where the retrofit of residential buildings is more promising in terms of energy savings. These areas are characterized by a dense urban tissue and the predominance of old buildings.

A map was drawn at the block level to show the cost-effectiveness of retrofit measures across the city (Fig. 6). The cost of energy savings depends on the type and period of construction of dwellings present in a specific area. Lower cost values indicate higher cost-effectiveness of retrofitting. The cost of energy savings decreases for older buildings, indicating an higher cost-effectiveness of retrofit measures (Table 3). The areas of Rotterdam where the distributed retrofit is expected to be more cost-effective are mainly located in the belt around the city center and in some of the suburbs where the presence of older buildings is larger. However, by comparison of this map (Fig. 6) with the energy savings potential map (Fig. 5) it emerges that not every area where the retrofit is more cost-effective has a large energy savings potential. This depends mainly on the urban density, for instance areas in the outskirts with old detached houses and low density tissue, have high cost-effectiveness values for retrofit but low energy savings potential. The two maps can be used in combination to support decision and prioritization of retrofit measures across the city.

TABLE 3, ENERGY SAVINGS POTENTIAL, CO₂ REDUCTION POTENTIAL AND MEAN COST OF ENERGY SAVINGS IMPLEMENTING STANDARD RETROFIT MEASURES FOR THE HOUSING STOCK OF ROTTERDAM.

Dwelling category	Tot. energy savings potential (GWh/a)	Tot. CO ₂ reduction potential (kton/a)	Mean cost of energy savings (€/MWh /a)
Period of construction			
<1946	853.0	162.2	657
1946-1964	344.9	68.0	867
1965-1974	164.2	32.1	939
1975-1991	218.3	50.8	2025
1992-2005	39.3	8.59	2284
Type of dwelling			
Houses	572.4	109.8	1134
Apartments	1046.6	211.9	1268
Whole stock	1619.7	321.7	1231

Results of the energy savings potential and CO₂ emission reduction computation for the whole housing stock of Rotterdam are reported in Table 3 distributed by period of construction and type of dwelling. The highest potential can be provided by buildings constructed before 1964 for a yearly saving of 1197,9 GWh, corresponding to the 74% of the total. Considering the type of dwelling, apartments have a yearly potential of 1046.6 GWh, almost 65% of the total. The total energy savings potential for the whole housing stock amounts to 1619.7 GWh per year while the CO₂ reduction potential to 321.7 kton per year.

V. Conclusions

A GIS-based statistical approach was developed to analyze the energy consumption of housing stocks at the urban scale and to prioritize the implementation of retrofit measures. The methodology was tested on the residential stock of Rotterdam city but can be generically applied to other contexts.

The linear regression model made it possible to disaggregate natural gas consumption data available at post-code area level accurately enough to predict energy consumption of single dwellings across the entire city. A preliminary evaluation of the spatial distribution of errors from the statistical analysis was carried out to detect the presence of possible spatial patterns and will be object of further spatial analysis. Maps of the energy consumption for space heating and domestic hot water in the current state, energy savings potential given by

standard retrofit measures and cost of energy savings were produced for the whole housing stock.

Results for Rotterdam City demonstrated that the energy savings and CO₂ reduction potential achievable by the retrofit of the existing housing stock are significantly high, respectively 1619.7 GWh and 321.7 kton CO₂. Retrofitting is particularly convenient and effective for the portion of the housing stock built before 1965 and for apartment blocks.

This approach can constitute a valid support to promote and prioritize the retrofit of the housing stock at the city scale based on energy savings, CO₂ emissions and costs. The results generated for the housing stock can be further used as support for planning renewable energy local production or urban heating networks.

References

- [1] EIFER European Institute for Energy Research. *Eifer 2.0*, 2012. http://www.eifer.uni-karlsruhe.de/IMG/pdf/120417_eifer_broschuere_ansicht_web.pdf
- [2] Directive 2012/27/EU of the European Parliament and of the Council of 25 October 2012 on energy efficiency.
- [3] L. Swan, V. Ugursal, "Modeling of end-use energy consumption in the residential sector: A review of Modeling techniques," *Renewable and Sustainable Energy Reviews*, **13**, pp. 1819-1835, 2009.
- [4] A. Mastrucci, O. Baume, F. Stazi, U. Leopold. "Estimating energy savings for the residential building stock of an entire city: A GIS-based statistical downscaling approach applied to Rotterdam," *Energy and Buildings*, **75**, pp. 358-367, 2014.
- [5] The MUSIC Project, Mitigation of CO₂ emissions in Urban areas: Solutions for Innovative Cities, 2013. <http://www.themusicproject.eu>
- [6] L. De Sousa, C. Eykamp, U. Leopold, O. Baume, C. Braun. "iGUESS – a web based system integrating urban energy planning and assessment modelling for multi-scale spatial decision making", *Proceedings International Environmental, Modelling and Software Society (iEMSS)*, Leipzig, Germany, 2012.
- [7] Agentschap NL, *Voorbeeldwoningen 2011 - Bestaandebouw*, publicatie-nr.2KPWB1034, 2011.
- [8] Normalisatie-instituut, NEN 7120:2011. *Energy performance of buildings -Determination method*. National Netherlands standard, 2011.
- [9] QGIS Development Team. *QGIS Geographic Information System, Open Source Geospatial Foundation*, 2009. <http://qgis.osgeo.org>



Parametric modeling of producer gas-combustor and heat exchanger integration for micro-gas turbine application

发生气参数化建模 – 用于微型燃气轮机之燃烧器与热交换器集成

Mackay A.E. Okure¹, Wilson B. Musinguzi^{2*}, Terese Løvås³

¹School of Engineering, Makerere University, P.O. Box 7062, Kampala, Uganda

²Faculty of Engineering, Busitema University, P.O. Box 236, Tororo, Uganda

³Department of Energy and Process Engineering, NTNU, Trondheim, Norway

*Corresponding Author: wilson.musinguzi@gmail.com

Accepted for publication on 14th September 2016

Abstract - An alternative way of improving the use of biomass resources in rural areas of developing countries is to design suitable combined heat, and power (CHP) small-scale plants for distributed generation. A gasification-based CHP system can potentially have higher electricity efficiency than a direct combustion-based CHP system. The combustible gas from wood gasification is fired in a combustor that is integrated with a heat exchanger to facilitate effective heat transfer from the hot flue gases to the 100kW_e micro gas turbine working fluid. Burning a gas in the combustor has an edge over the solid biomass because the gaseous fuel offers high heat exchanger temperature as well as stable combustion/continuous operation. Two parameters that have potential for efficiency advancement are investigated in this work: increased turbine inlet temperature and heat exchanger effectiveness. This paper presents a parametric model analysis of the combustion process in the combustor and heat transfer to the turbine working medium across the heat exchanger. Aspen Plus Process Modeling software (aspenONE® Engineering for Universities V7.3) was used for implementation and performing sensitivity analysis of the system. The heat exchanger and combustor integration process analysis has also shown good performance with the flue gases from combustion of producer gas providing sufficient thermal energy needed to raise the turbine working fluid to the required turbine inlet temperature. The analysis of the heat exchanger has provided parameters essential for decision making on the sizing of the heat exchanger. The practical value added was revealing the parameters needed in the design specification of the heat exchanger suitable for the heat duty of a typical 100kW_e externally fired micro gas turbine based on gasification of biomass and subsequent producer gas combustion. The heat exchanger effectiveness of 0.635 was achieved in this parametric study. Furthermore, the results

revealed that the heat exchanger effectiveness increased with decrease in adiabatic flame temperature. The heat duty of the hot combustion gases plays a role in the value of the adiabatic flame temperature that can give a desired effectiveness and at the same time satisfy the heat balance between the two streams.

Keywords - Parametric modeling, Producer-gas-Combustor, Heat Exchanger, Indirectly Fired Micro-gas Turbine.

I. INTRODUCTION

An alternative way of improving the use of biomass resources in rural areas of developing countries is to design suitable combined heat and power (CHP) small-scale plants for distributed generation. Among solid biomass thermochemical conversion processes, combustion is the most advanced and market-proven one, while pyrolysis and gasification can still be considered to be at a pre-commercial stage of development according to Maraver et al. [1]. A gasification-based CHP system can potentially have higher electricity efficiency than a direct combustion-based CHP system as demonstrated in [2]-[4]. Another of its advantages is that gas firing produces less CO₂ per unit power than does a liquid or solid fuel as shown by Pilavachi [5]. According to Leilei et al. [2], small-scale biomass-fuelled CHP systems have a particularly strong relevance in improving the quality of life, especially in rural communities in developing countries. The first step in designing a CHP plant is to determine the best configuration in terms of the thermodynamic integration of all the subsystems and the

optimization of the overall energy efficiency. Bassily [6] reports the main methods for improving the efficiency or power of the combined cycle as: increasing the turbine inlet temperature (TIT), inlet air-cooling, applying gas reheat, steam or water injection into the gas turbine (GT), and reducing the irreversibility of the heat recovery steam generator (HRSG).

By replacing the combustion chamber of a gas turbine with a high temperature heat exchanger, the electrical efficiency of a solid biomass fuelled power plant can be increased from 15-20% to 25-30% [7] for typical plant sizes of 100 kWel. The main reasons why hot air gas turbines (HGT) have not succeeded until now are the high operating air temperature of over 850°C, ash sintering, slagging and fouling, material problems on the heat exchanger due to the low heat transfer of

flue gas to air and large heat exchanger areas required as reported by Gaderer et al. [8]. In most applications, heat exchangers are very important to the overall efficiency, cost, and size of the system. Current heat exchanger designs rely heavily on fin-and-tube or plate heat exchanger designs, often constructed using copper and aluminum. Recent developments in material science, including advances in ceramics and ceramic matrix composites, open opportunities for new heat exchanger designs; Sommers et al. [9]. The major factors affecting heat exchanger performance are effectiveness, pressure drop and leakage of the heat transfer medium.

For process intensification, steam injection into the turbine working medium has shown greater increase in efficiency of externally fired microturbines due to increased specific heat of the turbine working medium. Delattin et al. [10] reports that steam addition of up to the surge limit of 3.3% of the mass of air flowing into the microturbine can increase the electric efficiency by 5%.

This paper reports on the parametric modeling of the high temperature heat exchanger and combustor integration utilizing a combustible gas from a wood gasifier for improved heat transfer to the turbine working medium. Thus the heat exchanger effectiveness is a key parameter to analyze.

II. MATERIALS AND METHODS

The researchers modeled the heat exchanger and combustor integration and analyzed its performance theoretically. The authors have carried out parametric modeling of the system to reveal the relationship of different parameters in the system in order to achieve the desired output of heat transferred to the turbine working fluid. The turbine inlet parameters are specified by the design model chosen and thus the turbine inlet temperature is set at 950°C. Attempt to have the highest possible practical value of the key parameter of heat exchanger effectiveness and thus high heat transfer to the turbine medium was made in the analysis.

Fig. 1 illustrates the system modeled in this paper. The hot wood gas from the gasifier and preheated combustion air enter the combustor integrated with the heat exchanger. The high temperature combustion gases flow through the shell-side of

the chamber packed with heat exchanger tubes carrying the turbine working medium (air plus a small amount of steam). The heated tube-side stream is led to the gas turbine for power generation. The exhaust from the turbine is led to the heat recovery steam generator (HRSG) which delivers the steam needed for injection into compressed air at the right compressor outlet pressure. The mixing takes place at common pressure. The exhaust from combustion is used for combustion air preheating.

Thermodynamic chemical equilibrium analysis of the combustor was carried out using the RGibbs reactor. This type of reactor uses the method of direct minimization of Gibbs free energy. It is useful when the reaction stoichiometry is not known or is high in number due to many components participating in the reaction. This is the only Aspen Plus block that deals with solid, liquid and gas phase equilibrium. For the heat exchanger, the HEATX block was used for shell-and tube analysis of the flow. Both the equation of state and ideal property methods were used in the simulation to compute the thermodynamic and flow properties of the streams. The producer fuel properties in Table I published by the authors in earlier work, were used for the modeling [11], [12].

Process optimization, under atmospheric combustion and heat exchange, used thermodynamic equilibrium and exergy analysis. Aspen Plus Process Modeling software (aspenONE® Engineering for Universities V7.3) was used for implementation and performing sensitivity analysis of the system. The thermodynamic analysis of this system considers continuous deterministic steady-state conditions. Stepwise procedure with simulation using

ASPEN PLUS process modeling is used in the thermodynamic analysis of the cycle. The ASPEN PLUS Gibbs reactor was used for combustion with the assumption that the reaction follows the Gibbs equilibrium. The process parameters in the analysis were correlated with those available in the literature by Schuster et al. [13], Kentaro et al. [14], Chiamonti et al. [15], Kautz et al. [7], Daniele et al. [16], Lieuwen et al. [17]. These parameters represent commercially available technologies or processes in advanced development stage.

Table I, Characteristic properties of the Producer gas generated in a downdraft fixed bed gasifier [11], [12].

Property	Value
Wood feed rate	0.02 (kg/s)
Steam (gasifying medium) flow rate at 500°C, 1 bar	0.012 (kg/s)
Reactor temperature in the gasification zone	820 (°C)
Net producer gas flow from the gasifier	0.028 (Nm ³ /s)
Component distribution in the wood gas	43.27% H ₂ , 14.42% CO, 7.84% CH ₄ , 17.31% CO ₂ , 17.16% H ₂ O (mol(%) / mol of wood gas)
HHV of gaseous fuel	13.9 (MJ/kg)
LHV of gaseous fuel	13.4 (MJ/kg)
\dot{m}_{pg}	0.02 (kg/s)
Sintering temperature of the carry-over ash in wood gas	1334 (°C)

Nomenclature			
Abbreviation			
CHP	combined heat and power	Pr	prandtl number
HGT	hot air gas turbine	A	Cross-section area of tube (m ²)
TIT	turbine inlet temperature	D	diameter of tube (m)
ε-NTU	effectiveness number of transfer units	T	temperature (K)
Fg	flue gas	St	stanton number
G _{Tm}	gas turbine medium	UA	overall thermal conductance (kW/K)
HHV	higher heating value (MJ/kg)	Wo	wobble number
HRSG	heat recovery steam generator	\bar{x}	Mole fraction
LHV	lower heating value (MJ/kg)	H	Enthalpy (kJ)
LMTD	logarithmic mean temperature difference	Greek letters	
N	number of tubes in the heat exchanger	Δ	difference (-)
P _g	producer gas	ε	heat exchanger effectiveness
SG	specific gravity	Φ	equivalent ratio
TO	theoretical oxidant	ρ	density (kg/m ³)
GT	gas turbine	ψ	volume flow rate (m ³ /s)
		μ	dynamic viscosity (Ns/m ²)
Roman letters			
n	number of moles	Subscripts	
C	Capacity rate (kW/K)	ad	adiabatic
h	Heat transfer coefficient (kW/m ² K)	i	i th component
\bar{h}	Enthalpy (kJ/kgmole)	o	outer
\bar{h}_f°	Standard heat of formation (kJ/kgmole)	s	surface
\dot{m}	Mass flow rate, kg/s	e	electric
P	Pressure (N/m ²)		

Fig. 1, Schematic of the system under study.

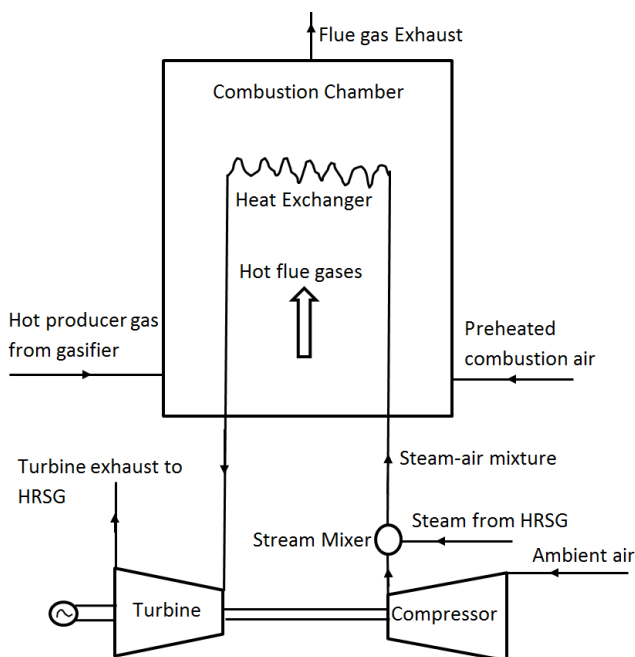
III. DERIVATION OF THE PARAMETRIC MODEL OF THE COMBUSTOR AND HEAT EXCHANGER

A number of important practical issues must be addressed in designing a wood gas combustion system in order to achieve sufficient stability in the operation of the combustor/heat exchanger combination. Indeed complex interactions between combustion phenomena and fluid mechanics have been sighted as not well understood [17]. In particular, burners involve complex, less understood interactions between swirling flow dynamics, flow field alterations induced by volumetric expansion across the flame, and flame propagation.

Unlike in natural gas combustion where premixed burners are used, combustion of wood gas from the gasifier favorably utilizes non-premixed burners as portrayed by the majority of the fundamental investigations on wood gas (syngas) combustion characteristics [17]. The non-premixed burners preferred in wood gas combustion are believed to significantly lower the operability issues that are detrimental to safe combustion. This study therefore exams two important parameters namely adiabatic flame temperature and heat exchanger effectiveness as theoretical basis for the interaction between the combustor and heat exchanger system.

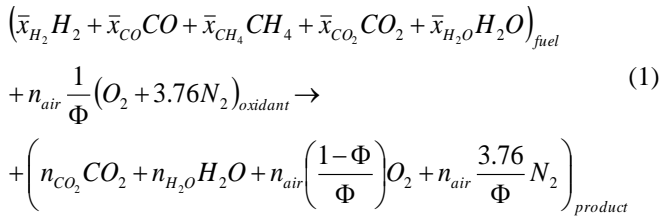
3.1 Adiabatic Flame Temperature

For purposes of analysis, it is assumed that the combustor operates at steady-state, steady flow conditions and that in this case, no work or power transfer occurs in addition to negligible changes in kinetic and potential energy fluxes. Energy transfer from the generated gases as heat to the surroundings (heat exchanger surfaces) due to combustion can be partly influenced by the properties of fuel burned, equivalent ratio, state of reactants (fuel and oxidant phase/temperature) and product state (completeness of combustion and product temperature) [18]. The adiabatic flame temperature gives insights on the maximum possible temperature in the combustor zone so that proper materials for combustor surfaces can be chosen for a given combustion



situation, and propose the necessary quenching or combustion mixture dilution (decreasing the equivalent ratio) among other interventions.

Knowing the composition of the combustible gas and taking air as the oxidant, the adiabatic temperature can be evaluated by setting a value of the equivalent ratio. Assuming one mole of wood gas, Eq. (1) then gives overall combustion expression.



n_{CO_2} , n_{H_2O} and n_{air} are the moles of carbondioxide, water vapour and air respectively.

Substituting the known values for moles of the producer gas components from Table I and setting the value of Φ initially

at 0.83333 or TO of 120, where $TO = \left(\frac{1}{\Phi} \right) 100$, Eq. (2) then

balanced overall equation:

$$\begin{aligned}
 & 0.4327H_2 + 0.1442CO + 0.0784CH_4 + 0.1731CO_2 + 0.1716H_2O + \frac{0.44525}{\Phi} (O_2 + 3.76N_2) \rightarrow \\
 & 0.3957CO_2 + 0.7611H_2O + 0.44525 \left(\frac{1-\Phi}{\Phi} \right) O_2 + (0.44525)(3.76) \left(\frac{1}{\Phi} \right) N_2
 \end{aligned} \tag{2}$$

Performing an energy balance in the combustor at constant pressure; $H_{products} - H_{reactants} = 0$, from Eq. (2),

$$\begin{aligned}
 & 0.4327 \left[\bar{h}_f^o \right]_{H_2} + 0.1442 \left[\bar{h}_f^o \right]_{CO} + 0.0784 \left[\bar{h}_f^o \right]_{CH_4} + 0.1731 \left[\bar{h}_f^o \right]_{CO_2} \\
 & + 0.1716 \left[\bar{h}_f^o \right]_{H_2O} + \frac{0.44525}{\Phi} \left[\left(\bar{h}_f^o \right)_{O_2} + 3.76 \left(\bar{h}_f^o \right)_{N_2} \right] = \\
 & 0.3957 \left[\bar{h}_f^o + \Delta \bar{h} \right]_{CO_2} + 0.7611 \left[\bar{h}_f^o + \Delta \bar{h} \right]_{H_2O} \\
 & + 0.44525 \left(\frac{1-\Phi}{\Phi} \right) \left[\bar{h}_f^o + \Delta \bar{h} \right]_{O_2} + 0.44525(3.76) \left(\frac{1}{\Phi} \right) \left[\bar{h}_f^o + \Delta \bar{h} \right]_{N_2}
 \end{aligned} \tag{3}$$

The values of $\Delta \bar{h}$ can be evaluated from appropriate tables by assuming an initial average temperature of reactant mixture in the reactor just before combustion to be around 700K since the fuel and oxidant are considered hot and preheated before the entry point, and then using trial-and-error for the unknown value of the adiabatic temperature. Standard values of enthalpy change and heat of formation are obtained from Keating [18]. The two temperature values that give the closest negative and positive value outcome in Eq. (3) are then iterated to obtain the temperature that gives zero value outcome of Eq. (3), which is taken as the estimated adiabatic flame temperature. The adiabatic temperature is evaluated for predicted equivalent ratio ($\Phi=1, 0.8333, 0.5, 0.4, 0.25$ and 0.2) all aimed at obtaining the adiabatic temperature that is logical to minimize the temperature at which thermal NOx is likely to occur. Another important condition crucial in

combustion phenomenon is the ignition temperature; the minimum temperature at which any fuel-air mixture begins to burn. The equivalent ratio therefore has to be appropriately selected because either too much fuel above the stoichiometric amount or too much air can extinguish the flame.

3.2 Parametric Analysis of the Heat Exchanger

The objective in heat exchanger design is to enhance the thermal contact between the heat-exchanging entities, that is, to minimize the temperature difference between the heat exchanging streams and thus reducing the rate of entropy generation (exergy destruction). Hence, a heat exchanger is a multifaceted engineering system whose design involves not only the calculation of the heat transfer rate across the heat exchanger surface but also the pumping power needed to circulate the fluids, the flow arrangements, the construction of the actual hardware and the ability to disassemble the apparatus for periodic cleaning [19]. In this paper, the discussion is centered on thermal design and optimization of the heat exchanger.

The two methods commonly used for heat exchanger design and analysis are the Logarithmic Mean Temperature Difference (LMTD) and the Effectiveness Number of Transfer Units (ϵ -Ntu). The two methods give similar outcome for a given heat exchanger analysis problem. In the determination of heat exchanger parameters in this paper, the ϵ -Ntu (NTU) method is applied. A base-case for a shell-and-tube heat exchanger is considered in establishing the characteristics for the heat exchange between the combustion gases (flue gas) and the turbine working medium (air and a small amount of steam). Fig. 2 illustrates the flow arrangement for heat exchange with known parameters indicated. The microturbine parameters indicated on Fig. 2 are for a commercially available unit that is required to deliver a net power of 100 kW. The microturbine working medium is air with steam injection (5% of flow). Parameters of the hot stream (flue gas) are obtained from the preceding discussion (sec 3.1) and the heat duty requirements in the heat exchanger.

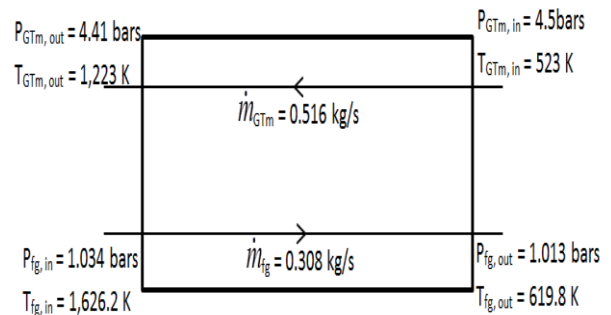


Fig. 2, Flow streams across the heat exchanger.

Compressed air and steam mixture which form the turbine working medium flows through n parallel tubes with inner diameter D, outer diameter D_o , and length L. The tubes are

mounted in a shell of cross-section area A_s . Combustion products (flue gas) flow through the tube-to-tube spaces, parallel to the tube in a counter flow mode. The problem at hand is therefore of sizing the heat exchanger i.e. determining the number of tubes and the heat exchanger dimensions. Although tubes are commercially available at only certain standard diameters and wall thicknesses, the ratio $D_o/D = 1.2$ holds true in most heat exchanger tubes. To determine the remaining four unknowns; n , D , L and A_s , the analysis must satisfy the heat transfer and fluid flow relations, making use of the specified inlet and outlet temperature and pressure values across the heat exchanger.

3.2.1 Heat Transfer Relations

The capacity rate on the high pressure side (the tube side) of the heat exchanger is

$$C_{GTm} = \dot{m}_{GT} c_{p,GTm} = (0.516 \text{ kg/s})(1.17 \text{ kJ/kgK}) = 0.6 \text{ kW/K} \quad (4)$$

The capacity rate on the low pressure side can be deduced from an energy balance across the heat exchanger

$$C_{fg} = \frac{C_{GTm}(T_{GTm,out} - T_{GTm,in})}{(T_{fg,in} - T_{fg,out})} = (0.6) \frac{1,223 - 523}{1,6262 - 6198} = 0.417 \text{ kW/K} \quad (5)$$

From Eq. (4) and Eq. (5), it is seen that the flow is unbalanced

$$\frac{C_{min}}{C_{max}} = \frac{C_{fg}}{C_{GTm}} \quad (6)$$

The effectiveness of the heat exchanger is obtained from

$$\varepsilon = \frac{T_{GTm,out} - T_{GTm,in}}{T_{fg,in} - T_{GTm,in}} \quad (7)$$

Then the Number of Transfer Units is calculated as

$$NTU = \frac{\ln \left[\frac{1 - \varepsilon C_{min} / C_{max}}{1 - \varepsilon} \right]}{1 - C_{min} / C_{max}} \quad (8)$$

The overall thermal conductance is

$$UA = C_{min} NTU \quad (9)$$

This value is related to the thermal conductances on the two sides of the heat transfer surface by

$$\frac{1}{UA} = \frac{1}{hn\pi DL} + \frac{1}{h_o n\pi D_o L} \quad (10)$$

where h and h_o are gas turbine medium-side and flue gas-side heat transfer coefficients.

3.2.2 Pressure Drop Relations

The pressure drop on the air/steam mixture stream (gas turbine working medium) is estimated from

$$\Delta P_{GTm} = f \frac{2L}{D} \frac{G^2}{\rho_{GTm}} + G^2 \left(\frac{1}{\rho_{out}} - \frac{1}{\rho_{in}} \right)_{GTm} \quad (11)$$

where f is fanning friction factor, G is the mass velocity of the stream and A is the channel cross-sectional area, and

$$G = \dot{m} / A = \rho_{in} V_{in} = \rho_{out} V_{out}$$

After simplification, Eq. (11) leads to

$$f \frac{2L}{D} + 2.2455 = 42,857 n^2 \left(\frac{D}{1 \text{ m}} \right)^4 \quad (12)$$

where $f = f(\text{Re}_D)$, and $\text{Re}_D = \frac{16,850.5}{nD}$ where f is

fanning friction factor.

Similar steps leading to Eq. (11) and Eq. (12) are followed for the flue gas side.

The area available for the flow of the flue gas is the difference between the total area of the shell, A_s , and the area occupied by n tubes:

$$A_{fg} = A_s - \frac{n\pi D_o^2}{4} \quad (13)$$

The evaluated expression for pressure drop on the flue gas side therefore becomes:

$$f_o \frac{2L}{D_h} - 1.1 = 8,606.6 \left(\frac{A_{fg}}{1 \text{ m}^2} \right)^2 \quad (14)$$

The development so far has provided one heat transfer related equation (Eq. 10) and two fluid-flow related equations (Eq. 12 and Eq. 14). These can be reduced further to obtain a final set of three equations as follows:

Invoking the Colburn analogy which relates the heat transfer and the momentum transfer for fully developed turbulent flow;

$$h = c_p G St, \quad St = \frac{1}{2} f \text{Pr}^{-2/3}; \text{ since}$$

$$UA = 0.582 \text{ kW/K}, \quad G_{fg} = \frac{\dot{m}}{A_{fg}}$$

$$1 = 0.3874 \frac{D}{fL} + 0.727 \frac{A_{fg}}{n f_o L D} \quad (15)$$

Since Reynolds number (Re_D) on both sides is proportional, and in the range $\text{Re}_D 10^4 - 10^6$, the friction factor varies as $\text{Re}_D^{-0.2}$, then f and f_o are also proportional resulting into simplification of Eq. (15).

$$\frac{\text{Re}_{D_h}}{\text{Re}_D} = 0.389 \frac{nD}{A_{fg}} D_h = 0.413,$$

$$\frac{f_o}{f} = \left(\frac{\text{Re}_{D_h}}{\text{Re}_D} \right)^{-0.2} = 1.1935$$

$$1 = 0.3874 + 0.61 \frac{A_{fg}}{n D f L}, \quad (16)$$

Eq. (14) can then be expressed as

$$8606.6 \hat{A}^3 n^2 \left(\frac{D}{1 \text{ m}} \right)^4 = f \frac{2L}{D} - 1.1 \hat{A} \quad (17)$$

where \hat{A} is the dimensionless cross-sectional area of the flue gas stream,

$$\hat{A} = \frac{A_{fg}}{nD^2} \tag{18}$$

Eliminating the group $2fL/D$ between Eq. (12) and Eq. (17)

$$n \left(\frac{D}{1m} \right)^2 = \left(\frac{2.2455 + 1.1\hat{A}}{42,857 - 8,606.6\hat{A}^3} \right)^{\frac{1}{2}} \tag{19}$$

Expressing Eq. (16) in terms of \hat{A} yields

$$\frac{fL}{D} = 0.3874 + 0.61\hat{A} \tag{20}$$

Combining Eq. (12) and Eq. (20)

$$n \left(\frac{D}{1m} \right)^2 = (7.05 \times 10^{-5} + 2.85\hat{A}) \tag{21}$$

With equations (16) – (21), the required numerical solution can be obtained

$$\begin{aligned} \hat{A} &= 6.341 \times 10^{-6} \\ nD^2 &= 9.41 \times 10^{-3} \end{aligned} \tag{22}$$

Substituting the values in Eq. (18),

$$A_{fg} = \hat{A}(nD^2) = 5.97 \times 10^{-8} m^2$$

From eq. (13),

$$A_s = A_{fg} + n \frac{\pi(1.2D)^2}{4} = 0.0106m^2$$

Noting that the shell area and the flue gas cross-section are fixed, the remaining design parameters (n, D, L) can vary, but only one can be chosen independently and must satisfy Eq. (20), i.e. $\left[\frac{fL}{D} = 0.3874 \right]$ and Eq. (22). When Re_D falls in the range $10^4 - 10^6$, $f = 0.046 Re_D^{-0.2}$ [13].

IV. RESULTS AND DISCUSSION

Table II gives the results for the values of adiabatic flame temperature at selected equivalent ratio, with resulting flow rate of the flue gas stream. The value of adiabatic flame temperature is seen to decrease with equivalent ratio. The mass flow rate of the combustion products increases as the adiabatic temperature decreases. The increase in flue gas flow is due to increase in oxidant (air) flow that result into dilution of the combustion mixture leading to decreased temperatures in the combustion zone. However the dilution which is desired for minimizing thermal stresses of the combustor materials has a limit below which it can compromise the heat duty of the flue gases for minimum permissible temperature difference in the heat exchanger flow streams. For purposes of heat exchanger analysis, the adiabatic temperature of 1626.2 K corresponding to the equivalent ratio of 0.25 is utilized as the fluegas

temperature at the heat exchanger inlet. The heat exchanger effectiveness of 0.635 was achieved for this optimization problem. For optimization purposes in the heat exchanger, it is necessary to determine the values of hot gas flow rate alongside the adiabatic flame temperature since the heat transfer to the cold fluid is dependent on both.

Table III shows the numerical results obtained by treating D as the independent variable. The values show that the variation of total heat transfer area $A = n\pi D_o L$ and overall heat transfer coefficient U with D or n is of a lesser extent. However the flow length L increases linearly with the tube diameter D. The volume of the heat exchanger ($A_s L$) increases too due to a fixed total area of the heat exchanger. The weight of the heat exchanger is controlled by the weight of the tubes, i.e. the tube material volume $n\pi(D_o^2 - D^2)L$ increases as D increases. In conclusion, a relatively small D would be selected if a small volume or a small weight is desired for the heat exchanger, keeping in mind the associated cost requirement.

Knowing that the most important parameter for optimal performance of the heat exchanger being the increased value of the heat exchanger effectiveness, the relationship of this effectiveness with the adiabatic flame temperature is established. Fig. 3 shows the variation of the effectiveness against adiabatic flame temperature with input data given in Table 4. The effectiveness of the heat exchanger increases with decrease in adiabatic flame temperature. The heat duty of the flue gases (turbine inlet temperature) determines the lower adiabatic temperature that gives reasonably high heat exchanger effectiveness. For effectiveness outside the range 0.3 – 0.8, the variation becomes asymptotic with reduced dependence on adiabatic temperature.

Table II, Values of adiabatic flame temperature and flue gas flow rate for given equivalent ratio Φ

Equivalent Ratio (Φ)	Adiabatic Flame Temperature (K)	Rate of flue gas flow into Heat Exchanger (kg/s)
1	2759	0.092
0.8333	2671	0.106
0.5	2101	0.164
0.4	1926	0.2
0.25	1626	0.308
0.2	1513	0.38

Table III, Heat exchanger parametric design values

D (m)	n	L (m)	Re _D 10 ⁵	L/D	A (m ²)	U (W/m ² .K)
0.01	94	0.84	1	84	2.98	195
0.02	24	1.93	2	97	3.49	167
0.03	10	3.33	4	111	3.76	155
0.04	6	5.11	8	128	4.62	126

Table IV, Heat exchanger effectiveness at evaluated values of adiabatic flame temperature

Adiabatic Flame Temperature (K)	Heat exchanger effectiveness
2759	0.313
2671	0.326
2101	0.444
1926	0.500
1626	0.635
1513	0.71

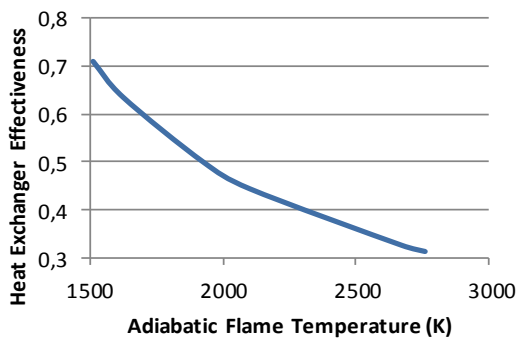


Fig. 3, Variation of heat exchanger effectiveness with adiabatic flame temperature.

V. SENSITIVITY ANALYSIS

Sensitivity analysis was performed in order to conveniently generate tables and plots showing how process performance varies with changes to selected equipment specifications and operating conditions. In the combustor, the varied parameters were the amount of oxidant (lean, stoichiometric and fuel-rich mixture of reactants) supplied and temperature in the vessel which determine the equilibrium component distributions in the hot combustion gases entering the heat exchanger. Increase in heat exchanger area led to

increased turbine inlet temperature, which is essential for achieving higher system efficiency.

Aspen Plus plot wizard was used to reveal the characteristic curve of the component distribution in the vessel with varying temperature for set conditions of lean, stoichiometric and fuel-rich reactant mixture as revealed in Fig. 4, Fig. 5 and Fig. 6. As shown in Fig. 4, the combustible components in the vessel are consumed in the presence of oxygen (oxidation reaction) in attaining the equilibrium. Thereafter the components distribution (concentration) remains independent of temperature until such a high temperature value that the water-gas-shift reaction and water dissociation start to occur.

At a temperature of about 1400 K, the concentration of water vapour and carbon dioxide start to decrease as the concentration of hydrogen and carbon monoxide start to increase due the shift reaction. Increase in oxygen concentration is brought about probably by dissociation of water vapour at elevated temperatures, which also further increases the hydrogen concentration thus shifting the water-gas-shift equilibrium towards conversion of carbon dioxide to carbon monoxide. A similar trend is observed for the stoichiometric conditions of reactants in Fig. 5.

For the case of fuel-rich mixture of reactants in Fig. 6, the supply of limited oxidant meant that some concentration of the combustible components remained at equilibrium. The extent to which the insufficient oxygen reacted with the combustible components in the vessel depended on the reactivity potential of the particular component with oxygen. Initially the concentration of methane and water vapour decreases as the concentration of carbon monoxide and hydrogen increases due to the steam reforming reaction. At higher temperatures the water-gas-shift reaction favours formation of more carbon monoxide and water vapour as the concentration of carbon dioxide and hydrogen decrease.

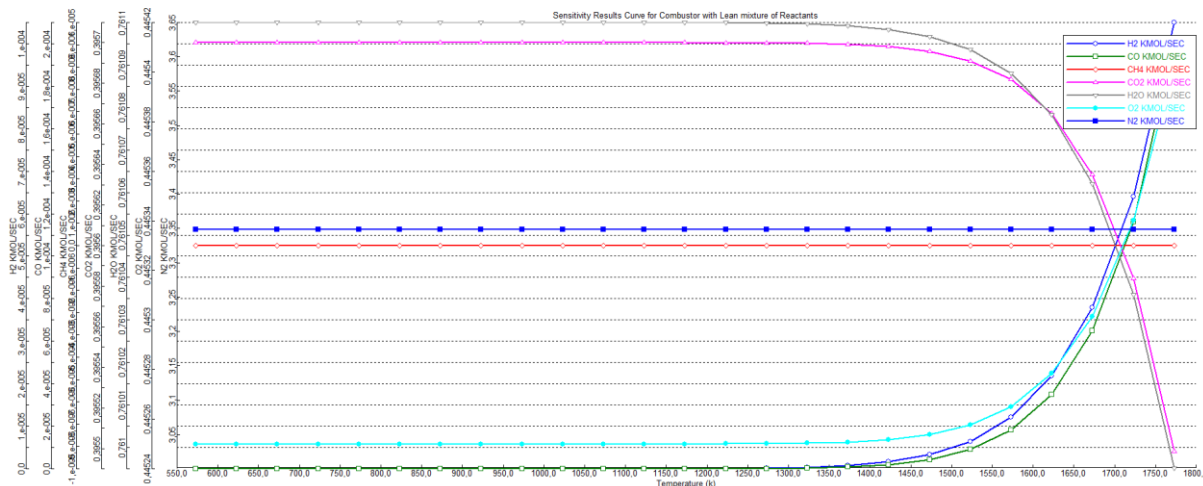


Fig. 4, Sensitivity Analysis Curve for Combustor with Lean Mixture of Reactants.

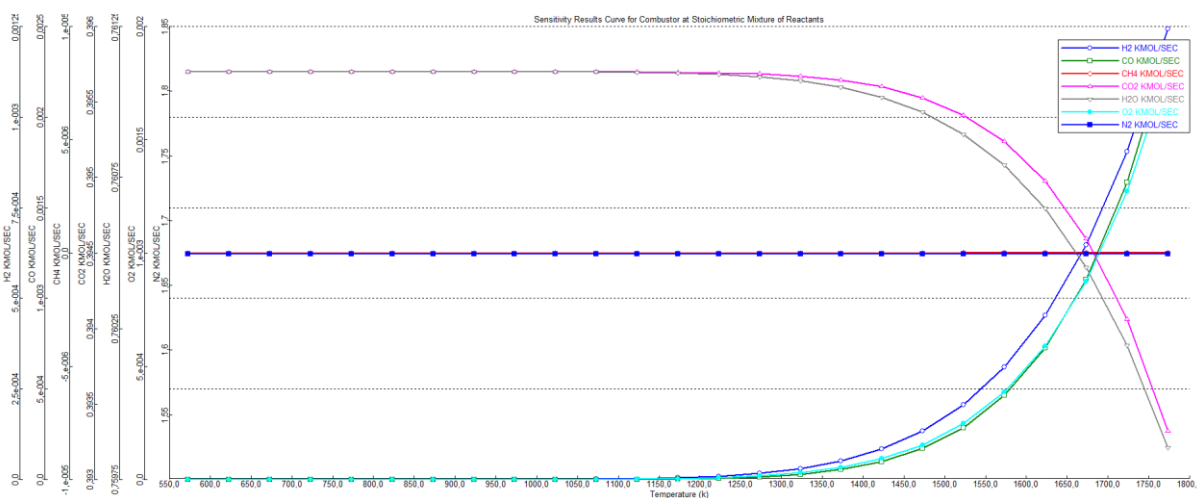


Fig. 5, Sensitivity Analysis Curve for Combustor with Stoichiometric Mixture of Reactants.

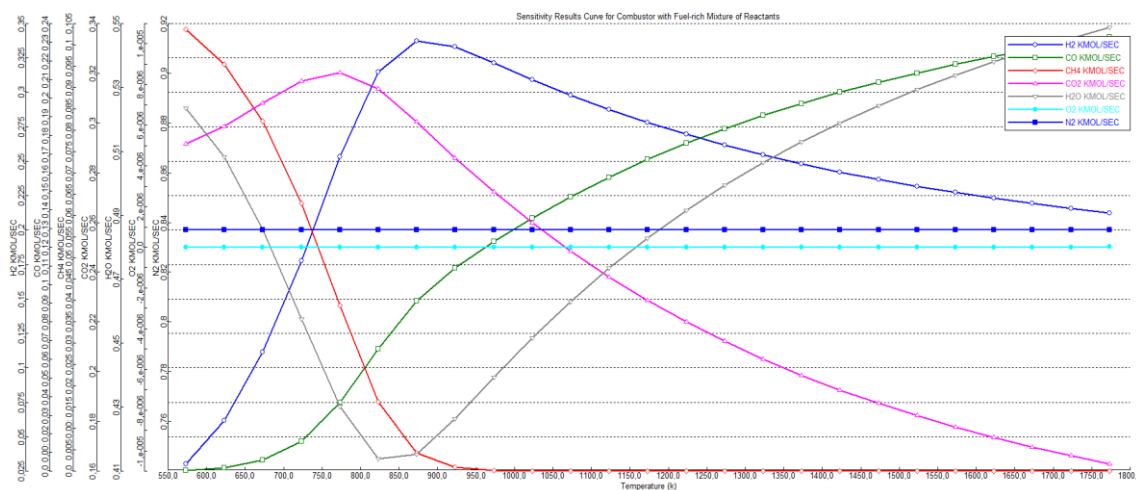


Fig. 6, Sensitivity Analysis Curve for Combustor with Fuel-rich Mixture of Reactants.

VI. CONCLUSION

The authors have carried out parametric modeling of the system to reveal the relationship of different parameters in the system in order to achieve the desired output of heat transferred to the turbine working fluid. The turbine inlet parameters are specified by the design model chosen and thus the turbine inlet temperature is set at 950°C. Though attempts to have the highest possible practical value of the key parameter of heat exchanger effectiveness and thus high heat transfer to the turbine medium were made, the author's cannot comfortably conclude that this is a generally accepted optimal value but rather a near optimal one.

The value of adiabatic flame temperature is seen to decrease with equivalent ratio. The mass flow rate of the combustion products increases as the adiabatic temperature decreases. The increase in flue gas flow is due to increase in oxidant (air) flow that results into dilution of the combustion mixture leading to decreased temperatures in the combustion zone. However the dilution which is desired for minimizing thermal stresses of the combustor materials has a limit below which it can compromise the heat duty of the flue gases for minimum permissible temperature difference in the heat exchanger flow streams. For purposes of heat exchanger analysis, the adiabatic temperature of 1626.2 K corresponding to the equivalent ratio of 0.25 is utilized as the flue gas temperature at the heat exchanger inlet. For optimization purposes in the heat exchanger, it is necessary to determine the values of hot gas flow rate alongside the adiabatic flame temperature since the heat transfer to the cold fluid is dependent on both. The stoichiometry of the combustion products determines the equilibrium concentrations and parameters of the combustion gas as revealed by the Aspen Plot wizard curves.

The analysis of combustion of the wood gas has revealed that high temperatures can be achieved in the combustor region. The heat exchanger and combustor integration process analysis has also shown good performance with the flue gases

from combustion of producer gas providing sufficient thermal energy needed to raise the turbine working fluid to the required turbine inlet temperature. The analysis of the heat exchanger has provided parameters essential for decision making on the sizing of the heat exchanger. The practical value added was revealing the parameters needed in the design specification of the heat exchanger suitable for the heat duty of a typical 100kW_e externally fired micro gas turbine based on gasification of biomass and subsequent producer gas combustion. The heat exchanger effectiveness of 0.635 was achieved in this parametric study. Due to high temperature involved in the process, materials that can withstand high temperature stresses have to be chosen.

The choice of a suitable Gasification system is driven by the need and local conditions at the target end user, keeping in mind that the system integration should have a good balance of being most efficient, cost effective, reliable, least polluting, sustainable in the long run and socially beneficial. Innovative systems which take into consideration the local conditions such as biomass fuel characteristics have shown great success in other countries. Therefore issues of unpredictable fuel behavior during thermochemical conversion, unreliable operating conditions, and low overall efficiency need to be addressed through continued research to make the gasification technology more attractive.

ACKNOWLEDGEMENT

This work was funded by the Norwegian Agency for Development Cooperation (NORAD) through the Energy and Petroleum (EnPe) Project, as part of the collaboration between The Norwegian University of Science and Technology (NTNU), Trondheim, Norway and Makerere University, Kampala, Uganda.

REFERENCES

- [1] D. Maraver, A. Sin, J. Royo, F. Sebastián. "Assessment of CCHP systems based on biomass combustion for small-scale applications through a review of the technology and analysis of energy efficiency parameters", *Applied Energy*, **102**, pp. 1303-1313, 2013.
- [2] D. Leilei, L. Hao, R. Saffa. "Development of small-scale and micro-scale biomass-fuelled CHP systems – A literature review", *Applied Thermal Engineering*, **29**, pp. 2119-2126, 2008.
- [3] J.H. Juan, A.A. Guadalupe, B. Antonio. "Gasification of biomass wastes in an entrained flow gasifier: Effect of the particle size and the residence time", *Fuel Processing Technology*, **91**, pp. 681-692, 2010.
- [4] M. Puig-Arnavat, C.B. Joan, C. Alberto. "Review and Analysis of Biomass Gasification models", *Renewable and Sustainable Energy Reviews*, **14**, pp. 2841-2851, 2010.
- [5] P.A. Pilavachi. "Power generation with gas turbine systems and combined heat and power", *Applied Thermal Engineering*, **20**, pp. 1421-1429, 2000.
- [6] A.M. Bassily. "Enhancing the efficiency and power of the triple-pressure reheat combined cycle by means of gas reheat, gas recuperation, and reduction of the irreversibility in the heat recovery steam generator", *Applied Energy*, **85**, pp. 1141-1162, 2008.
- [7] M. Kautz, H. Ulf. "The externally-fired gas-turbine (EFGT-Cycle) for decentralized use of biomass", *Applied Energy*, **84**, pp. 795-805, 2007.
- [8] M. Gaderer, G. Gallmetzer, H. Spliethoff. "Biomass fired hot air gas turbine with fluidized bed combustion", *Applied Thermal Engineering*, **30**, pp. 1594-1600, 2010.
- [9] A. Sommers, Q. Wang, X. Han, C. T'Joen, Y. Park, A. Jacobi. "Ceramics and ceramic matrix composites for heat exchangers in advanced thermal systems—A review", *Applied Thermal Engineering*, **30**, pp. 2137-2152, 2010.
- [10] F. Delattin, B. Svend, J.D. Ruyck. "Effects of steam injection on microturbine efficiency and performance", *Energy*, **33**, pp. 241-247, 2007.
- [11] W.B. Musinguzi, M.A.E. Okure, L. Wang, A. Sebbit, T. Løvås. "Thermal characterization of Uganda's *Acacia hockii*, *Combretum molle*, *Eucalyptus grandis* and *Terminalia glaucescens* for gasification", *Biomass and Bioenergy*, **46**, pp. 402-408, 2012.
- [12] W.B. Musinguzi, M.A.E. Okure, A. Sebbit, T. Løvås, I.P. Da Silva. "Thermodynamic Modeling of Allothermal Steam Gasification in a Downdraft Fixed-bed Gasifier", *Advanced Materials Research*, **875- 877**, pp. 1782 -1793, 2014.
- [13] G. Schuster, G. Löffler, K. Weigl, H. Hofbauer. "Biomass steam gasification – an extensive parametric modeling study", *Bioresource Technology*, **77**, pp. 71-79, 2001.
- [14] U. Kentaro, Y. Kouichi, N. Tomoaki, Y. Kunio. "High temperature steam-only gasification of woody biomass", *Applied Energy*, **87**, pp. 791-798, 2009.
- [15] D. Chiamonti, R. Giovanni, M. Francesco. "Preliminary design and economic analysis of a biomass fed micro-gas turbine plant for decentralized energy generation in Tuscany," Paper GT2004-53546, *The American Society of Mechanical Engineers (ASME) Turbo Expo proceedings*, Vienna, Austria, June 14-17, 2004.
- [16] C. Daniele, D. Paolo, C. Giorgio. "Performance evaluation of small size externally fired gas turbine (EFGT) power plants integrated with direct biomass dryers", *Energy*, **31**, pp. 1459-1471, 2005.
- [17] T. Lieuwen, V. McDonell, D. Santavicca, T. Sattelmayer. "Burner Development and Operability Issues Associated with Steady Flowing Syngas Fired Combustors", *Combustion Science Technology*, **180**, pp.1169-1192, 2008.
- [18] E.L. Keating. *Applied Combustion*. New York: Taylor & Francis Group, 2007.
- [19] A. Bejan, G. Tsatsaronis, M. Moran. *Thermal Design and Optimization*. New York: John Wiley and Sons Inc., 1996.



Behavior, cutting property and environmental load of machine tool in mist of strong alkaline water

机床在强碱性水雾中的行为，切割性能与环境负荷

Ikuro Tanabe^{1*}

¹Department of Mechanical Engineering, Nagaoka University of Technology, 1603-1 Kamitomioka Nagaoka Niigata, 940-2188 JAPAN

tanabe@mech.nagaokaut.ac.jp

Accepted for publication on 11th August 2016

Abstract - In the 21st century, as it is important to produce products with care for protecting the earth, a producer must be careful to conserve energy, save resources and reduce waste which pollutes environment. Further, in case of a machine tool, much lubricating oil was used for smooth drive, electrical energy of forced cooling was used for high accuracy and much cutting oil was also used for lubrication and cooling. This is a large problem for protecting the earth. Therefore, the behavior of a machine tool in the mist of strong alkaline water was investigated and evaluated. Properties of strong alkaline water were firstly investigated for alkali-proof, corrosion and safety of health. Then the bench lathe was remodeled in the vessel with the mist of strong alkaline water (pH12.5), thermal deformation between the spindle and the tool post was measured for evaluation of accuracy. And cutting using CNC milling machine in the vessel with the mist of strong alkaline water was performed for investigating the effect of water evaporation in the strong alkaline water. It is concluded from the results that; (1) Alkali-proof regarding several elements of a machine tool and safety of health were cleared in the experiment, (2) The forced cooling using mist of strong alkaline water had a very strong influence. Thus, it could be said that the thermal deformation of structure can be effectively cooled by using a mist of strong alkaline water, (3) Thermal deformation of the bench lathe was very small despite no-forced cooling, (4) Accuracy of the machine tool was very good and the tool life was very long despite no-cutting oil, (5) Mist of strong alkaline was eco-friendly.

Keywords - forced cooling, machine tool, high accuracy, strong alkaline water, cutting, eco-Friendly

I. INTRODUCTION

Since the beginning of the 21st century, the importance to manufacture products in an environmentally-conscious [1] way has been highlighted. In this regard, manufacturers not only need to conserve energy, but they also need to scrutinize in order to save resources and reduce environmentally-harmful pollutants. Nowadays, there are many researches related to the environmental impact of men [2], as well as countermeasures

to reduce it [3]; however, these are still insufficient. Particularly, in the field of manufacturing, most machine tools highly depend on cutting and cooling oils to achieve the high accuracy. This represents a large environmental problem, since in most cases the cutting and cooling oils are misused, introduced into the environment and generate undesired pollution [4]. Consequently, the importance of developing new manufacturing ideas that consider parameters such as high accuracy, high quality and a low environmental impact had been underlined. Hence, manufacturers will be in the need of daring plans, unique ideas and new technologies [5].

Therefore, even though the cutting concept of this research is *ecology*, it also included other concepts related to the industrial sector. Among these are: suitable cost of a machine tool, low running and maintenance cost with high precision machining. Thus, this study is to achieve the application of the *ecology* and multiple industrial sector-related concepts, in conjunction with the advances of production engineering technology. For instance, regarding machine tool technology, while restraint of the thermal deformation on a machine tool was attempted to achieve high accuracy and quality, it was at the expense of using costly equipment and a large quantity of electrical energy. Even then, those countermeasures taken were not enough to satisfy these parameters [6].

Therefore, behavior of a machine tool in mist of strong alkaline water were investigated and evaluated. Properties of strong alkaline water were firstly investigated for alkali-proof, corrosion and safety of health. Then the bench lathe was remodeled in the vessel with mist of strong alkaline water (pH12.5), thermal deformation between the spindle and the tool post was measured for evaluation of accuracy. And cutting using CNC milling machine in the vessel with mist of strong alkaline water was performed for investigating the effect of water evaporation in the strong alkaline water.

II. THE CORROSION RESISTANCE OF MATERIALS IN STRONG ALKALINE WATER

The strong alkali water with pH value above 12.5 has high interfacial permeability, dissolving, emulsification, and separation properties. For these properties, it is well using for washing, sterilization, corruption prevention. Moreover, when strong alkaline water is kept long time in the air, it lost alkali property and become normal water of pH 7.0. This fact also regarded as very excellent for using it as cleaning agent with improved environmental protection.

In this section, the reactions of the various materials in strong alkaline water are tested. The specification of the device for making alkaline water is shown in Table 1. It is small and compact for making alkaline water of pH12.5. Fig. 1 shows the measurement results of pH values for keeping 10 L of strong alkaline water (pH12.5) in three containers (diameter ϕ 25 mm, height 230 mm) and kept exposed to air for 2 months, in three different environment conditions. These conditions are different temperatures of 20°C, 40°C and 12°C with humidity 60% respectively. It is confirmed that the change in pH value even for the most decreasing condition with 40°C is just drop from pH 12.5 to pH12.0 during two months experiment. In the practical application of this method, there exist natural evaporation and evaporation due to generated cutting heat and it is necessary to fill up alkaline water to keep maintain the amount and pH value of water. However, from this experiment, it can be considered that this decreasing rate of pH value is quite enough to endure for the practical application of proposed method.

In the corrosion engineering, logarithmic value of metal ion concentration lesser than (-6) could not be corroded at equilibrium state. Here, according to the corrosion characteristic [7] of strong alkaline water, steel could not corrode in the alkaline water above pH10. Similarly, Nickel in the Nickel based alloys shows no chemical reaction in the range of pH8.5~pH13.0. Moreover, titanium alloys also shows no effect under pH13.0 range. From these facts, it can be considered that it is possible to operate underwater metal

cutting processing of Titanium and Nickel alloy materials for compulsory water evaporative cooling with using the optimum range of pH values between pH10.0~pH13.0. The corrosion characteristics of these materials are also confirmed by experiment.

In the experiment, the tested materials are steel, titanium alloy, nickel alloy and those being used well in industries such as, copper, aluminum, brass and carbide (tool material) as shown in Table 3.

These materials are put in the test tubes containing water with three pH values, pH7.0, pH10.0, pH12.5 and keep in a room with constant temperature of 20 ± 1 °C and 60% moisture for two months (see Table 2). The pH value is made to kept constant by changing alkaline water once per week.

The result of the experiment regarding to alkali resistance of the materials are shown in Table 3. The results shown there was no corrosion exhibit for the tested materials placing inside strong alkaline water for two months except aluminum. From this result, it was confirmed that the underwater cutting process for titanium alloys and nickel alloys can be applicable for compulsory tool cooling effect with the exception of aluminum. For cutting aluminum, it is necessary to take precaution and improvement as it is corroded in strong alkaline water. For the case of copper and brass, there occurred change in color.

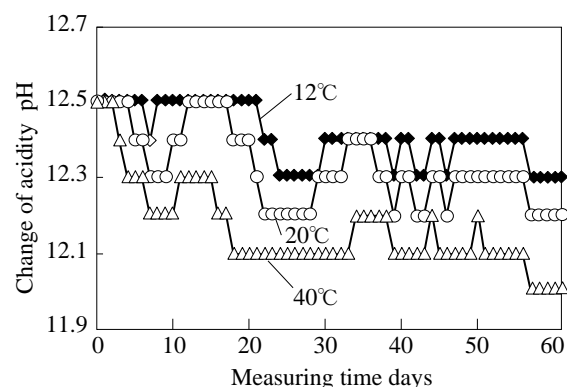


Fig. 1 Variation of pH values in different temperatures

Table 1 Specification of the system for making strong alkaline water and safty of health for strong alkaline water

Method of generation	Closed generation type	Assistant material	Potassium carbonate
Value of pH	pH 12.5	Safety of health	○ Odourless
Quantity of generation	10 ℓ/h		△ Wear gloves & glasses
Voltage & Power	100 V & 300W		△ Wear mask
Size	495W × 430D × 1100H		×

○ : No problem △ : Avoid × : Prohibition

Table 2 Materials and conditions used in corrosion test

Medium in the vessel	Strong alkaline water (pH 12.5)
Ambient conditions	Room temp.: 20 ± 1 °C, Humidity: 60%
Period	Two months

Table 3 Results of the proof test for two month in alkaline water with pH12.5

Machine tool structure	S45C	○	Changeless condition	Machine element	Rubber bushing	○	Changeless condition
	SUS304	○	Changeless condition		Exhaust cleaner	×	Corrode and discoloration
	Cast iron	○	Changeless condition		Thinned cylinder	△	Only screw corroded
Work piece	Ti	○	Changeless condition	Air chack	○	Changeless condition Same function	
	Ti6Al4V	○	Changeless condition	Check valve	△	Only screw corroded	
	Inconel 718	○	Changeless condition	Lubricator	○	Changeless condition Same function	
	S45C	○	Changeless condition	Regulator	△	Only screw corroded	
Tool	Copper	△	Only discoloration	Push-button switch	△	Terminal corroded Screw corroded	
	Brass	△	Only discoloration	Command switch	△	Terminal corroded Screw corroded	
	Aluminum	×	Corrode	Optoelectronic switch amplifier	△	Terminal corroded Screw corroded	
Coating material of tool	HSS	○	Changeless condition	Servomotor	△	Only screw corroded	
	Carbide	○	Changeless condition	Box terminal	○	Changeless condition	
	Cermet	○	Changeless condition	Electromagnetic contactor	×	Electromagnet corroded	
	Diamond	○	Changeless condition	Solenoid valve	△	Only discoloration	
	CBN	○	Changeless condition	Solenoid valve base	△	Only discoloration	
	Ceramic	○	Changeless condition	Flat cable	○	Changeless condition	
Machine element	DLC	○	Changeless condition	Cable connector	○	Changeless condition	
	Ti AlN	×	Discoloration	Direct acting two port solenoid valve	△	Only screw corroded and discoloration	
	TiAlCr	×	Discoloration	Basic material	Acrylic acid resin	○	Changeless condition
	V-belt	×	Small crack		Vinyl chloride	○	Changeless condition
	Drive belt	○	Changeless condition Same function		Nylon	○	Changeless condition
	Timing belt	○	Changeless condition Same function		Polyurethane	○	Changeless condition
	O-ring	○	Changeless condition Same function		Polycarbonate	○	Changeless condition
	Bearing	○	Changeless condition		Nitrile rubber	○	Changeless condition
	Linear guide	○	Changeless condition Same function		Polyurethane rubber	○	Changeless condition
	Ball screw	○	Changeless condition Same function		Fluoro rubber	○	Changeless condition
Oil seal	△	Spring corroded	Chloroprene rubber		○	Changeless condition	
Oil pump	×	Terminal corroded No work	Chlorosulfonated Polyethylene rubber,		○	Changeless condition	
Paint	Wire hose	○	Changeless condition	Oilproof vinyl mixture	○	Changeless condition	
	Excel hose	○	Changeless condition	Urethane elastomer	○	Changeless condition	
	Cap connector	△	Only screw corroded	Paint	Lacquer paint	○	Changeless condition
	Tube fitting	○	Changeless condition		Urethane resin paint	○	Changeless condition
	Oil level gauge	○	Changeless condition		Epoxy resin paint	○	Changeless condition

○ : Enable △ : Only discoloration or only screw corroded × : Disable

III. COOLING PROPERTY FOR MIST WITH STRONG ALKALINE WATER

New nozzle was manufactured for making mist of strong alkaline water such as Fig. 2. The nozzle consists of an air tube (1x7 mm) and a tube (7x7 mm) of strong alkaline water. Then cooling property for mist with strong alkaline water was measured in experiment. Experimental set-up is shown in Fig. 3. A sensor for measuring heat transfer coefficient and a manufactured nozzle were set in the center of the vessel (556x386x310 mm). Sensor for measuring heat transfer coefficient is self consists of a ceramic heater (5x5x1.75 mm), two steel plates (5x5x0.06 mm) and 4 thermo-couples. The ceramic heater got caught between both two steel plates and is inputted electric power E (7.8 W). At this time, temperature on the steel plate becomes about 100 °C in the air. Two thermo-couples are measured temperatures T_{w1} and T_{w2} on the center of the each steel plate respectively. Other two thermo-couples are measured temperatures T_{M1} and T_{M2} of mist with strong alkaline water on the 5 mm distance from the each steel plate respectively. Heat transfer coefficient α is calculated by equation (1).

$$\alpha = \left(\frac{E / 2}{A (T_{w1} - T_{M1})} + \frac{E / 2}{A (T_{w2} - T_{M2})} \right) / 2 \quad (1)$$

where A (5x5 mm) is area of steel plate. Average of heat transfer coefficient on twice steel plates is calculated. Because influence of radiation is also included in this heat transfer coefficient, this value is appearance heat transfer coefficient. However we thought that this is used for evaluation of cooling property because of similar condition to several manufacturing or machining fields.

Furthermore, the existing relationship between the heat transfer coefficient and the mixture ratio of air and strong alkaline water is shown in Fig. 4. In this case, the length L from output nozzle to measuring point was 225 mm. Moreover, the parameter considered here is the total flow rate of strong alkaline water. There are two plots in this figure; one is the mist condition (fine strong alkaline water) which has very

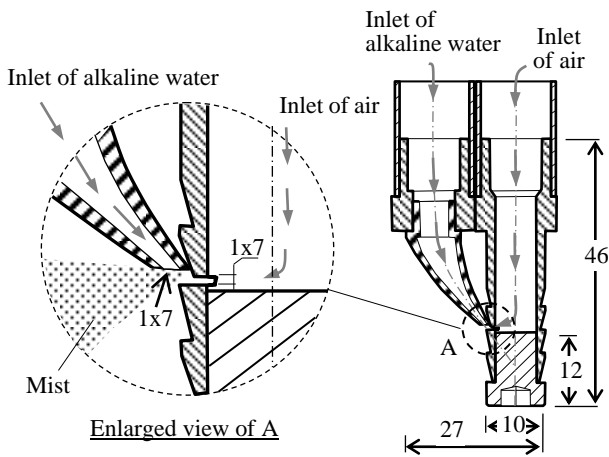


Fig. 2 Schematic view of nozzle for mist of strong alkaline water

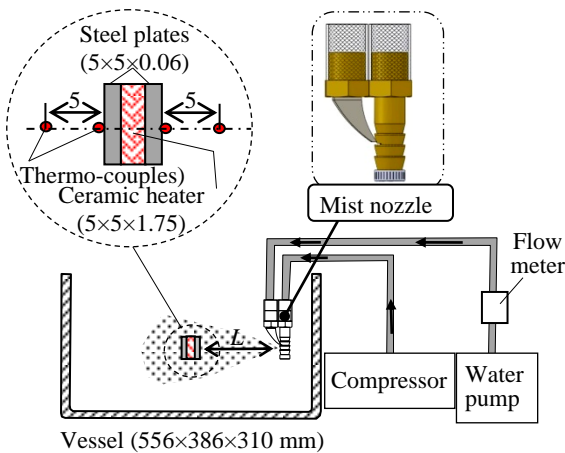


Fig.3 Experimental set-up for measuring heat transfer coefficient regarding mist of strong alkaline water

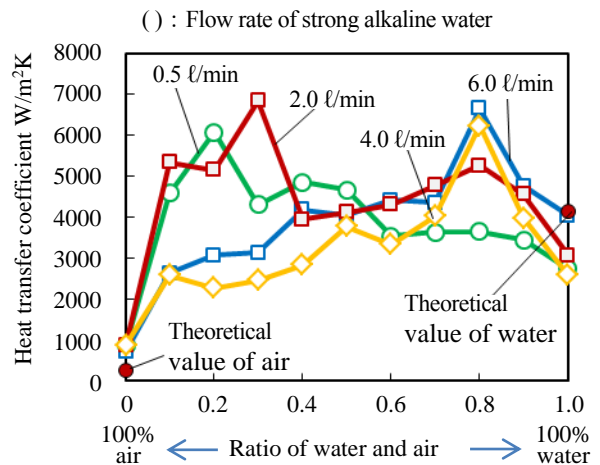


Fig. 4 Relationship between the heat transfer coefficient and the mixture ratio of air and strong alkaline water

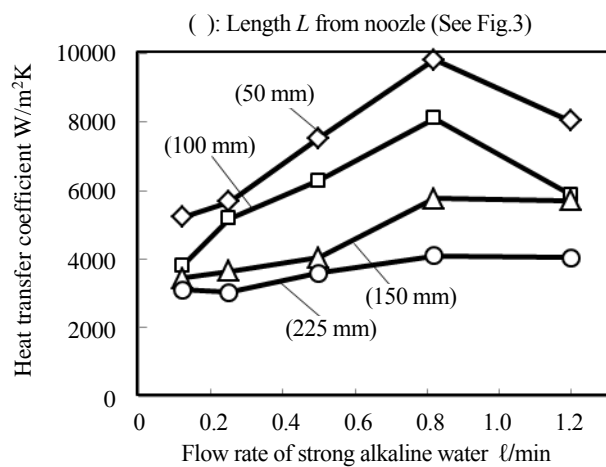


Fig.5 Relationship between the heat transfer coefficient and the optimum amount of air and strong alkaline water

large forced cooling effect because of the heat of vaporization, and the other one is the fluid condition (fine air pockets) which has a very large heat transfer coefficient because it presents a high speed.

The relationship between the heat transfer coefficient and the optimum amount of air and strong alkaline water is shown in Fig. 5. The parameter considered here is length L mm from output nozzle to measuring point. When the distance (L) becomes smaller, the heat transfer coefficient becomes larger. In this figure, there is a peak in each plot near 0.8 l/min of total flow rate of strong alkaline water, and when amount of air is 113.3 l/min, the total flow rate of strong alkaline water is 0.82 l/min. At this point, the distance L mm from output nozzle to measuring point is 50 mm, and the heat transfer coefficient is about 10000 W/m²K. These results clearly show that the forced cooling using mist of strong alkaline water has a very strong influence. Thus, it can be said that the thermal deformation of structure can be effectively cooled by using a mist of strong alkaline water.

IV. EVALUATION OF MANUFACTURING IN MIST OF STRONG ALKALINE WATER

The cutting fluids [8] or MQL (minimum quantity lubrication) [9] are commonly used for forced cooling during multiple processes. However, most cutting fluids pollute the environment and most MQL agents cooling performance is inferior to other cooling alternatives. In this research, a forced cooling method using a mist of strong alkaline water for restraining thermal deformation on a machine tool was developed and evaluated for only cooling effect. Additionally, among the reasons to choose strong alkaline water are that it shows a pH value above 12.5, has high interfacial permeability, dissolving, emulsification, and separation properties. Furthermore, after multiple corrosion tests of different machine tool components and materials for up to 2 months, it was observed that most components did not corrode under the influence of strong alkaline water. In contrast, it had a very large cooling effect because vaporization of the mist occurred due to the heat involved. Thus, mist of strong alkaline water was supplied around the structure of the machine tool and the machining area, in order to restrain the thermal deformation and alleviate the heat generation during machining. Accordingly, a bench lathe and a CNC milling machine were used for the experimentation. In the first instance, thermal deformation of the bench lathe was measured to evaluate the forced cooling effect that the mist of strong alkaline water possesses. Subsequently, the effects of mist of strong alkaline water were also evaluated with respect to the tool temperature during cutting, surface roughness and the tool life parameters on a CNC milling machine [10]. In this regard, the entirety of the experimental data and further explanation about it can be consulted in a parallel research [10].

4.1. THERMAL DEFORMATION OF BENCH LATHE IN MIST OF STRONG ALKALINE WATER

Thermal deformation cause by heat from the friction of bearing unit can affect the machining accuracy of final cutting result. Here, the thermal deformation of bench lathe in the mist of strong alkaline water was measured.

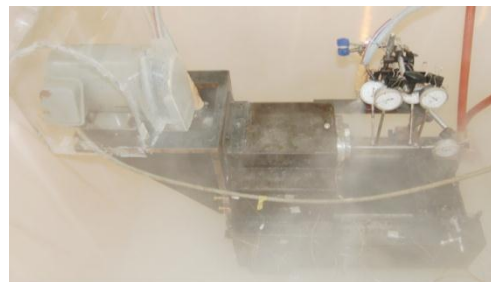
The same setup of bench lathe machine showed in Table 4 and Fig. 6 was used. There are 2 photographs before and after supplying mist of strong alkaline water in Fig. 6. The bench lathe is installed in vessel which sizes are L 1190×W 980×H 790 mm. The detail setup for this experiment is shown in Fig.7. Test bar was inserted into lathe chuck and the 4 dial gauges were used to measure the displacement of the test bar in horizontal and vertical direction during experiment. The experiment data was taken by compare between dry condition and using mist of strong alkaline water. The bench lathe was operated at spindle speeds 3600 min⁻¹. Red circles are positions of thermo-couples for measuring temperatures on the machine structure. The developed nozzles were set up on near centers of front and rear surfaces of the head stock. The mixed air (113.3 l/min) and strong alkaline water (0.82 l/min) is supplied by each nozzle. Distance between the nozzle and the machine structure is 50 mm.

Table 4 Specification of the bench lathe in the experiment

Head stock	Height of center from bed	177 mm
	Height of center from floor	337 mm
	Spindle speed	Max. 3600 min ⁻¹
Bed	Size (W×L×H)	600×360×660
Tool	Stroke of Y axis	30 mm
Table	Stroke of Z axis	200 mm
Motor	Power	0.75 kW
	Mass	200 kg



(a) Without mist of strong alkali water



(b) With mist of strong alkali water

Fig. 6 Photograph of the experimental setup

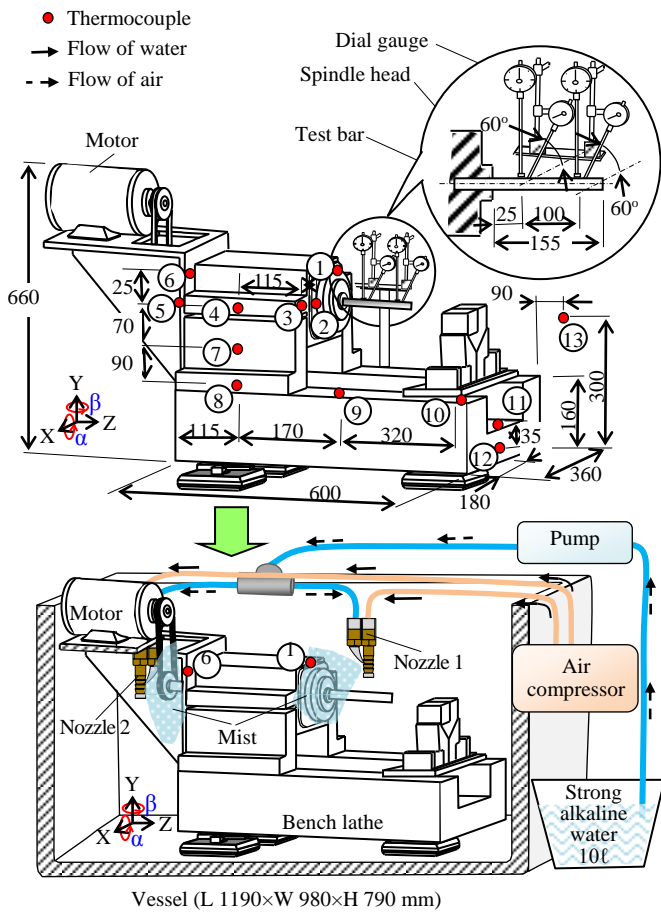


Fig. 7 Schematic view of the experiment using the bench lathe in strong alkali water mist

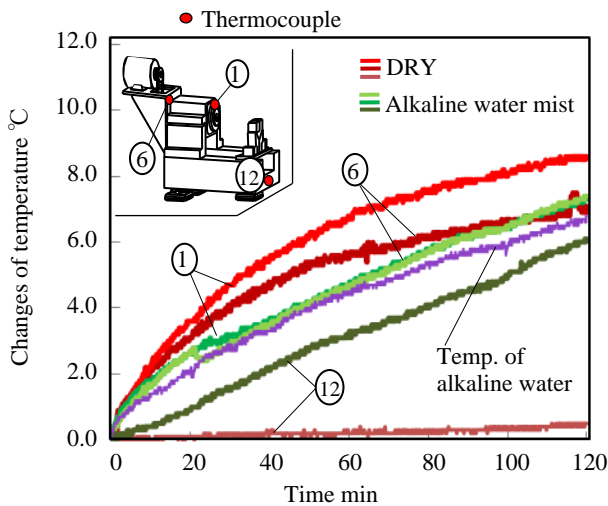
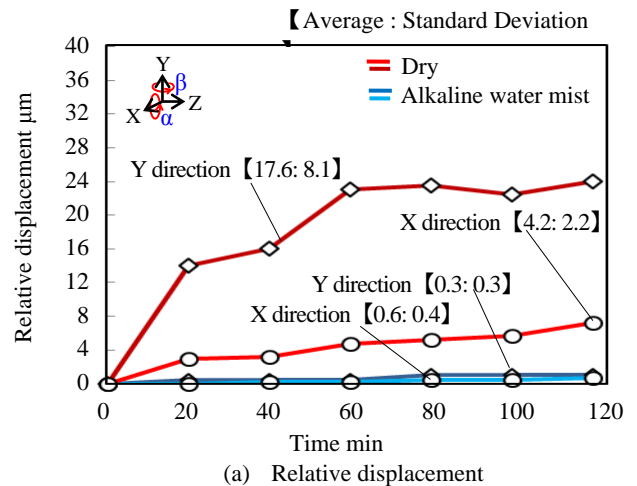


Fig. 8 Temperature change of the bench lathe using strong alkaline water mist operated in 3600 min⁻¹

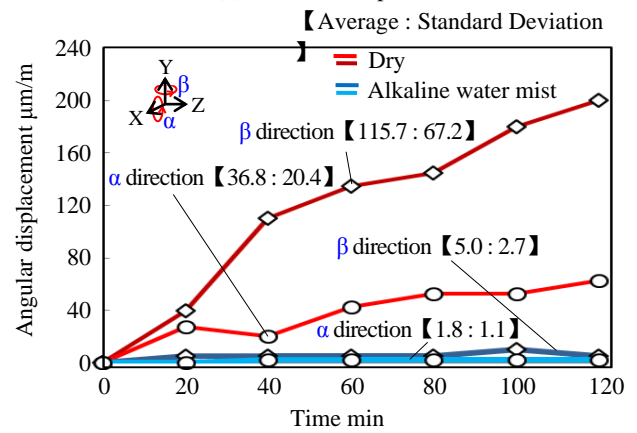
Fig. 8 shows the experimental result of the temperature on the bench lathe at spindle tip surface ①, ⑥ and end of bed ⑫. At spindle speed 3600 min⁻¹, the rise in temperature

(the maximum values at steady state condition) at the spindle tip surface ① which is the most influencing part of the machining accuracy were 8.3°C at dry cutting, 6.4°C for mist of strong alkaline. Temperature rising for mist of strong alkaline occurred because the heat generated by microbubble device caused the pump become warm during continuously operation in two hours. At that time, if the forced cooling is used, temperature rising is restrained. However the forced cooling is never used in this research, because this research is performed for earth-friendly. In case of dry cutting, as temperature distribution on the machine structure is very large, thermal deformation will also become very large. On the other hand, in case of mist of strong alkaline water, as temperature distribution is very small, thermal deformation will also become very small.

The relative displacement (X and Y directions) and angular displacement (α and β directions) of the tip of test bar measured at operation a speed 3600 min⁻¹ are shown in Fig. 9. In the same way, the data between 20 min to 120 min were divided into 6 intervals and the average values and standard deviations of each of the six intervals are plotted. The results show that, in dry cutting, relative displacements are large with $\Delta X=6.0\mu\text{m}$, $\Delta Y=24.0\mu\text{m}$ and angular displacements were $\alpha=55\mu\text{m/m}$ and $\beta=200\mu\text{m/m}$, in mist of strong alkaline water, the relative displacements are $\Delta X=0.6\mu\text{m}$, $\Delta Y=0.9$



(a) Relative displacement



(b) Angular displacement

Fig. 9. Thermal deformation of the bench lathe in strong alkaline water mist at 3600min⁻¹

μm and angular displacements are $\alpha=3.6 \mu\text{m}/\text{m}$ and $\beta=9.0 \mu\text{m}/\text{m}$. This means that, when operated under a mist of strong alkaline water, the thermal deformations due to operation speeds reduced significantly. However, since standard deviations are very small in this case, temperature changes are also very small and therefore thermal behavior highly stable.

These results clearly show that relative displacement and angular displacement were restrained by using mist of strong alkaline water and showed a very strong influence. Therefore, it can be said that by using mist of strong alkaline water in bench lathe, the thermal deformation of machine structure can be effectively suppressed and resulting in a high machining accuracy.

4.2. CUTTING PROPERTY OF CNC MILLING MACHINE IN STRONG ALKALINE WATER

Cutting area on the CNC milling machine was filled by mist of strong alkaline water, and two tool temperatures were measured for evaluation of cooling property. Cutting conditions for tool temperature measurement are shown in Table 5. This is middle cutting. Experimental set-up is shown in Fig. 10. Amount of air is 113.3 ℓ /min, total flow rate of strong alkaline water is 0.82 ℓ /min and L mm from output nozzle to measuring point is 50 mm. Workpiece was fixed to the spindle and tool was set to the vise on the table, because it is that the tool temperatures were measured without a hitch by thermo-couples. Then temperature on the top of the tool was estimated by the measured temperatures and FEM analysis. Here the tool model is firstly made, and tool temperatures with transient state are calculated by FEM analysis.

Table 5 Cutting conditions for tool temperature measurement

Cutting conditions		
Cutting speed 80 m/min	Feed speed 0.25 mm/rev	Depth of cut 0.4 mm
Work piece		
Material : S50C		
Tool (Bite)		
Rake angle: 5°	Coated carbide	

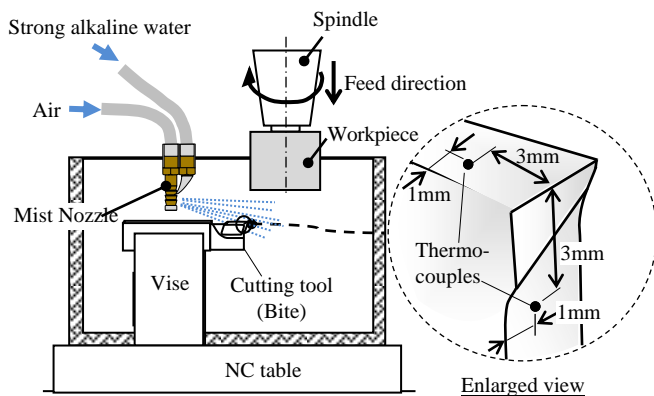


Fig. 10 Experimental setup for measurement of tool temperature

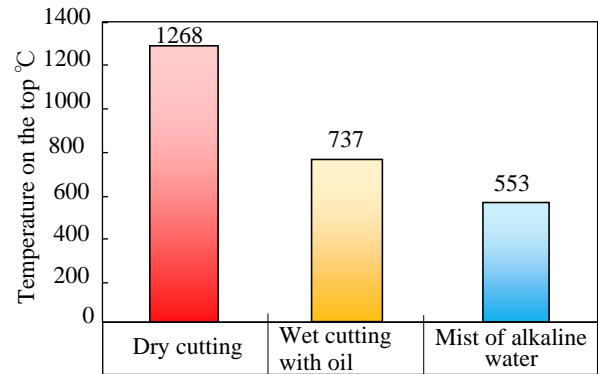


Fig. 11 Experimental results for temperature on the top

At that time, heat transfer coefficient and heat generation on the top of the tool for input data are changed one by one. When the result of the FEM analysis became same to the result of the two measured temperature, the calculated temperature on the top of the tool is adopted for its temperature.

Temperatures on the top of the tool were shown in Fig. 11. Dry cutting and wet cutting with oil were also shown for reference. Material of the used tool is coated carbide and its optimum temperature for cutting is about 800 °C. Temperature on the top of the tool using mist of strong alkaline water was 44% of one of dry cutting and 75% of one of wet cutting with oil respectively. Mist of strong alkaline water is effective method for cooling tool.

Tool life for evaluation of cutting using mist of strong alkaline water was performed. Cutting conditions for tool life test are shown in Table 6. This is middle cutting. Experimental set-up is shown in Fig. 12. Amount of air is 113.3 ℓ /min, total flow rate of strong alkaline water is 0.82 ℓ /min and L mm from output nozzle to measuring point is 50 mm. Dry cutting and wet cutting with oil were also performed for reference. End-mill with 2 throw away tips was used for milling machining, because it is easy and certain for judgment of limit of tool life.

Table 6 Cutting conditions for tool life measurement

Cutting conditions			
Cutting speed 100 m/min	Feed/ tooth 0.15 mm/tooth	Width of cut 3 mm	Depth of cut 2 mm
Work piece			
Material : S50C			
Tool (Endmill with 2 throw away tips)			
Rake angle: 5°	Coated carbide		

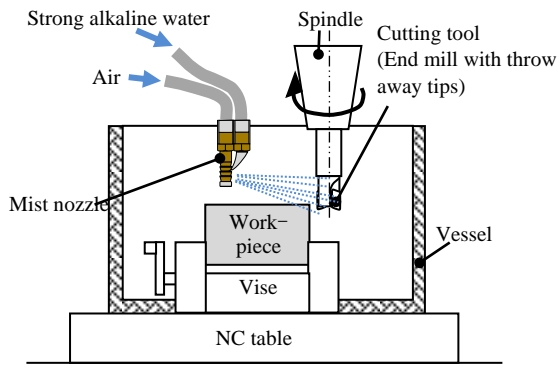


Fig. 12 Experimental set-up for measurement of tool life and surface roughness

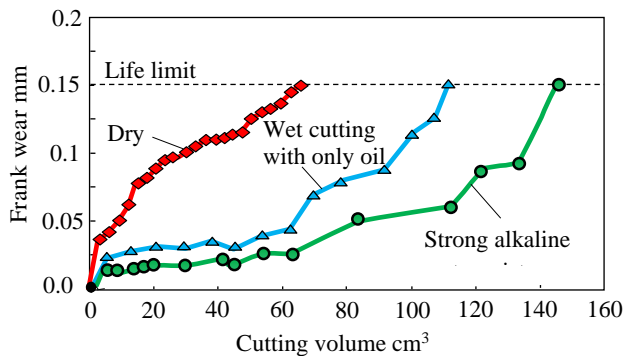


Fig. 13 Results of tool life test

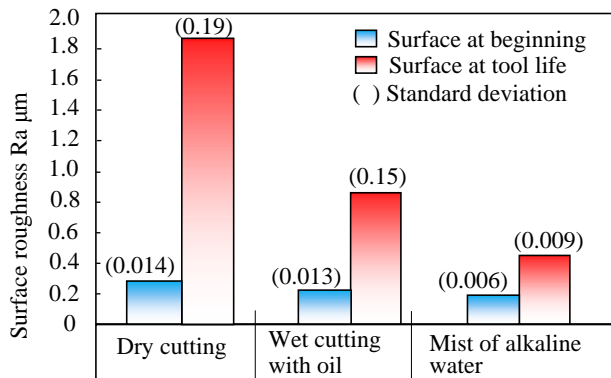


Fig. 14 Results of surface roughness

Similarly, the results of the tool life test were shown in Fig. 13 and dry cutting and oil wet cutting were also shown for reference. It was observed that that the tool life of the tool using mist of strong alkaline water was 2.5 times of one of dry cutting and 1.4 times of one of wet cutting with only oil respectively. Hence, it is thought that a mist of strong alkaline water is an effective method for extending the tool life during machining. To support this, in the case of the cutting using mist of strong alkaline water, defects were not observable in the microscope.

In addition, surface roughness test results are shown in Fig. 14 and dry cutting and wet cutting with only oil were also shown for reference. After machining, surface roughness on the workpiece using mist of strong alkaline at limit of tool life water was 22 % of one of dry cutting and 50 % times of one of wet cutting with only oil respectively. Surface roughness on the workpiece using mist of strong alkaline at start of the test is similar to that of dry cutting and wet cutting with only oil. However, a mist of strong alkaline water is thought to be an effective method for the improvement of surface roughness on the workpiece. Thus, it can be said that by using practice CNC milling machine with mist of strong alkaline water, the heat generation for cutting can be effectively removed; resulting in a low tool temperature, long tool life and fine surface roughness.

Lastly, nevertheless, a deep understanding of the thermodynamics field was also necessary to evaluate the water evaporation effect. Similarly, the alkaline water mist employed in this research also made use of the chemical engineering field. In the end, this makes the technology an environmentally-friendly and affordable one by reducing parameters that involve higher costs.

V. EVALUATION AND CONSIDERATION FOR MANUFACTURING IN MIST OF STRONG ALKALINE WATER

Since the developed technology was created to support the intensity of production at a low-environmental impact level with the highest cost-effectiveness, in this section both the environmental and economic aspects of this technology will be assessed. In the first instance, the proposed model evaluates the degree of how “environmentally-friendly” a technology is through the CO₂ emissions involved. On the other hand, the economic aspect of the presented technologies will be based on a general overview of the technical requirements involved in this research.

Firstly, the environmental impact of this technology will be assessed based on a comparison of the amount of exhaust CO₂ using the proposed and conventional cooling. This was calculated through the relationship between the electricity consumption per hour and the CO₂ emissions. For this, it was considered that the electricity used by the coolant pump on the milling machine during conventional wet cutting was 1.2kW per hour and a working year being composed of 250 days and 8-hours per day. Furthermore, the amount of CO₂ emissions, CL_{CO_2} , is calculated by using the equation (2).

$$CL_{CO_2} = 0.468 \times W_E \tag{2}$$

Where, W_E is the amount of used electricity (kWh) used in coolant pump and 0.468 the conversion value for kg-CO₂/kWh.

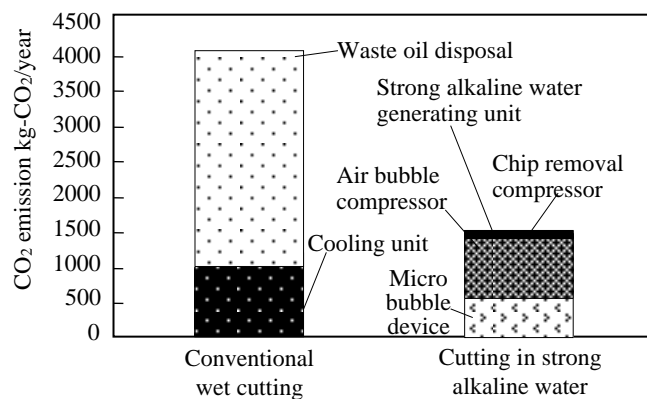


Fig. 15 Comparison of CO₂ emissions (Environment)

Table 7 General overview of proposed cooling and the conventional cooling expenses (Cost-profit)

Cooling method	Proposed cooling	Conventional cooling
Cooling capacity	Very large ◎	Average △
Initial cost	Alkaline water Pump ○	Refrigerator ×
Running cost	Oil supply × Electricity ×	Oil supply × Electricity ×
Maintenance	Little ◎	Need ×
Remarks	Low-environmental impact and profitable	High-environmental impact

◎ : Excellent, ○ : Good, × : Weak

The corresponding calculated amount of CO₂ emissions for the coolant pump is 1123.2 kg-CO₂. Subsequently, the amount of CO₂ emissions due to the oil disposal was calculated. In this case, the amount of oil is assumed to be 340 L and disposal times to be 2 times/year a year. However, milling machines require a monthly oil fill-up which is assumed to be 30 l a month (30 l × 12 month = 360 l). Hence, the total amount of disposed oil was assumed to be 1040 l and the CO₂ emissions were calculated based on this value and using the equation (3) [11].

$$CO_2 \text{ emission (kg-CO}_2) = \text{Disposed oil k}\ell \times \text{Emitted heat energy GJ/k}\ell \times \text{Carbon emission t-C/TJ} \times (44 \div 12) \quad (3)$$

Where, the emitted heat energy is 40.2 GJ / kℓ and the amount of carbon emission is 19.22 t-C / TJ, and by using equation (2), the amount of CO₂ emission due to disposed oil was calculated and a value of 2946.3 kg-CO₂ was obtained. Therefore, the total amount of CO₂ emitted from both cases was 4069.5 kg-CO₂. Furthermore, the comparison between the conventional wet cutting method and the proposed method is shown in Fig. 15.

In contrast, the amount of CO₂ emissions of cutting in strong alkaline water mist can be reduced to 2634.9 kg-CO₂,

(64.7 % reduced) in a year. This is due to the less power consumption for the cooling of the tool; as well as, the lower emissions that represent not using cutting oil in the proposed method. Thus, it can be considered that this method is not only effective in cooling the machine tool but also capable of reducing the impact to the environment.

Ultimately, a comparison between the expenses involved in the proposed cooling and the conventional cooling during machining is shown in Table 7. It can be noted that the proposal is more affordable, given that the initial costs would be considerably less because of the low market price of alkaline water. Thus, the proposed system goal of simultaneously reaching a “highly cost-effective” and “environmentally-friendly” technology is achieved.

VI. CONCLUSION

From this research, the following was possible to conclude; (1) Alkali-proof regarding several elements of a machine tool were cleared in the experiment.

(2) Thermal deformation of the bench lathe for bathing was very small in spite of no-forced cooling.

(3) Accuracy of the machine tool was very good and the tool life was very long in spite of no-cutting oil

(4) The application into real production engineering problems and technology is proposed and presented “Forced cooling using mist of strong alkaline water” researches.

(5) It was concluded from the experimental results of this technology, that improvements in the environmental pollution, mechanical properties and cost parameters were achieved through the proposed research.

REFERENCES

- [1] Tanabe I. and Hong M. T. “Cutting with an environment-friendly cooling method using water evaporation”, Transactions of Japan Society of Mechanical Engineers, Vol. 67 No.664, Series C , pp. 4011–4016(in Japanese), 2001.
田辺郁男, TRUONG HONG Mihn, 環境にやさしい気化熱冷却を用いた切削加工, 日本機械学会論文集 C 編, Vol. 67, No. 664 pp.4011-4016, 2001.
- [2] e-Gov Japan, Ordinance related to calculation for carbon dioxide equivalent greenhouse gas emissions with their business activities of specified emitters, Article 2 (2013), available from <<http://law.e-gov.go.jp/htmldata/H18/H18F15002002003.html>> (accessed on 22 April, 2014) (in Japanese).
e-Gov, 特定排出者の事業活動に伴う温室効果ガスの排出量の算定に関する省令第2条 (2013), available from <<http://law.e-gov.go.jp/htmldata/H18/H18F15002002003.html>> (参照日2014年4月22日).
- [3] Tanabe I., Truong H. M., Yoshii K. “Turning with environment-friendly cooling method using water evaporation”, Transactions of the Japan Society of Mechanical Engineer, Series C, Vol. 66, No. 643, pp. 1026-1030(in Japanese), 2000.

- 田辺郁男, TRUONG HONG Mihn, 吉井一夫, 環境にやさしい気化熱冷却を用いた切削加工 (第1報, 気化熱冷却の効果と旋盤チップ冷却への適用), 日本機械学会論文集 C編, Vol. 66, No. 643, pp.1026-1030, 2000.
- [4] Tanabe, I., Ikeda, S. and Urano, K., Estimation of optimum temperature for cooling oil on a spindle using inverse analysis of neural network (Effect of relearning), Transactions of Japan Society of Mechanical Engineers, Series C, Vol. 69, No.679, pp. 819-824 (in Japanese), 2003.
田辺郁男, 池田祥生, 浦野好市, ニューラルネットワークの逆解法による主軸冷却油最適温度の推定 (再学習の効果), 日本機械学会論文集 C編, Vol. 69, No. 679, pp.819-824, 2003.
- [5] Tanabe I., Yamanaka K., Mizutani J. and Yamada Y. "A new design of lathe structure for reducing thermal deformation (Design of zero-center on three directions, self-compulsory cooling and design of thermal synchronism)", Transactions of Japan Society of Mechanical Engineers (Series C), Vol. 65, No.639, pp. 4508-4513 (in Japanese),1999.
田辺郁男, 山中邦彦, 水谷淳之介, 山田泰宏, 熱変形抑制のための新しい旋盤構造設計 (三次元零芯設計, セルフ強制冷却, 熱同期設計), 日本機械学会論文集 C編, Vol. 65, No. 639, pp.4508-4513, 1999.
- [6] Tanabe I., Ye H. S., Iyama T. and Abe Y. "Control of tool temperature using neural network for machining work-piece with low thermal conductivity", Transactions of Japan Society of Mechanical Engineers (Series C), Vol. 77, No.776, pp. 1556-1564 (in Japanese), 2011.
田辺郁男, イエー・トット・ソー, 井山徹郎, 阿部洋太朗, 低熱伝導材料加工のためのニューラルネットワークを用いた工具温度管理, 日本機械学会論文集 C編, Vol. 77, No. 776, pp.1556-1564, 2011.
- [7] Shiddaira S., Material science for corrosion and corrosion resistance (in Japanese), AGNE technological center, pp.30-32, 255-257, 287-288, 1995.
下平三郎, 腐食・防食の材料科学, アグネ技術センター, pp.30-32, 255-257, 287-288, 1995.
- [8] Shintani S., Hand book for cutting fluid, Kogyo Chosakai Publishing Co., Ltd., (2004), pp. 33-48 (in Japanese).
新谷滋記, 切削油剤ハンドブック, 株式会社工業調査会, pp. 33-48, 2004.
- [9] Okada M., Hosokawa A., Asakawa N., Fujita Y. and Ueda T. "Influence of minimum quantity lubrication on tool temperature in end milling of difficult-to-cut materials having low thermal conductivity", Transactions of Japan Society of Mechanical Engineers (Series C), Vol. 78, No.792, pp. 3093-3103 (in Japanese), 2012.
岡田将人, 細川晃, 浅川直紀, 藤田祐介, 上田隆司, 低熱伝導率難削材のエンドミル加工におけるMQLの工具温度への影響, 日本機械学会論文集C編, Vol. 78, No. 792(2012), pp.3093-3103.
- [10] Tanabe I. "Development of forced cooling using mist of strong alkaline water for restraining thermal deformation on a machine tool", MM-science journal, DECEMBER , pp. 521-526, 2014.
- [11] Enviroment agency, "Law (enforce No3) for Global Warming Countermeasures in Japan-(Exhaust coefficient list)", 2006.



Korea's policies, R&D investment and competitiveness in the LED industry

韩国在光敏二极管行业的政策，研发投资和竞争力

Joon Han(韓準)¹, Chul-Ho Park(朴哲皐)^{1*}, Ji-Sun Ku(具智善)¹, Ho-Sik Chon(全浩植)²

¹ Center for Climate Technology Cooperation, Green Technology Center Korea, Seoul, Korea

² Division of Policy Research, Green Technology Center Korea, Seoul, Korea

joonie@gtck.re.kr (Joon Han); park5085@gtck.re.kr (Chul-Ho Park)

Accepted for publication on 8th January 2017

Abstract - The Korean government released its plan to carry out intensive short-term investment in LED-related R&D projects to develop LED as a growth engine for Korea in the near future. It also announced ambitious goals regarding how to support LED technology and distribute it. In addition, it designated LED as a suitable business for small- and medium-sized enterprises (SMEs) to encourage the development of SMEs in the field. However, Korea's LED industry faces difficulties because of strong challenges from globalized multinational companies and the lack of fundamental technology. This research is to review Korea's LED policies and plans, its R&D investment in the field for years, and its competitiveness so as to assess the correlations of the three. The amount of R&D investment in the field can be a clear example of the government's support to nurture the industry and its competitiveness in the LED industry can be a good index to determine whether such investment is successful or not. Lastly, the research provides some suggestions for the vitalization of the LED industry in Korea.

Keywords - LED, Policy, R&D investment, Competitiveness, Korea

I. INTRODUCTION

LED (Light-emitting diode) lighting is a lighting fixture consisting of a LED light source and module. It has advantages such as long-life and highly efficient lighting, which contribute to reducing energy consumption and CO₂ emissions. Because of these advantages, the Korean government designated it as one of 27 Core Green Technologies¹ (NST, 2009). And the Korean government

planned to promote the domestic LED industry as an export-led green industry through intensive short-term investment which can lead to improved price competitiveness and localized technology (PCGG, 2009).

However, the Korean LED industry experiences a lot of difficulties as, basically, it lacks fundamental technology and is aggressively challenged by foreign businesses equipped with vertical integration, high quality and low cost. Moreover, there was a serious conflict between SMEs and large businesses over the issue of designating the industry as an SME-suitable industry, which, some evaluated, might further lower Korea's LED competitiveness. In this regard, it is required to evaluate the current situations from diverse perspectives as they happened despite the government's policies to nurture the industry.

This research is to review the Korean government's policies and plans to develop, and distribute LED technology. It deals with the government's R&D investment in the field for years

Non-silicon based solar cells (5) Bio energy (6) Light water reactors (7) Next-generation fast reactors (8) Nuclear fusion energy (9) Hydrogen energy (10) Fuel cell (11) Plant growth promotion (12) Integrated gasification combined cycle (13) Green cars (14) Infrastructure for intelligent transport and logistics (15) Green city and urban renaissance (16) Green buildings (17) Green Process technology (18) LED/green IT (19) IT-combined electric machines (20) Secondary batteries (21) CO₂ capture, storage, and sequestration (22) Non-CO₂ sequestration (23) Assessment and management of water quality (24) Alternative water resources (25) Waste reduction, recycling and energization (26) Monitoring and processing of hazardous substances (27) Virtual reality

¹ 27 core green technologies are as followings. (1) Monitoring and modeling for climate change (2) Climate change assessment and adaptation (3) Silicon-based solar cells (4)

and its competitiveness so as to assess the correlations of the policies, R&D investment and competitiveness. The amount of R&D investment of the government in the LED industry can be a clear example that shows the level of the government's nurturing policies. Its competitiveness in the LED industry, which is the result of such investment, can be an important index to determine whether the investment is successful or not. Through this, the research also provides some suggestions for the vitalization of the LED industry in Korea.

II. METHODS

For this study, three different aspects were examined: national LED promotion policies and plans, government expenditure on LED R&D, and the level of LED technology. First, the national master plan released by the government and its reports on LED were reviewed.² It also goes over the issue of designating the LED industry as an SME-suitable industry because the SME-suitable industry designation scheme has a lot of impact on Korea's LED industry. Second, the government's expenditure on LED R&D in Korea was analyzed. The national R&D database named 'National Science & Technology Information Service (NTIS)' was used. It is a portal service offered by the National Science & Technology Council and provides information on national R&D projects including R&D-related businesses, projects, human resources, lab equipment & devices, research outcomes, etc.³ Third, the competitiveness of Korea's LED technology was assessed compared with those of major developed countries. Finally, based on the analysis, this study suggests some points for policies to promote the LED industry.

III. NATIONAL POLICY AND PLANS FOR THE LED INDUSTRY IN KOREA

3.1. NATIONAL STRATEGY TO PROMOTE THE LED INDUSTRY

The previous Korean government (Feb. 2008 ~ Feb. 2013) announced "Green Growth" as a national agenda and emphasized green technology which could facilitate not only economic development but also environmental conservation. It designated LED technology as green technology that should be quickly developed, demonstrated, distributed and timely commercialized through intensive short-term investment. By localizing LED components and enhancing their price competitiveness, the LED industry was expected to be

² The statistics related to the distribution of LED in Korea hasn't been properly accumulated by the government yet so this research doesn't deal with the evaluation on it.

³ NTIS homepage (<http://www.ntis.go.kr>)

developed as a leading export industry of Korea (PCGG, 2009).

The Korean government set the goals for the world market share of Korean LED products at 20% and their luminous efficiency (210 lm/W) by 2020 (joint assessment by related departments, 2012). The LED Lighting 2060 Plan was announced where the national goals for the LED distribution rate would be 100% in public offices and 60% in the whole country by 2020. It was also planned to improve LED efficiency and decrease its price through increased R&D investment, to enhance consumer awareness about domestic LED lighting through follow-up services, and to establish a collaboration system between large companies and SMEs (MKE, 2011). Under the National Energy Master Plan 2.0, all lamps installed in subway, tunnels, public offices and passenger terminals should be replaced with LED ones by 2020.

3.2. DESIGNATION OF LED AS AN SME-SUITABLE INDUSTRY

Designating LED as an SME-suitable industry was an important issue in the Korean LED market in that it substantially affects Korea's competitiveness in the industry. The Korean government introduced the SME-suitable industry designation scheme in 2011. It is aimed to foster the competitiveness and growth of Korea's SMEs by restricting the entry and expansion of large companies into the field. And LED production was included in the scheme in November 2011. After the decision, large companies' sales and production of LED and its components in the consumer market were prohibited in Korea except for multi-faceted reflector (MR), parabolic anodized reflector (PAR), and bulb type LED. It was expected to ease economic polarization between large companies and SMEs in the LED industry. However, there was a serious conflict between them over the policy. While SMEs supported the scheme, large domestic companies opposed it. Large companies insisted that domestic SMEs would play just a simple role of assembling parts in LED production while foreign companies would make inroads into the domestic market. Looking at the result after the designation, they insisted it was doubtful whether the scheme really contributed to improving domestic competitiveness and supporting the economic growth of SMEs in the domestic market. Actually, the competition among domestic SMEs in the LED market has become intensified and has made domestic SMEs concentrate on producing low price LED products. This caused an invasion of foreign LED companies with low-priced, high-quality LED products and the deterioration of the technological competitiveness of SMEs. It was reported that foreign LED companies occupied up to 60~70% of the consumer LED market in Korea (KCCP, 2013).

In January 2015, the Korean government finally cancelled the designation of LED as a suitable market for SMEs. In line with it, large domestic companies and SMEs made a 'cooperation agreement for the development of LED lighting

products' without government enforcement to strengthen global competitiveness of the Korean LED industry and promote mutual cooperation. (KCCP, 2015). According to the agreement, large domestic companies would not enter the domestic LED procurement market until 2018, making an effort to promote the domestic LED industry through signing an Original Equipment Manufacturing (OEM) and/or an Original Design Manufacturing (ODM) with SMEs.

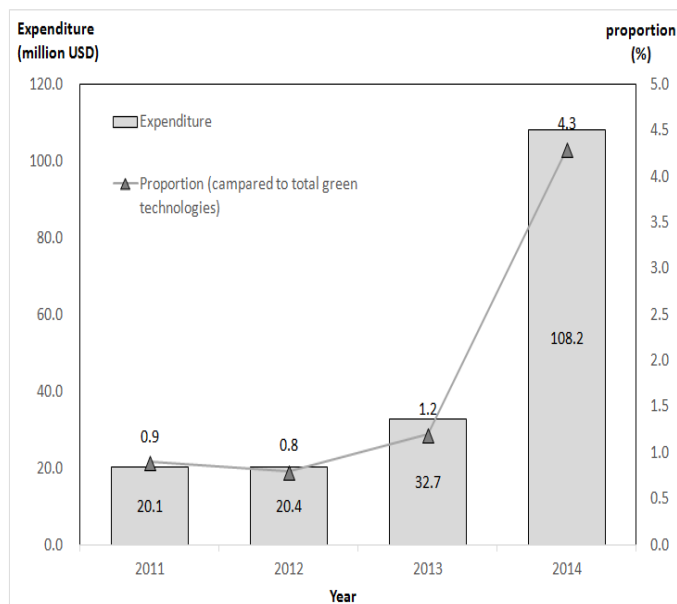
This agreement could be reached because of the understanding that it is necessary for the two players to cooperate for the vitalization of Korea's LED industry and mutual growth and prosperity. In fact, the global LED lighting market is dominated by three major lighting companies - namely Osram, Philips and GE - which strengthen their competitiveness through vertical integration (Sanderson et al, 2008). Against this backdrop, it is essential to establish such collaboration system in Korea. In fact, there used to be some attempts led by large companies to achieve vertical integration in the Korean LED industry; however, such plans were given up in the middle or substantially changed soon. It was because the vertical integration by large domestic businesses didn't create much comparative advantage while foreign businesses entering the Korean market could expand their production capacity and lower production costs through it. In this regard, it is necessary to strengthen collaboration between SMEs and large companies so that such close cooperation can produce advantages like the ones vertical integration can create.

IV. GOVERNMENT EXPENDITURE ON LED R&D IN KOREA

4.1. ANNUAL GOVERNMENT EXPENDITURE ON LED R&D IN KOREA

Annual government expenditure on LED R&D⁴ in Korea and its relative proportion to total government R&D expenditure on green technology between 2011 and 2014 are presented in Fig. 1. The Korean government spent 20.1 million USD in 2011, 20.4 million USD in 2012, 32.7 million USD in 2013 and 108.7 million USD in 2014, accounting for 0.9%, 0.8%, 1.2% and 4.3% of annual total government R&D expenditure on green technology respectively. During the period from 2011 to 2014, the rate of government expenditure on LED R&D had increased by 5.4 times. It is quite a big figure considering the fact that Korea's total R&D investment in green technology increased by 1.1 times during the period. (MSIP>C, 2014). Such huge increase in the government's R&D investment in LED fit its policy to nurture the industry.

⁴ Ministry of Science, ICT and Future Planning (MSIP) and Green Technology Center (GTC) provide a report including annual government expenditure on green technology.



Source: MSIP & GTC (2015)

Fig.1. Annual government expenditure on LED R&D in Korea between 2011 and 2014

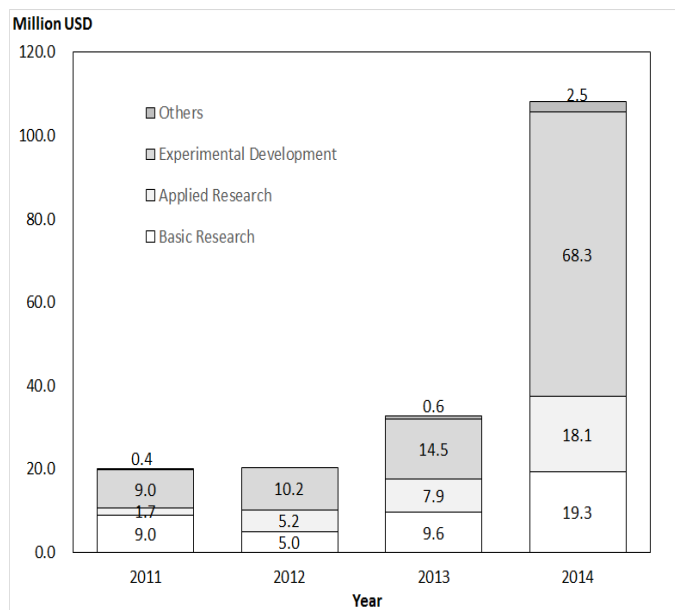
4.2. ANNUAL GOVERNMENT EXPENDITURE ON DIFFERENT STAGES OF LED R&D

Depending on R&D stages, the national R&D could be classified into 'basic research', 'applied research' and 'experimental development' (OECD, 2002). Investment in basic research is the investment to support theoretical or experimental researches to be conducted to acquire new knowledge of natural phenomena or observable facts without any particular use or application. Private enterprises invest in basic research to prepare technologies required for the next generation. Applied research is the creative study to obtain the new scientific knowledges for specific practical aim or objective and typically utilizes results obtained from basic researches. The business enterprise sector creates new project to explore promising results of basic research program. The results of applied research are typically valid for limited number of products, methods, operations or systems. Experimental development is systematic work to improve those already produced or installed or to produce new materials, products and devices through knowledge gained from basic research, applied research and practical experience.

The annual government expenditure on different stages of LED R&D in Korea between 2011 and 2014 is shown in Fig. 2. A large amount of LED R&D budget was used for the stage of 'experimental development' research in Korea, ranging from 44.3% ~ 63.1% of total government expenditure on LED R&D annually. The share of experimental development increased greatly at 63.1% in 2014. Such increase can be interpreted as the result of the Korean government's LED promotion policies, one of which considered LED lighting as the technology needed to be developed, demonstrated, and distributed within a short period of time. (PCGG, 2009). In order to obtain a tangible outcome, the Korean government

intensively invested in LED R&D, especially in the stage of 'experimental development' research.

However, in order for LED technology to be a real growth engine, Korea should have fundamental technology. It can be possible by expanding investment in basic research among the four LED R&D stages. As Korea's LED R&D is concentrated on experimental development and Korea's LED companies fail to obtain fundamental LED technology, the investment hasn't made noticeable results like the industry's growing rapidly and becoming a growth engine as the government expected. In this regard, it is very important to increase LED R&D budgets for 'basic research not only for the development of the LED industry, but also for the development of next-generation LED products in Korea.

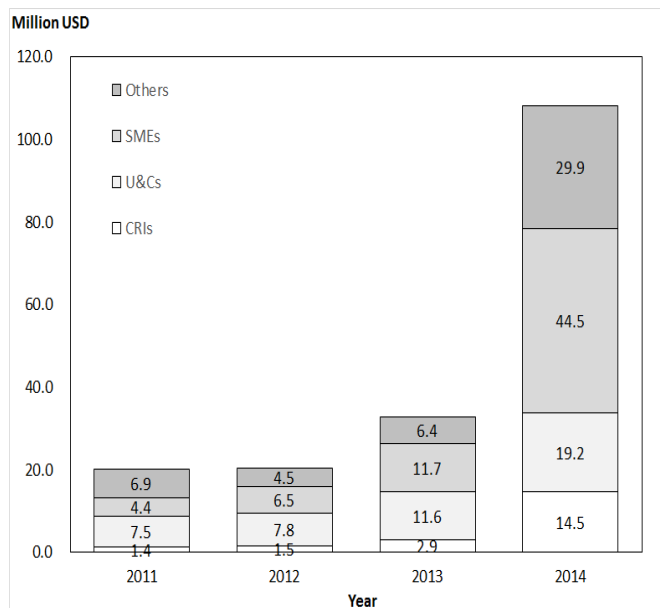


Source: MSIP & GTC (2015)

Fig.2, Annual government expenditure on different stages of LED R&D in Korea between 2011 and 2014

4.3. ANNUAL GOVERNMENT EXPENDITURE ON LED R&D LED BY DIFFERENT INSTITUTIONS AND COMPANIES

In Korea, most national projects for LED R&D are carried out by Combined Research Institutions (CRIs), University and Colleges (U&Cs), and SMEs. Others include Public Research Institutions (PRIs), Large Enterprises (LEs) and High Potential Enterprises (HPEs). As presented in Fig. 3, 37.1% and 38.4% of annual total government expenditure on LED R&D in 2011 and 2012 were allocated to U&Cs respectively, contributing to its highest proportion of R&D activities in Korea. Then from 2013, SMEs started to take the largest share and it reached at 41.2% in 2014. This seems to be affected by the decision of the Korean government to designate LED production as a suitable business for SMEs.



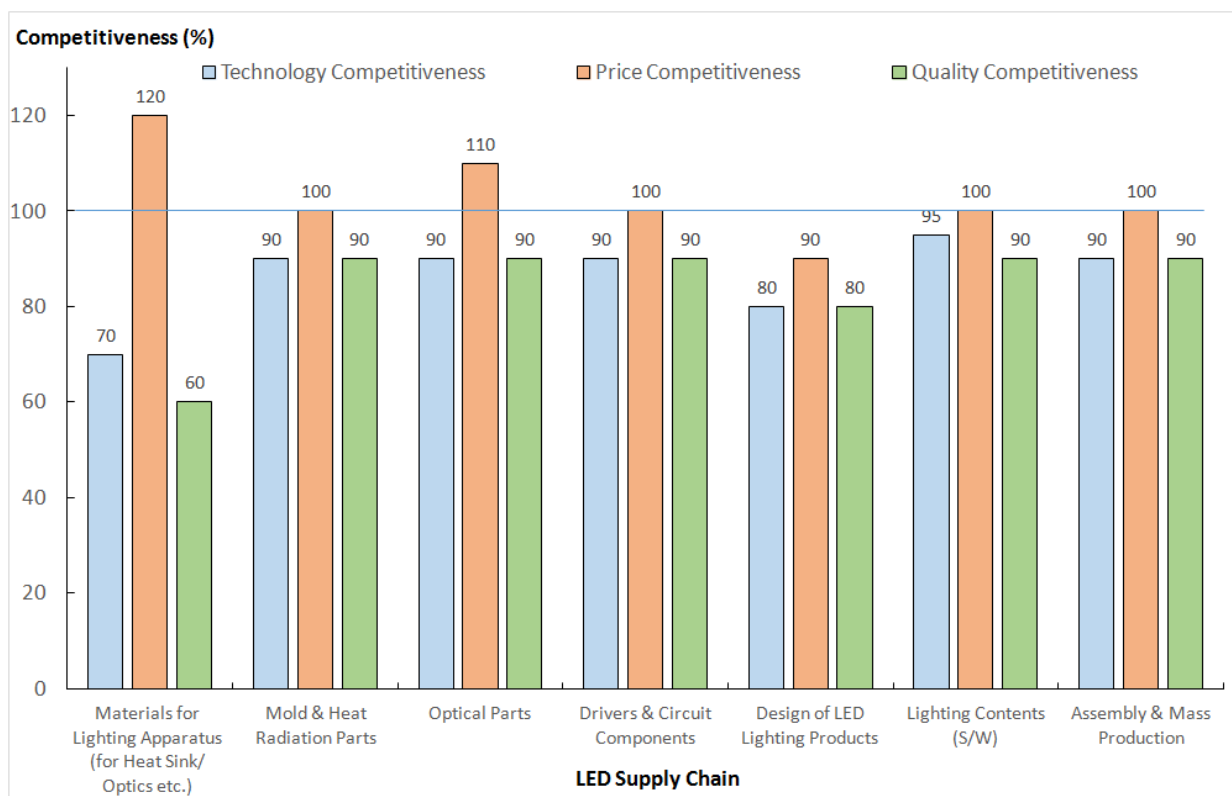
Source: MSIP & GTC (2015)

Fig.3, Annual government expenditure on LED R&D carried out by different institutions and companies between 2011 and 2014

V. COMPETITIVENESS OF KOREA'S LED TECHNOLOGY

It is a global trend to make a high-efficient, low-priced LED lighting. Competition among LED companies is more intensified than ever before, especially in the field of lighting modules and lighting engines. At present, Korean companies have LED technologies with 190lm/W of luminous efficiency and over 50,000 hours of lifetime and have made efforts to improve energy efficiency and price competitiveness of LED products.

This study evaluated the competitiveness of Korean LED lighting products by comparing it with those of major developed countries. Fig. 4 shows Korea's technology competitiveness, price competitiveness, and quality competitiveness on different stages of the LED supply chain against major competitors, namely, the US, Japan and European countries (Germany, Italy, the Netherlands, etc.) As shown in Fig. 4, Korean LED price levels are quite competitive in comparison to those of major developed countries. However, the competitiveness of Korean LED product's quality and technology is relatively inferior to those of major developed countries. In addition, the localization ratio of LED materials is only 40% in Korea, while those of chips, modules, optical parts and heat sinks used for LED production are 60 to 80% (KAPID, 2014). The reason why the competitiveness of Korean LED materials is low is that Korean companies do not have enough fundamental technology. The Korean LED industry lacks fundamental technology such as a LED packaging technology and has a



※ Values in each column denote the relative competitiveness of the Korean LED technology compared with the level of the best technology (100) in each supply chain
 Source: KAPID (2014)

Fig.4. Levels of competitiveness of Korean LED technologies

vulnerable infrastructure for the promotion of the LED market. In order to develop related technology and the quality competitiveness of Korean LED products, it is necessary for Korean LED businesses to develop fundamental LED technology. It is a fundamental way to promote the Korean LED industry and win over fierce global LED competition.

VI. DISCUSSION & CONCLUSIONS

This study analyzed Korea's national policies and plans for LED R&D, annual government expenditure on LED R&D and the competitiveness of LED technology in Korea for the past years. In terms of policies and plans, the Korean government designated LED technology as the one that should be quickly developed, demonstrated, distributed and timely commercialized, set up goals to achieve regarding the level of LED technology and distribution and established plans like requiring the installation of LED lighting in public places. In addition, it designated the LED industry as an SME-suitable industry and tried to encourage the development of LED by SMEs. Such plans were reflected on its intensive short-term investment which led to the substantial increase in LED R&D investment by the government and increased share of SMEs in LED R&D investment.

However, in spite of the government's efforts along with intensive short-term investment, the LED industry in Korea is in trouble due to lack of fundamental LED technology. In addition, a large portion of Korea's LED market is occupied by aggressive global companies with low-priced, high-quality products and the competitiveness of Korean companies has been much weakened. It seems to be the result of Korea's R&D investment which was concentrated not on basic research but on experimental development research, which led to the difficulties in developing fundamental LED technology.

Based on this, two suggestions can be made for the vitalization of the LED industry in Korea. First, the government should expand its R&D investment in basic research so that Korea could obtain fundamental technology. Moreover, regarding LED chips, it can stimulate the development of next generation optical semi-conductor while utilizing Korea's highly advanced technology in memory semi-conductor and IT fields. Second, the government should help strengthen the collaboration between SMEs and large businesses in the LED industry, which started to collaborate with the recently reached cooperation agreement for development of LED lighting products. Through vertical integration, global players have acquired price competitiveness of LED lighting. The agreement could play a key role to cope with the market penetration of global companies with low-priced, high-quality LED products.

REFERENCES

- [1] Joint assessment by related departments in Korea. *Assessment on LED development and distribution policies and follow-up measures*. an agenda for the 6th assessment meeting. 2012.
- [2] Korea Association for Photonics Industry Development (KAPID). *Survey on the Utilization of lighting Apparatus and Study on Saving Lighting Power Consumption*. Ministry of Trade, Industry and Energy (MOTIE), 2014.
- [3] Korean Commission for Corporate Partnership (KCCP). *KCCP's position on the article of The Seoul Economic Daily(11.17) related with businesses suitable for SMEs*. 2013.
- [4] Korean Commission for Corporate Partnership (KCCP). *Corporate partnership for cooperation and development of LED lighting product between large companies and SMEs*. 2015.
- [5] Ministry of Science, ICT and Future Planning (MSIP) and Green Technology Center (GTC). *Statistics Yearbook 2014 of Green Technology - Research and Development*. 2015.
- [6] Ministry of Knowledge Economy (MKE). *Proposing "2060 LED Lighting Plan" for Green Lighting Society*. 2011.
- [7] National Research Council of Science & Technology (NST). *Green Technology R&D Comprehensive Plan*. 2009.
- [8] OECD. *Frascati Manual: Proposed standard practice for surveys on research and experimental development*. 2002. <http://www.oecd.org/sti/frascatimanual>
- [9] Presidential Committee on Green Growth (PCGG). *Core Green Technologies and Commercialization Strategies. Agenda for the 3th Meeting of Committee on Green Growth*. 2009.
- [10] S. W. Sanderson, K. L. Simons, J. L. Walls, and Y. Lai. "Lighting Industry: Structure and Technology in the Transition to Solid State," 2008 *Industry Studies Conference Paper*, 2008.